January 2017

The Role Of A-Synuclein In Brain Lipid Metabolism And Inflammation

Drew R. Seeger

Follow this and additional works at: https://commons.und.edu/theses

THE ROLE OF α-SYNUCLEIN IN BRAIN LIPID METABOLISM AND INFLAMMATION

Dissertation

Presented in Partial Fulfillment of the Requirements for the Degree Doctor of Philosophy
in the Graduate School of the University of North Dakota

By

Drew Richard Seeger
Bachelor of Arts, Saint John's University, 2010

Graduate Program in Pharmacology, Physiology, and Therapeutics

The University of North Dakota

2017

Dissertation Committee:

Dr. Eric J. Murphy, Advisor

Dr. Colin K. Combs

Dr. Mikhail Y. Golovko

Dr. Thad A. Rosenberger

Dr. James D. Foster

This dissertation, submitted by Drew Richard Seeger in partial fulfillment of the requirements for the Degree of Doctor of Philosophy from the University of North Dakota, has been read by the Faculty Advisory Committee under whom the work has been done and is hereby approved.

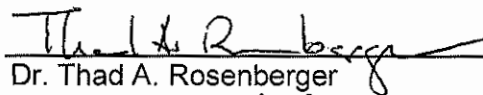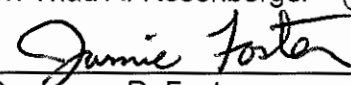Dr. Eric J. Murphy, Chairperson

Dr. Colin K. Combs

Dr. Mikhail Y. Golovko

Dr. Thad A. Rosenberger

Dr. James D. Foster

This dissertation is being submitted by the appointed advisory committee as having met all of the requirements of the School of Graduate Studies at the University of North Dakota and is hereby approved.

Grant McGimpsey
Dean of the School of Graduate Studies

July 28, 2017
Date

iii

PERMISSION

Title   The Role of α-Synuclein in Brain Lipid Metabolism and Inflammation

Department   Pharmacology, Physiology, and Therapeutics

Degree   Doctor of Philosophy

       In presenting this dissertation in partial fulfillment of the requirements for a graduate degree from the University of North Dakota, I agree that the library of this University shall make it freely available for inspection. I further agree that permission for extensive copying for scholarly purposes may be granted by the professor who supervised my dissertation work or, in his absence, by the Chairperson of the department or the dean of the School of Graduate Studies. It is understood that any copying or publication or other use of this dissertation or part thereof for financial gain shall not be allowed without my written permission. It is also understood that due recognition shall be given to me and to the University of North Dakota in any scholarly use which may be made of any material in my dissertation.

<div align="right">

Drew Richard Seeger
April 1, 2017

</div>

TABLE OF CONTENTS

LIST OF FIGURES

Figure   Page

LIST OF TABLES

ACKNOWLEDGMENTS

I would like to express my deepest gratitude to the members of my advisory committee for their guidance and assistance in completing my dissertation work. And a special thank you to my advisor, Dr. Murph for fostering my scientific understanding, ethics, and for passing on valuable anecdotal references and idioms.

To my family, parents Barb and Richard, brother Grant, sisters Lisa and Alayna, wife Ashley, and children Aurora and Orion. You have all helped me on the path of becoming the son, brother, husband, father, and scientist I am today.

ABSTRACT

Alpha-synuclein (Snca) is a small cytosolic protein that is ubiquitously expressed in the nervous system and comprises 0.5-1% of all cytosolic protein, but its biological function is poorly understood. Although Snca function has been studied in lipid metabolism, the function of Snca in brain lipid metabolism under inflammatory conditions is yet to be elucidated. We utilized several model systems including primary cultured astrocytes and microglia, *Snca* deficient and mutant knock-in mice, and a radiolabeled free fatty acid steady state-kinetic mouse model to determine Snca role in neuroinflammation. Herein, we have determined several major roles of Snca during inflammation: (i) dBcAMP treatment increases 20:4n-6 uptake in astrocytes and this increase appears to be due to increased expression of long chain acyl-CoA synthetases 3 and -4 coupled with a reduction in acyl-CoA hydrolase expression in the presence of reduced *Snca* expression. (ii) *Snca* deficient mice have higher basal brain 2-arachidonyl glycerol (2-AG) levels compared to wildtype and lipopolysaccharide (LPS) stimulation further exacerbated 2-AG synthesis.(iii) In primary microglia, LPS-treatment reduced released 2-AG into medium concomitantly with reduced *Snca* expression and *Snca* deficient microglia had a delayed response to LPS stimuli. This supports the hypothesis that *Snca* expression is linked to 2-AG release in primary microglia and may contribute to regulating the phagocytic phenotype.(iv) Using *Snca* gene-ablated mice, we determined the impact of Snca on brain 20:4n-6 metabolism during LPS-induced inflammatory response in vivo using an established steady-state kinetic model. In *Snca* deficient mouse brain, 20:4n-6 uptake was significantly increased 1.3-fold. In the organic fraction,

tracer entering into *Snca* deficient mouse total brain phospholipids was significantly

increased 1.4-fold, accounted for by increased incorporation into choline

glycerophospholipids and phosphatidylinositol. In the neutral lipid fraction, 20:4n-6

incorporation into diacylglycerol of *Snca* deficient mice was significantly reduced by

75%. Hence, under inflammatory conditions where 20:4n-6 release is enhanced, Snca

has a crucial role in modulating 20:4n-6 metabolism, and the absence of Snca results in

increased uptake and incorporation into lipid pools associated with enhanced lipid-

mediated signaling during neuroinflammatory response. Herein, we focus on the role of

Snca in downstream eicosanoid biosynthesis, inflammatory mediators, and lipid

signaling molecules linking Snca to inflammatory response elucidating a key step in

neuroinflammation.

.

CHAPTER I

INTRODUCTION

Snca and Parkinson's disease

Snca is a 140-amino acid intrinsically unfolded protein which comprises 0.1-1%
of all brain cytosolic proteins and is predominantly found in the nervous system (Jakes *et
al.* 1994). Snca is an in intrinsically disordered protein but upon binding the lipid bilayers
its N-terminus develops an amphipathic helical structure. The C-terminal tail however,
remains disordered (Ahn *et al.* 2002). Snca is ubiquitously expressed in neurons
(Krüger *et al.* 2000), astrocytes (Castagnet *et al.* 2005), microglia (Austin *et al.* 2011),
and oligodendroglia (Richter-Landsberg *et al.* 2000). Snca is highly conserved in
vertebrates and was originally studied in neurons due to its predominate presynaptic
localization in neurons (Adamczyk *et al.* 2005; Raghavan *et al.* 2004). This has led Snca
to be highly studied in regards to its function in neurons and neurodegenerative
diseases.

A widely accepted hallmark of Parkinson's disease (PD) and of other
synucleinopathies is the accumulation of aggregated Snca in plaques known as Lewy
bodies (Iseki *et al.* 1998). PD is the second most common neurodegenerative disorder
in the United States affecting nearly 3% of individuals over the age of 65 (Kowal *et al.*
2013). Rare familial missense mutations (A30P, A53T, E46K, H50Q, or G51D) or
multiple gene replications in Snca result in early onset PD (Krüger *et al.* 2000;
Polymeropoulos *et al.* 1997) suggesting Snca plays a key role in PD pathogenesis. PD
however, is not the only disorder that has been linked to Snca aggregation named

"synucleinopathies", as Lewy bodies which are commonly found in patients with dementia and glia in multiple system atrophy contain Snca fibrils (Farrer *et al.* 1999). Although Snca function in neurons has been studied by others, we have focused on Snca lipid mediating effects in the nervous system. Snca has a robust impact on lipid metabolism and lipid mediated signaling having a critical role in neuroinflammation found in neurodegenerative disorders including PD.

Snca has several diverse roles in the nervous system including synaptic vesicular movement (Cabin *et al.* 2002), dopamine transporter modulation (Lee *et al.* 2001), and regulation of dopamine levels (Lotharius and Brundin 2002). However, recent studies suggest Snca has a role in brain fatty acid metabolism. Previous research suggested that Snca is a fatty acid binding protein (FABP) due to similar protein homology and structure (Sharon *et al.* 2001). Although Snca facilitated fatty acid uptake its binding constant for fatty acids is two orders of magnitude less than a classical FABP and its impact on lipid metabolism is clearly different (Murphy *et al.* 2005; Barceló-Coblijn *et al.* 2007; Martin *et al.* 2003). However, like FABP (Murphy *et al.* 2005), Snca increases long chain acyl-CoA synthetase (Acsl) activity, but this effect is limited to arachidonic acid but hypothesized to affect other acyl-CoA formation (Golovko *et al.* 2006a). Effects of Snca on lipid metabolism are brain specific and it is hypothesized that Snca directly modulates Acsl activity. Furthermore, *Snca* deficiency results in decreased palmitic acid (PAM) and arachidonic acid (ARA) uptake, incorporation rate and fractional turnover in PL (Golovko *et al.* 2005; Golovko *et al.* 2006a). However, in PAM infusion studies, incorporation into choline glycerophospholipids (ChoGpl) is increased while incorporation and turnover into all other major phospholipids are reduced (Golovko *et al.* 2005). Furthermore, in *Snca* deficient microglia n-butanol treatment partially attenuates phospholipase D (PLD)-dependent signaling resulting in increased cytokines and

cytosolic phospholipase A_2 ($cPLA_2$) and cyclooxygenase 2 (Cox-2) protein levels (Austin *et al.* 2011). This finding is significant because it suggests Snca affects PLD function, which is crucial in inflammatory response and has a pivotal role in PD progression. Our data supports this idea through increased ChoGpl recycling by increased PLD activity in the absence of Snca as well as increased prostaglandin formation resulting from dysfunctional ARA metabolism. Although Snca function has been studied in lipid metabolism, the function of Snca in lipid metabolism and microglia following LPS stimulation remains to be elucidated. This contribution is significant because it will identify key roles of Snca in ARA metabolism as well as modulation of microglia phenotype in neuroinflammatory response.

Our group has shown that Snca facilitates PAM and ARA uptake in astrocytes (Castagnet *et al.* 2005) and brain (Golovko *et al.* 2005; Golovko *et al.* 2006a), as well as playing a role in brain neutral lipid metabolism (Barceló-Coblijn *et al.* 2007). We have established that Snca deficiency results in a marked reduction in PAM and ARA incorporation and turnover kinetics using a steady-state kinetic model. Interestingly, Snca deficient brain microsomes have decreased Acsl activity and incubation with physiological levels of recombinant Snca restored this activity (Golovko *et al.* 2006a). However, mutant forms (A53T and A30P) failed to restore activity. Basal prostanoid levels are not affected by *Snca* ablation. However, Under ischemic conditions *Snca* gene ablation results in increased formation of prostaglandins (PG) (Golovko and Murphy 2008), demonstrating a lipid mediated link to the inflammatory response.

Although Snca affects fatty acid uptake and modulates trafficking into specific lipid pools *in vivo,* the function of Snca during neuroinflammatory response is poorly defined. Because Snca activity is crucial in brain fatty acid uptake, phospholipid fatty acid turnover and fatty acid trafficking into specific lipid pools, it is important to asses if

2

Snca has a role in brain inflammation. Our objective is to determine the significance *Snca* expression *in vivo* on ARA uptake and trafficking into lipid pools following LPS (i.p.) stimulation. The arachidonic acid infusion following LPS stimulation will apply a well-defined radiotracer steady-state kinetic model to determine fatty acid uptake and turnover (Robinson *et al.* 1992). The rationale for this is that Snca is known to affect brain fatty acid uptake and trafficking into specific lipid pools by modulating ER-localized Acsl activity (Golovko *et al.* 2006a). Snca binds free fatty acids at a low *Kd*, but does not target fatty acids for β-oxidation, or produce a change in lipid mass after gene ablation suggesting it does not act as a FABP(Golovko *et al.* 2006a). Interestingly though, Snca has been hypothesized to have these similar roles of a FABP by enhancing ER-based lipid synthetic enzyme activity (Golovko *et al.* 2006a).

ARA and PAM are prepared for utilization by the addition of CoA by Acsl, which in turn allows the FA-CoA to participate in biosynthetic or catabolic pathways. There are five long chain acyl-CoA synthetase isoforms in humans and rodents (Watkins *et al.* 2007). These isoforms differ in their substrate preferences, regulation, enzyme kinetics, alternative splicing and location. Of these 5 isotypes Acsl-4 and-6 are prominently found in the brain (Cao *et al.* 2000; Kee *et al.* 2003; Van Horn *et al.* 2005).   Acsl-6 is alternatively spliced into four variants Acsl-6v.1-4 (Van Horn *et al.* 2005; Lee *et al.* 2005b). Acsl-4 presents high affinity for PAM and Acsl-6v.1 shows high affinity for ARA. Incubation with wildtype, but not mutant forms of Snca (A53T and A30P) recombinant protein restores Acsl activity to make ARA-CoA in isolated gene deficient microsomes from *Snca* ablated mice (Golovko *et al.* 2006a). This lack of Acsl modulation by the mutants gives reason to believe that mutant forms function like the null. However, the role of hSnca and its mutant forms on Acsl activity and fatty acid uptake and trafficking is

unknown. Furthermore, *Snca* ablation has shown a significant decrease in phospholipid targeting in PAM treated mice (Barceló-Coblijn *et al.* 2007; Golovko *et al.* 2005). However, incorporation of PAM into ChoGpl is increased possibly due to increased activity of PLD_2 resulting in increased ChoGpl turnover. This increase in turnover should also be reflected in mutant *Snca* expressing mice, directly linking mutant Snca dysfunction to lipid signal transduction. Hence, these data contributes an important missing, yet fundamental element in Snca physiology. Acquisition of this knowledge is crucial to understanding the fundamental roles of Snca not only in PD, but to a broad spectrum of CNS disease that result in neurodegeneration. We expect to determine if Snca has an important role in facilitating fatty acid uptake and trafficking in phospholipid pools during neuroinflammation. Such a finding is important because it illuminates key functions of a ubiquitously expressed, yet poorly defined, protein that is established as the center of all synucleinopathy type neurodegenerative diseases.

Progressive Parkinson's disease is associated with the presence of activated microglia and neuroinflammation (Austin *et al.* 2006; Teismann and Schulz 2004). Snca inhibits PLD activity in yeast (Outeiro and Lindquist 2003) as well as in animal studies (Jenco *et al.* 1998). PLD activity is essential for activation of microglia required for inflammatory response including expression of key cytokines such as IL-1 and TNF-α (Austin *et al.* 2011). Similarly, dysfunctional ARA metabolism in *Snca* ablated mice results in increased prostaglandin biosynthesis (Golovko and Murphy 2008). Furthermore, Snca stimulates PLCβ (Narayanan *et al.* 2005), which in turn generates diacylglycerol which can then be hydrolyzed by diacylglycerol lipase to produce 2-arachidonyl glycerol (2-AG) (Blankman *et al.* 2007). 2-arachidonyl glycerol is important in both microglia motility and phenotypic state (Walter *et al.* 2003). However, it is unknown if Snca have a similar effect on 2-AG levels and subsequent

neuroinflammation. LPS treatment is needed because *Snca* deficient mice display a basal inflammatory profile similar to wild type. However, during inflammatory insult, such as LPS treatment, the depressed PLD_2 inhibition and ability to recycle ARA result in an increased inflammatory profile. Our rationale is that Snca is known to affect ARA metabolism producing inflammatory metabolites as well as PLD_2 and PLCβ activity modulation by Snca, would produce key players in lipid signal transduction. *Snca* deletion increases prostaglandin formation after ischemic injury, suggests that Snca has a role in brain response to injury and inflammation (Golovko and Murphy 2008). The increased prostaglandin profile and reduced Acsl activity is consistent with reduced ARA-CoA turnover causing increased ARA release into the free FA pool and subsequent metabolism into eicosanoids. An increase in downstream inflammatory mediators and cytokines released in microglia suggests involvement of PLD_2 activity (Austin *et al.* 2011). Increased turnover of ChoGpl found in *Snca* deficient mouse brain is consistent with tonic inhibition of PLD_2 by Snca (Jenco *et al.* 1998). Furthermore, butanol treatment attenuates PLD-mediated generation of phosphatidic acid (PA), by transphosphatidylation of ChoGpl into phosphatidylbutonal causing a resultant drop in PA release, is consistent with reduced cytokine secretion observed in gene ablated microglia (Austin *et al.* 2011). Herein, we focus on the role of Snca in downstream eicosanoid biosynthesis, inflammatory mediators, and lipid signaling molecules linking Snca to inflammatory response elucidating a key step in neuroinflammation

In this manuscript I will present several lines of evidence indicating that Snca plays a vital role in brain lipid metabolism and has an impact on the inflammatory state of the brain. I will utilize several model systems including primary cultured astrocytes and microglia, *Snca* deficient and *Snca* mutant knock-in mice, and a radiolabeled free fatty acid steady state-kinetic mouse model to determine the role of Snca in

neuroinflammation. In chapter I, I will determine how phenotypic shift of astrocytes by dBcAMP affects PAM and ARA uptake and trafficking and expression of enzymes that regulate these changes. This is important because astrocyte-derived lipids are critical in brain function and dBcAMP treatment results in an activated phenotype in astrocytes similar to what is found in neuroinflammation. In chapter II,   Because Snca affects ARA metabolism, we will determine whole brain 2-AG levels in wild type, *Snca* gene-ablated, and *Snca* knock-in animals at basal levels and following LPS stimulation. This is important because 2-AG is synthesized from ARA containing DAG and is a neuroprotective bioactive lipid that plays a role in lipid signal transduction and can modulate inflammatory response. In chapter III, using primary microglia we will determine how 2-AG levels are related to *Snca* expression. This is important because, 2-AG affects microglia motility and 2-AG levels may contribute to the reduced phagocytic ability found in *Snca* deficient microglia. Finally in chapter IV, we will determine the impact of *Snca* deficiency on brain ARA metabolism during LPS-induced inflammatory response in vivo using an established steady-state kinetic model. This is important because, under inflammatory conditions where ARA release is enhanced, Snca has a crucial role in modulating 20:4n-6 uptake and incorporation into lipid pools associated with lipid-mediated signaling and may enhance fatty acid uptake and metabolism during neuroinflammatory response. In the following chapters we will elucidate the role of Snca in lipid metabolism and downstream neuroinflammatory mediators.

CHAPTER II

INTRODUCTION

Arachidonate and palmitate uptake and metabolism is differentially modulated by dibutyryl-cAMP treatment

Brain injury results in astrocytosis, a process that involves activation of astrocytes within hours after injury and this activation is sustained for weeks following injury (Csuka *et al.* 2000; Bye *et al.* 2011). In cultured astrocytes, treatment with dibutyryl-cAMP (dBcAMP), a cell permeable cAMP analog, induces a phenotypic shift to a fibrous morphology characteristic of a reactive astrocyte (Fedoroff *et al.* 1987; Fedoroff *et al.* 1984; Miller and Raff 1984) and is similar to activated astrocytes following traumatic brain injury. Consistent with this phenotype, dBcAMP treated astrocytes express increased levels of glial fibrillary acidic protein (Bignami and Dahl 1976) and vimentin (Ciesielski-Treska *et al.* 1984) as well as broad changes in modulation of protein phosphorylation (Neary *et al.* 1987). In dBcAMP treated astrocytes, actin is reorganized (Goldman and Abramson 1990; Ciesielski-Treska *et al.* 1984) with an increased number of tightly packed intermediate filaments (Goldman and Chiu 1984) and microfilament ring formation (Fedoroff *et al.* 1987), producing stellate processes that are a hallmark of reactive astrocytes *in vivo.* Although astrocytosis has been highly studied in central nervous system (CNS) trauma, ischemia, and stroke using dBcAMP treated astrocytes, differences in fatty acid metabolism between non-treated and dBcAMP treated primary astrocytes are poorly defined.

9

Astrocytes have a crucial role in brain cholesterol metabolism and overall CNS function. Apolipoprotein E (ApoE) is synthesized in the central nervous system and is predominantly expressed in astrocytes (Boyles *et al.* 1985; Elshourbagy *et al.* 1985; Krul and Tang 1992). Although, ApoE and B receptors are expressed on astrocyte endfeet near the arachnoid space (Pitas *et al.* 1987), it is widely accepted that plasma-derived ApoE lipoprotein containing cholesterol does not cross the blood-brain barrier and cholesterol within the CNS is a result of synthesis in astrocytes *de novo* (Dietschy *et al.* 1983; Dietschy and Turley 2001; Osono *et al.* 1995; Hanaka *et al.* 2000). ApoE with bound cholesterol is released by cultured astrocytes (Krul and Tang 1992; Boyles *et al.* 1985), which is important as it combines ApoE and cholesterol production in the same cell. Neurons normally express low-density lipoprotein receptors (LDLR) (Swanson *et al.* 1988; Motoi *et al.* 1999; Beffert *et al.* 2004), which stimulate axonal growth and synaptogenesis (Hayashi *et al.* 2004; Mauch *et al.* 2001). However, after injury and during neuronal repair, neurons have increased expression of LDLR on growth cones and rely on ApoE derived cholesterol for remodeling (Poirier *et al.* 1993; Ignatius *et al.* 1987; Swanson *et al.* 1988; Posse de Chaves *et al.* 1997; Krul and Tang 1992; Yin *et al.* 2012). Interestingly, in transgenic mice expressing human ApoE, purified human ApoE contains abundant ethanolamine glycerophospholipids (EtnGpl) and choline glycerophospholipids (ChoGpl), as well as cholesterol (DeMattos *et al.* 2001), suggesting phospholipids are also taken up by neurons via ApoE/LDLR mechanisms (Staub *et al.* 1995; Moore *et al.* 1991; Bernoud *et al.* 1998).

Fatty acid binding proteins (FABP) act as fatty acid chaperons that facilitate fatty acid uptake and targeting (Murphy 1998; Murphy *et al.* 1996; Prows *et al.* 1995; Binas *et al.* 1999; Murphy *et al.* 2004; Murphy *et al.* 2005) and also affect cellular phospholipid

metabolism (Murphy *et al.* 2004; Murphy *et al.* 2005; Murphy *et al.* 2000a; Jolly and Murphy 2002). The brain expresses three different fatty acid binding proteins, FABP3, FABP5, and FABP7 (Owada and Kondo 2003; Owada *et al.* 1996; Owada 2008; Veerkamp and Zimmerman). FABP7 is developmentally expressed in radial glial cells (Kurtz *et al.* 1994; Owada *et al.* 1996) and is then expressed at lower levels in adult mouse astrocytes (Myers-Payne *et al.* 1996; Owada *et al.* 1996). It has a preference for binding of the *n-3* fatty acid family (Myers-Payne *et al.* 1996; Feng *et al.* 1994). FABP7 may serve as a plasma derived biomarker useful for diagnosing patients with dementia-related diseases, such as Alzheimer's and Parkinson's disease (Teunissen *et al.* 2011). FABP5 is expressed primarily in gray matter in glial cells, although there does appear to be limited expression in white matter, in the adult animal (Owada *et al.* 1996). FABP5 has less specificity and impacts both *n-3* and *n-6* fatty acid uptake into the cell and spinal cord (Liu *et al.* 2008; Figueroa *et al.* 2016). In PC-12 cells it enhances neurite extension (Allen *et al.* 2000) and protects cells from lipotoxicity through a potential NFκB mechanism (Liu *et al.* 2015). FABP3 is expressed in the brain primarily in neurons, with the highest expression in cortical layers, in hippocampus, and in dentate gyrus (Owada *et al.* 1996; Sellner *et al.* 1995). FABP3 has a binding preference for *n-6* fatty acids (Hanhoff *et al.* 2002), suggesting that this protein may be involved in neuronal 20:4n-6 uptake and trafficking.

Arachidonic acid (20:4n-6) is highly esterified into ethanolamine glycerophospholipids (EtnGpl) and its biosynthesis can occur within astrocytes, which may be crucial for maintaining brain 20:4n-6 levels in brain signal transduction events (Moore *et al.* 1991). Although neurons and blood-brain barrier endothelium are capable of elongation and desaturation of fatty acids, the bulk of 20:4n-6 is provided through

plasma derived 20:4n-6 or by that provided by astrocytes (Moore *et al.* 1991; Bernoud *et al.* 1998; Rapoport *et al.* 2001). Cultured astrocytes can either take up 20:4n-6 or synthesize it from linoleic acid (18:2n-6) and subsequently esterify it into lipid pools following activation by formation of its CoA thioester, which is catalyzed by long chain acyl-CoA synthetases (Acsl). Astrocytes readily take up the precursor of 20:4n-6,18:2n-6, which is preferentially elongated and desaturated into 20:4n-6, resulting in increased 20:4n-6 incorporation into phospholipid pools (Williard *et al.* 2002; Murphy 1995). This is important because 20:4n-6 is the major polyunsaturated fatty acid (PUFA) at the *sn*-2 position in EtnGpl and ChoGpl (Svennerholm 1968; Murphy 1984; López *et al.* 1995). These phospholipid pools are reservoirs for 20:4n-6 that can be directly released as free fatty acids (FFA) by Ca^{+2}–dependent activation of PLA_2, via inositide signal transduction pathways, resulting in 20:4n-6 release from phospholipids (Wilkin *et al.* 1991) and subsequent metabolization into prostanoids exerting a downstream signal (Keller *et al.* 1987; Strokin *et al.* 2003). Treating astrocytes with dBcAMP causes a substantial increase in elongation and desaturation pathway and increase in 20:4n-6 mass, suggesting a larger releasable pool of 20:4n-6 (Murphy *et al.* 1997). Thus, events regulating 20:4n-6 metabolism have a major role in CNS function and understanding the modulation of 20:4n-6 in phenotypically shifted astrocytes is crucial to understanding the changes in 20:4n-6 uptake and trafficking in reactive astrocytes.

Because dBcAMP treated astrocytes show phenotypic similarities to reactive astrocytes and 20:4n-6 metabolism is crucial during events associated with astrocytosis, we examined the impact of dBcAMP phenotypic shift on 20:4n-6 uptake into astrocytes and its incorporation into lipid pools. A predominately *sn*-1 position fatty acid, palmitic acid (16:0), was used to determine the potential changes in *sn*-1 position fatty acid

metabolism. dBcAMP treatment specifically increased 20:4n-6 uptake and incorporation into phospholipid pools, while 16:0 uptake was unaffected. Interestingly, Acsl gene expression was effected by dBcAMP treatment. We demonstrate for the first time that in dBcAMP treated astrocytes, 20:4n-6 uptake and incorporation was enhanced, suggesting that dBcAMP had a significant impact on 20:4n-6 metabolism via modulation of Acsl expression in astrocytes and potentially impacts 20:4n-6 use in downstream signal transduction (Seeger *et al.* 2016).

MATERIALS AND METHODS

Cells

Mouse cortical astrocytes were isolated from brains of 1 day old 129/SvEv mice under an approved protocol by the University of North Dakota (Grand Forks, ND) Animal Care and Use Committee (UND protocol #1106-1C). Cortices were triturated in Dulbecco's modified Eagle's medium (DMEM) to separate cells, filtered through 80 μm Nylon mesh, and resuspended in DMEM containing 10% fetal bovine serum (FBS). Astrocytes were cultured in DMEM containing 10% FBS, 3.7 g/L bicarbonate, 2 mM glutamine, 100 μg/mL penicillin/streptomycin, and 5 mM HEPES at pH 7.4 in a water jacketed incubator at 37°C in 5% CO_2 atmosphere. Astrocytes were expanded by subculturing on T-75 flasks (4:1) by loosening the adherent cells with 0.25% trypsin. The third passage (3:1) was plated on 100 mm polystyrene cell culture plates prior to treatment with dBcAMP. Confluent astrocytes were treated with 0.25 mM dibutyryl-cAMP in serum containing medium for a period of four days prior to incubation with fatty acid radiotracers (Hertz 1990; Murphy *et al.* 1997). Because changes in phospholipid fatty acid composition occur in primary astrocytes over time, cells in this study were subcultured for more than 28 days in culture (Murphy *et al.* 1997).

Fatty Acid Incubation

The effect of dBcAMP treatment on fatty acid uptake and trafficking in primary cortical astrocyte cultures was determined by incubating the cells with 2 μM [1-^{14}C]20:4n-6 or 2 μM [1-^{14}C]16:0 (Moravek Biochemicals, Brea, CA, USA) in FBS-free DMEM. These concentrations are well below the critical micellar concentration for each

14

fatty acid. Tracers were dissolved in ethanol and the final concentration of ethanol added to the culture was < 0.2% (Castagnet *et al.* 2005). The final tracer specific activity was 4.87 nCi/nmol for [1-^{14}C]20:4n-6 and 4.73 nCi/nmol for [1-^{14}C]16:0, which was used to calculate the mass of tracer taken up into cells. Astrocytes were incubated with fatty acids for 1, 5, 15, and 30 min at 37°C in 5% CO_2.

Lipid Extraction

Prior to cell lipid extraction, FBS free-DMEM was removed and cells were rinsed twice with 2 mL of ice cold phosphate buffered saline (PBS) to remove residual tracer and medium (Murphy *et al.* 1997). The plate was then immediately floated on liquid nitrogen to stop enzymatic activity and 2 mL of 2-propanol added. Then the cells were removed from the plate using a Nylon cell scraper and the 2-propanol containing the cellular debris was then transferred to a test tube containing 6 mL of hexane (Murphy *et al.* 1997; Castagnet *et al.* 2005). The plate was then washed using a second addition of 2-propanol, which was added to the tube contain the first aliquot of 2-propanol resulting in a solution of n-hexane:2-propanol (HIP 3:2 v/v) (Radin 1988). Cell extracts were then dried under $N_{2(g)}$ until ~1 ml of the solvent remained. The extracts were then subjected to centrifugation (3,000xg) for 20 minutes at 4°C to the pellet cellular debris and denatured protein. The lipid containing supernatant was decanted and saved for analysis. Cellular debris was washed with 2 ml HIP (3:2 v/v) and the debris pelleted by centrifugation (3,000x g) and the wash combined with the initial extract. The debris pellet containing cellular protein was air dried overnight at room temperature and saved to quantify the protein. Lipid extracts were stored under a $N_{2(g)}$ atmosphere at -80°C in HIP.

Protein Quantification

The dried cellular debris was subjected to hydrolysis with 0.2 M KOH at 65°C overnight (Murphy and Horrocks 1993). Proteins were then quantified using a modified dye-binding assay (Bradford 1976). Bovine serum albumin dissolved in 0.2 M KOH as a standard and was used to convert absorbance to concentration via standard curve.

Thin Layer Chromatography

After drying the lipid extracts under $N_{2(g)}$ and dissolving them in chloroform ($CHCl_3$), the phospholipid and neutral lipid fractions were separated using silicic acid column chromatography (Clarkson Chemical Company, Inc., Williamsport, PA, USA). The neutral lipid fraction was eluted with chloroform:methanol (58:1 by vol) and the phospholipid fraction eluted with methanol (Murphy *et al.* 1997). Radioactivity of phospholipid and neutral lipid fractions was determined by liquid scintillation counting after silicic acid column separation to determine a total radioactivity of each fraction. Following fractionation, neutral and phospholipids were separated using thin-layer chromatography (TLC) on heat-activated (110°C) Whatman silica gel-60 plates. Neutral lipids were separated using petroleum ether:diethyl ether:acetic acid (75:25:1.3 by vol) (Marcheselli *et al.* 1988). Phospholipids were separated using chloroform:methanol:acetic acid:water (50:37.5:3:2 by vol) (Jolly *et al.* 1997). Bands containing individual lipid classes were identified using commercially available standards (Avanti, Polarlipids Alabaster, AL; NuChek Prep., Elysian, MN, USA). Samples were then visualized using iodine (phospholipids) or 6-(p-Toluidino)-2-naphthalenesulfonic acid (TNS) (neutral lipids) (Jones *et al.* 1982). Bands were removed by scraping and put into 20 ml glass liquid scintillation vials to which 0.5 ml of H_2O was added to facilitate lipid desorption from the silica. Then 8 ml of ScintiVerse BD cocktail (Fisher Scientific,

Pittsburg, PA, USA) was added and the samples were mixed by vortexing and were counted 1 h after mixing to allow silica to settle using a Beckman LS 6500 liquid scintillation counter equipped with low level detection software (Fullerton, CA, USA).

Quantitative real-time PCR

RNA was extracted from astrocytes using the Qiagen RNeasy Kit and quantified on an Epoch spectrophotometer system (BioTek, Winooski, VT, USA). Optical density was used to verify RNA concentration at 260 nm and genomic DNA contamination by 260/280 nm ratio. Then 2 µg of poly(A)+ RNA was used for first strand synthesis using the iScript cDNA Synthesis Kit (Bio-Rad Hercules, CA, USA). cDNA was quantified using a Cepheid Smart Cycler detection system with FastStart SYBR green (Roche, Indianapolis, IN, USA) spiked with Taq DNA polymerase (New England BioLabs, Ipswich, MA, USA). Primers used for all *Acsl* isoforms, *Acot-7, Fabp, SDHA*, and *Snca* are shown in Table 1. Samples were pre-denatured (95°C for 120 s) then a polymerase-activation program (45 cycles of 95°C for 15 s, 60-53°C for 30 s, and 72°C for 30 s) was followed by post-annealing at 72°C for 120 s. Then a melting temperature (T_m) curve program (60-95°C ramp at 0.2°C/s) was used to identify amplification contaminants.

Table 1. Primer sequences used for astrocyte qRT-PCR

Isoform	Forward Primer	Reverse Primer
Acsl1	CTTAAATAGCATCGCAACCCG	TCGAAAATACCGGAACAATTCATG
Acsl3	TCTGAGGAGCAGCCAGG	GGAGGCTAAGACAGATGGATC
Acsl4	TTCCTCTTAAGGCCGGGA	GTTAGTAATCTTTGGAAGCCAGC
Acsl5	CAGAAAGCCTCACTCGGAAG	AAACGTCAGGAGGCAGATC
Acsl6_v1	CTTTCCGAGACAGGACGATG	GAGCCTTCATGTCATCTGAGAG
Acsl6_v2	CGTCCACTTTTCCTACTTGCC	GGAGAGCCTTCATGTCATCTG

Acsl6_v3	CACTTCAGCATGTGCACTTTC	CTCCTGGGTCTGCATCTTC
Acsl6_v4	GATGTGGTAACCTCTTTCCCTG	CTCCTGGGTCTGCATCTTC
Acot7	CCTCCCAGGCTCATTCA	ACATCTTGGCTGCGACG
Fabp3	ACCTGGAAGCTAGTGGACAG	TGATGGTAGTAGGCTTGGTCAT
Fabp5	CAAAACCGAGAGCACAGTGA	AAGGTGCAGACCGTCTCAGT
Fabp7	CCAGCTGGGAGAAGAGTTTG	TTTCTTTGCCATCCCACTTC
SDHA	CCTACCCGATCACATACTGTTG	AGTTGTCCTCTTCCATGTTCC
Snca	GCCCTTGCCTCTTTCATTG	GTCCTTTCATGAACACATCCATG

Table 1 continued. Primer sequences used for astrocyte qRT-PCR

A common threshold of fluorescence was set and using the absolute standard curve method, the number of cycles (Ct) was used to determine absolute number of copies of target gene cDNA. Endogenous control succinate dehydrogenase complex, subunit A, (flavoprotein) SDHA, was used to normalize target gene copy number found by qRT-PCR, resulting in a ratio of target gene to house-keeping gene.

Statistics

Statistical analysis was done using Instat® statistical program (Graphpad, San Diego, CA). Multiple comparisons were assessed using a one-way ANOVA and a Tukey-Kramer *post hoc* test, with $p < 0.05$ considered to be significant. Where appropriate (Fig. 6, 9, 10, 11, and 12) Student's two-tailed *t*-test was used to determine significance between treatment groups, with $p < 0.05$ considered to be significant. Each time point contains samples from five (n=5) individually treated separate cell cultures. For analysis of gene-expression, n=3.

RESULTS

dBcAMP treatment increases arachidonate but not palmitate uptake in astrocytes

dBcAMP treatment of astrocytes increased [1-^{14}C]20:4n-6 uptake 1.9-fold compared to non-treated astrocytes (control), while no change was observed in total [1-^{14}C]16:0 uptake (Fig. 1). Consistent with [1-^{14}C]20:4n-6 total uptake, the rate of [1-^{14}C]20:4n-6 uptake was appreciably faster in treated astrocytes (229 pmol x mg prot^{-1} x min^{-1}) as compared to non-treated astrocytes (143 pmol x mg prot^{-1} x min^{-1}) between 5-15 min (Fig. 1). Treatment increased the rate and extent of [1-^{14}C]20:4n-6 uptake, but not of [1-^{14}C]16:0 uptake, suggesting that dBcAMP treatment has an impact on specific fatty acid uptake in astrocytes.

dBcAMP treatment differentially modulates free fatty acid metabolism

Although dBcAMP treatment enhanced the rate and extent of [1-^{14}C]20:4n-6 uptake, we determined if it altered the distribution of fatty acid between the free fatty acid (FFA) pool and esterified pool. In dBcAMP treated astrocytes, total esterification of [1-^{14}C]20:4n-6 was increased 2.0-fold, but there was no change in the amount of tracer in the FFA pool (Fig. 2). However, at the initial time point (1 min), there was a slight, but significant increase in the mass of free tracer in the FFA pool, but this increase was rapidly shifted to the esterified pool by 5 min
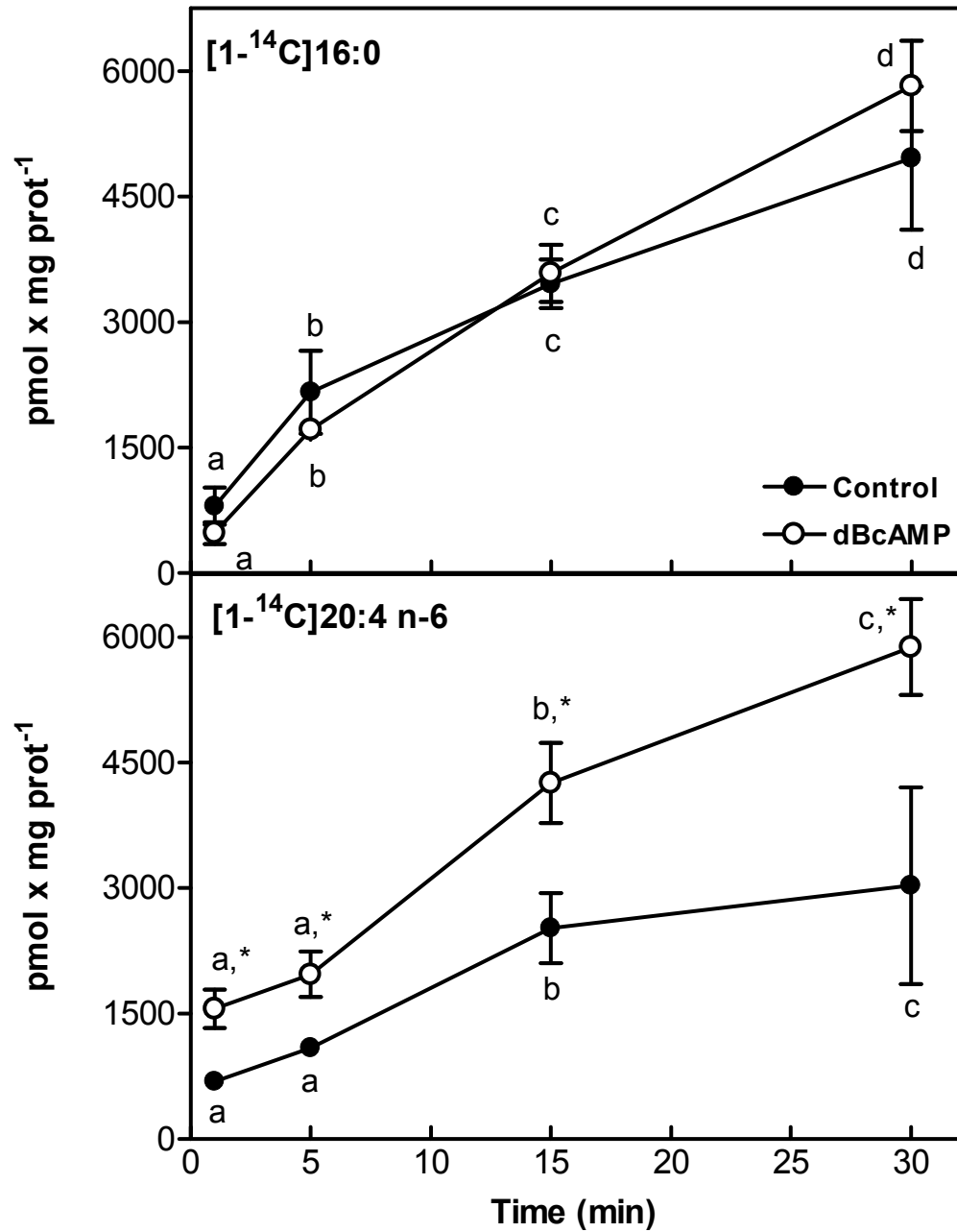
Figure 1. Effect of dBcAMP treatment on [1-14C]20:4n-6 or [1-14C]16:0 uptake in

astrocytes. Astrocytes were incubated with 2 μM radiolabeled [1-14C]20:4n-6 or

[1-14C]16:0 from 1 to 30 minutes. Untreated (Control, filled-circle) and dBcAMP treated

(dBcAMP, unfilled-circle) astrocytes were incubated with [1-14C]16:0 (upper panel) and

[1-14C]20:4n-6 (lower panel). Values represent means ± standard deviation (n=5). The

asterisk indicates a statistically significant difference from untreated (control) to treated (dBcAMP) astrocytes while lettering denotes statistically significant differences within groups using a one-way ANOVA and a Tukey-Kramer *post hoc* test ($p < 0.05$). Reproduced with permission.

Expressing these data as fractional distribution of tracer (Fig. 2), it becomes apparent that dBcAMP treatment enhanced the movement of tracer from the free [1-^{14}C]20:4n-6 pool to the esterified pool.

For [1-^{14}C]16:0, there was a 1.5-fold increase in total esterified tracer, accompanied by a profound 71% reduction in tracer entering the FFA pool in dBcAMP treated astrocytes (Fig. 3). This large reduction in tracer found in the FFA pool of dBcAMP treated astrocytes accounted for the lack of increased [1-^{14}C]16:0 uptake (Fig. 1). Fractional distribution of [1-^{14}C]16:0 was significantly different between groups (Fig. 3), which mirrors the changes in mass of fatty acid esterified, indicating that more tracer was being targeted for esterification. Although there was no net change for total [1-^{14}C]16:0 uptake, unlike [1-^{14}C]20:4n-6, dBcAMP treatment produce profound changes in the distribution of [1-^{14}C]16:0 into metabolic pools, enhancing its transfer from the FFA pool to the esterified pool.
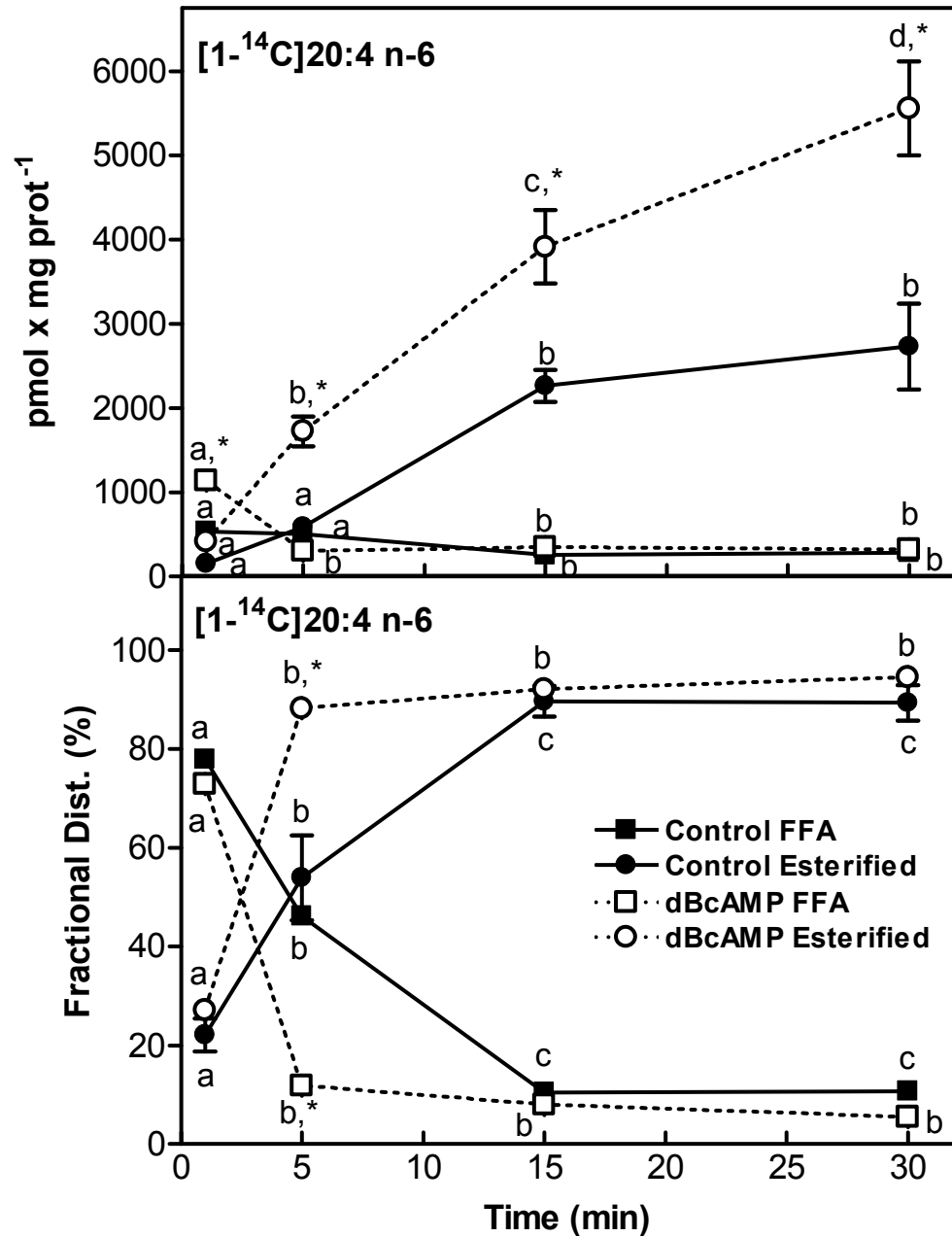
Figure 2. Mass of [1-14C]20:4n-6 esterified or unesterified in dBcAMP treated and untreated astrocytes expressed as total uptake (upper panel) and fractional distribution (lower panel). Untreated (Control FFA, filled-square and Control Esterified, filled-circle) and dBcAMP treated (dBcAMP FFA, unfilled-square and dBcAMP Esterified, unfilled-circle) astrocytes were incubated [1-^{14}C]20:4n-6 from 1 to 30 minutes. Values represent

22

means ± standard deviation (n=5). The asterisk indicates a statistically significant

difference from untreated (control) to treated (dBcAMP) astrocytes while lettering

denotes statistically significant differences within groups using a one-way ANOVA and a

Tukey-Kramer *post hoc* test ($p < 0.05$). Reproduced with permission.
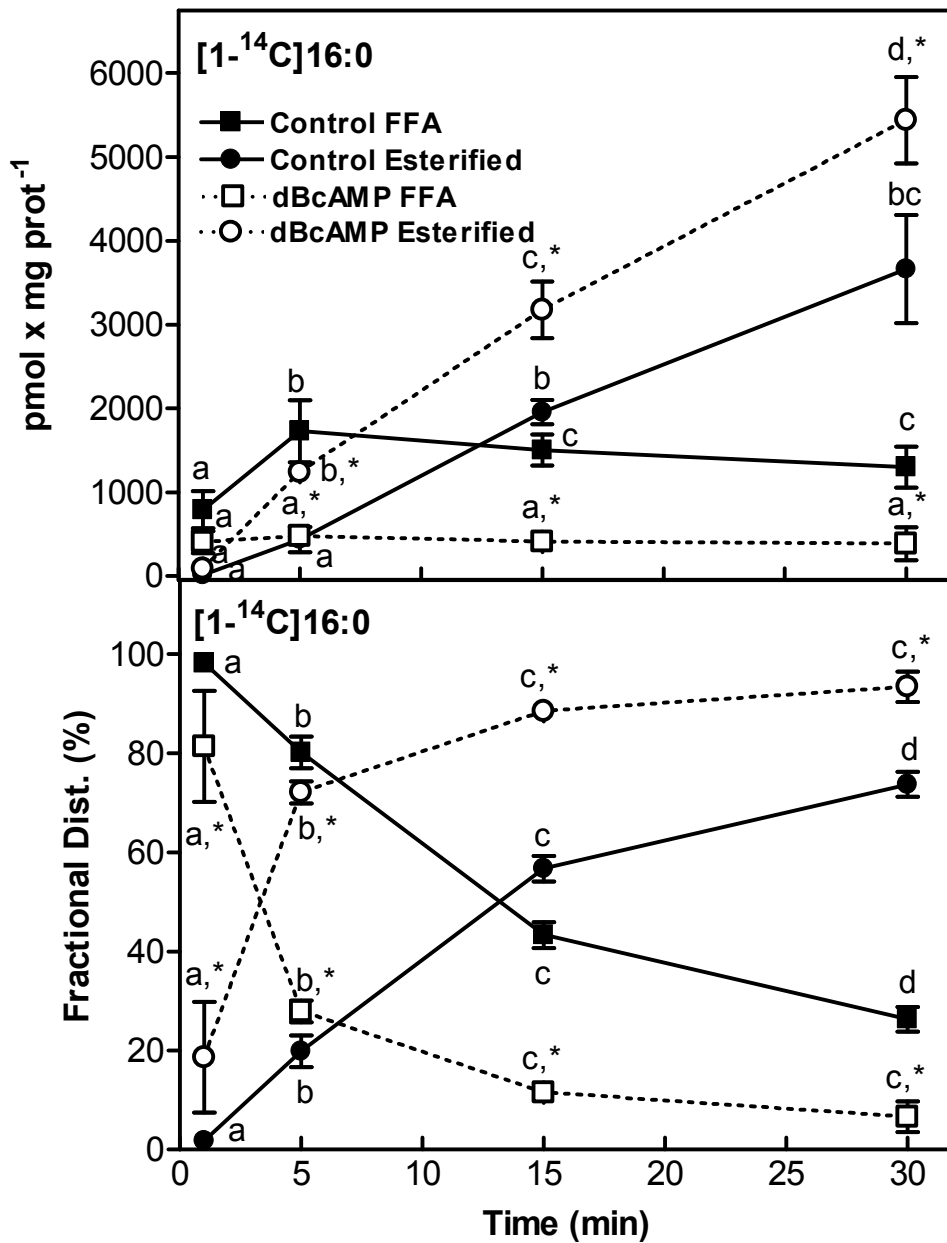
Figure 3. Mass of [1-14C]16:0 esterified or unesterified in dBcAMP treated and untreated

astrocytes expressed as total uptake (upper panel) and fractional distribution (lower

panel). Untreated (Control FFA, filled-square and Control Esterified, filled-circle) and

dBcAMP treated (dBcAMP FFA, unfilled-square and dBcAMP Esterified, unfilled-circle)

astrocytes were incubated with [1-14C]16:0 from 1 to 30 minutes. Values represent

means ± standard deviation (n=5). The asterisk indicates a statistically significant

difference from untreated (control) to treated (dBcAMP) astrocytes while lettering

denotes statistically significant differences within groups using a one-way ANOVA and a

Tukey-Kramer *post hoc* test ($p < 0.05$). Reproduced with permission.

dBcAMP treatment increases esterification and trafficking of [1-^{14}C]20:4n-6 and [1-^{14}C]16:0 into phospholipid pools

Because dBcAMP treatment increased the esterification of [1-^{14}C]20:4n-6 and

[1-^{14}C]16:0, we determined its effect on tracer movement into the phospholipid pools.

There was a significant 2.2-fold increase in the extent of [1-^{14}C]20:4n-6 esterified into

phospholipids at 30 min in dBcAMP treated astrocytes (Fig. 4). This is consistent with

the increased rate of esterification into phospholipids of dBcAMP treated cells from 5-15

min, (191 pmol x mg prot^{-1} x min^{-1}) as compared to non-treated astrocytes (158 pmol x

mg prot^{-1} x min^{-1}) (Fig. 4). The fractional distribution clearly demonstrated the enhanced

rate of targeting of [1-^{14}C]20:4n-6 to the phospholipid fraction, but both treated and non-

treated astrocytes reached saturation by 15 min (Fig. 5). These data indicate that

dBcAMP treatment increased initial rate of [1-^{14}C]20:4n-6 movement into phospholipid

pools.

Although total uptake for [1-^{14}C]16:0 was not increased by dBcAMP treatment

(Fig. 1), more [1-^{14}C]16:0 was esterified into phospholipids (Fig. 5), which is consistent

with the observed increase in its total esterification (Fig. 3). Interestingly, this occurred

at a nearly constant rate over the 30 min incubation and unlike [1-^{14}C]20:4n-6

esterification did not reach saturation.

25

Figure 4. Effect of dBcAMP treatment on tracer incorporation into phospholipids in

dBcAMP treated and untreated astrocytes. The extent of esterification of [1-^{14}C]16:0

(upper panel) and [1-^{14}C]20:4n-6 (lower panel) for untreated (Control, filled-downward

triangle) and treated (dBcAMP, unfilled-downward triangle) astrocytes from 1 to 30

minutes. Values represent means ± standard deviation (n=5). The asterisk indicates a

statistically significant difference from untreated (control) to treated (dBcAMP) astrocytes while lettering denotes statistically significant differences within groups using a one-way ANOVA and a Tukey-Kramer *post hoc* test ($p < 0.05$). Reproduced with permission.

Fractional distribution of [1-^{14}C]16:0 into phospholipids was immediately (1 min) increased and remained enhanced at all time points over non-treated cells (Fig. 5), indicating that dBcAMP treatment resulted in sustained increased targeting of [1-^{14}C]16:0 into the phospholipid pool. Although a similar event occurred for [1-^{14}C]20:4n-6 (Fig. 5), only about 65% of the [1-^{14}C]16:0 fatty acid mass was found associated with the phospholipid pools as opposed to nearly 85% of [1-^{14}C]20:4n-6 in treated astrocytes.

Individual phospholipid classes were similarly altered by dBcAMP treatment

Because dBcAMP treatment enhanced the extent of tracer entering the total phospholipid pool, we determined its impact on tracer uptake into individual phospholipid classes. At 30 min of incubation, dBcAMP treatment resulted in a marked increase in the mass of [1-^{14}C]20:4n-6 found in sphingomyelin (Cer<u>P</u>Cho), ChoGpl, phosphatidylinositol (PtdIns), with an even more profound effect on the mass targeted to EtnGpl (Fig. 6), which is consistent with the increase in total phospholipid incorporation (Fig. 4). Interestingly, dBcAMP treated astrocytes also had increased [1-^{14}C]20:4n-6, but not [1-^{14}C]16:0, incorporation into phosphatidylserine (PtdSer). Although there is a difference between the magnitude of [1-^{14}C]20:4n-6 and [1-^{14}C]16:0 esterification into individual phospholipid classes, there is a similar increase between the dBcAMP treated astrocytes as compared to the non-treated astrocytes.
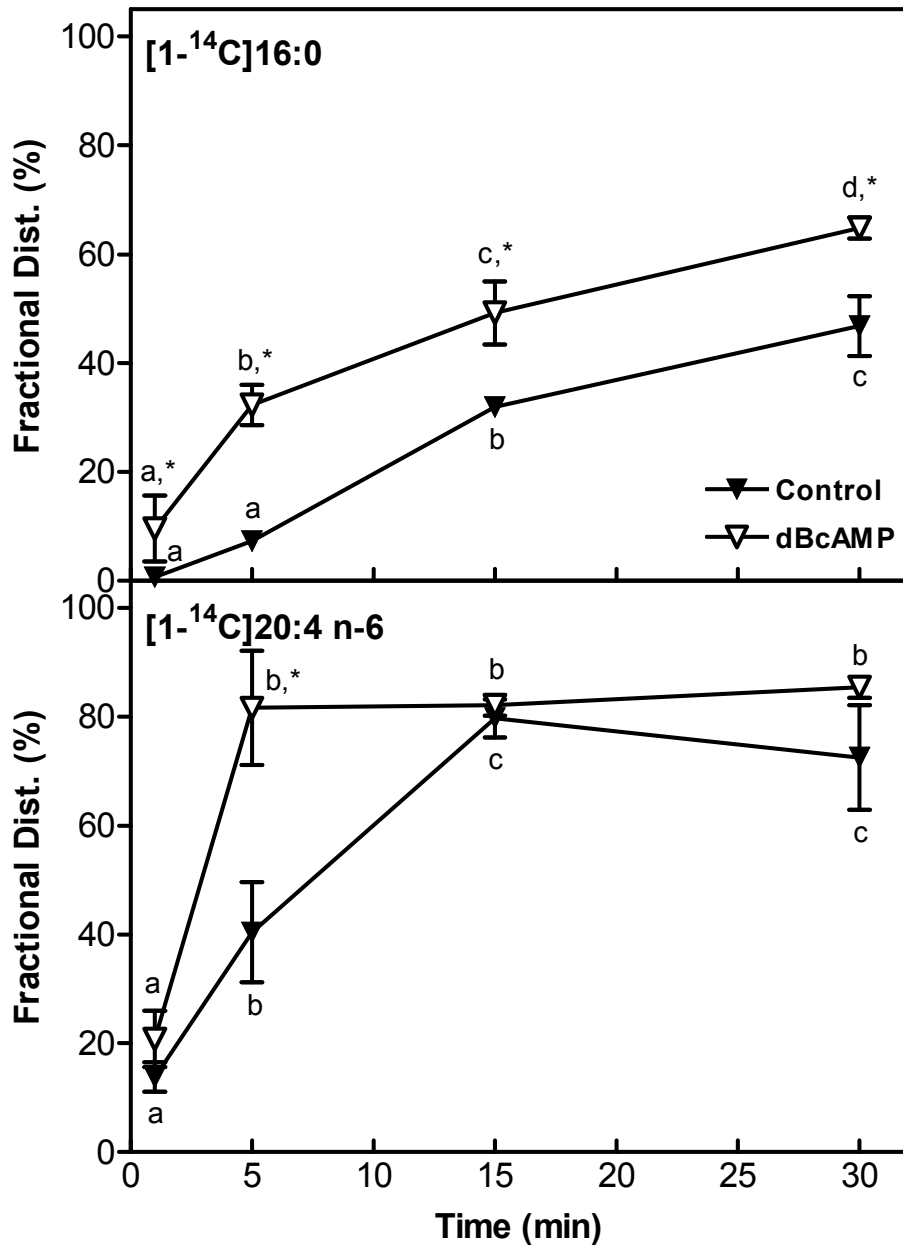
Figure 5. Fractional distribution of tracer into phospholipid fraction in dBcAMP treated and untreated astrocytes. The Fractional Distribution of [1-^{14}C]16:0 (upper panel) and [1-^{14}C]20:4n-6 (lower panel) for untreated (Control, filled-downward triangle) and treated (dBcAMP, unfilled-downward triangle) astrocytes from 1 to 30 minutes. Values represent means ± standard deviation (n=5). The asterisk indicates a statistically

significant difference from untreated (control) to treated (dBcAMP) astrocytes while

lettering denotes statistically significant differences within groups using a one-way

ANOVA and a Tukey-Kramer *post hoc* test ($p < 0.05$). Reproduced with permission.

This broad increase in targeting of tracer to individual phospholipid classes is

consistent with the increased targeting of both $[1\text{-}^{14}C]16{:}0$ and $[1\text{-}^{14}C]20{:}4n\text{-}6$ into the

phospholipid pool (Fig. 4), however, a more substantial increase in EtnGpl suggests that

dBcAMP treated astrocytes may be specifically targeting tracer to EtnGpl.

Figure 6. Tracer esterification into individual phospholipids in dBcAMP treated and untreated astrocytes. The extent of esterification of [1-^{14}C]16:0 (upper panel) and [1-^{14}C]20:4n-6 (lower panel) for untreated (Control, filled) and treated (dBcAMP, unfilled) astrocytes from 30 minutes. Values represent means ± standard deviation (n=5). The

asterisk indicates a statistically significant difference from untreated (control) astrocytes using Student's *t*-test ($p < 0.05$). Reproduced with permission.

dBcAMP treatment alters esterification and trafficking of [1-^{14}C]16:0 and [1-^{14}C]20:4n-6 to neutral lipids

Although the bulk of the tracer taken up in astrocytes is esterified into phospholipids, nearly 35% and 15% of esterified [1-^{14}C]16:0 or [1-^{14}C]20:4n-6, respectively, was incorporated into neutral lipids therefore, we determined the effect of dBcAMP treatment on fatty acid trafficking into esterified neutral lipid classes. In dBcAMP treated astrocytes, total incorporation of [1-^{14}C]20:4n-6 into neutral lipids was not increased at 30 min (Fig. 7) However, there was a small but significant increase in rate between 5-15 min in treated astrocytes which shifted back to control levels by 30 min (Fig. 7). Fractional distribution of [1-^{14}C]20:4n-6 into neutral lipids in treated astrocytes was significantly less then untreated at 5 and 30 min, suggesting that although minor, the amount of [1-^{14}C]20:4n-6 being targeted to neutral lipids in dBcAMP treated astrocytes was reduced (Fig. 8).

Although there was no net change in total uptake of [1-^{14}C]16:0 (Fig. 1), dBcAMP treatment resulted in a marked increase in its targeting to the neutral lipid fraction at early time points (5-15 min), similar to the enhanced targeting of [1-^{14}C]16:0 to phospholipids, but returned to levels found in untreated cells by 30 min (Fig. 7). Similar to total neutral lipid uptake, fractional distribution of tracer, indicates dBcAMP treatment increased [1-^{14}C]16:0 incorporation into neutral lipids at the initial time point (1 min) as a result of rapidly transferring tracer to esterified neutral lipid and phospholipid fractions (Fig. 8). Interestingly, incorporation and trafficking of [1-^{14}C]16:0 in dBcAMP treated astrocytes returns to control levels by 30 min indicating its incorporation into neutral

lipids is saturable. While dBcAMP treatment enhanced the magnitude of tracer

esterification and the magnitude of tracer initially entering the different fractions, its

impact on the fractional distribution of the tracer into the esterified neutral lipid pool at 30
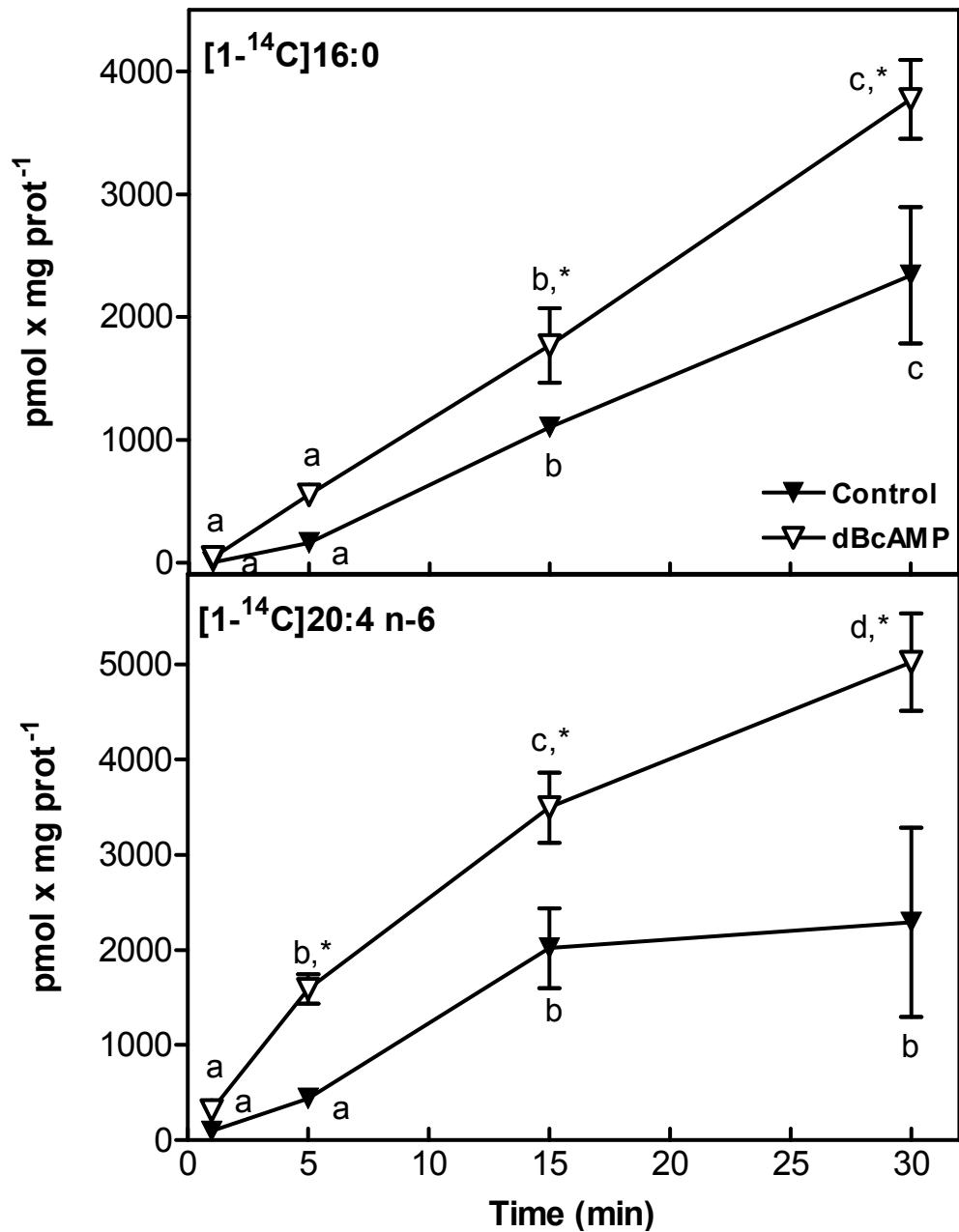
min was minor.
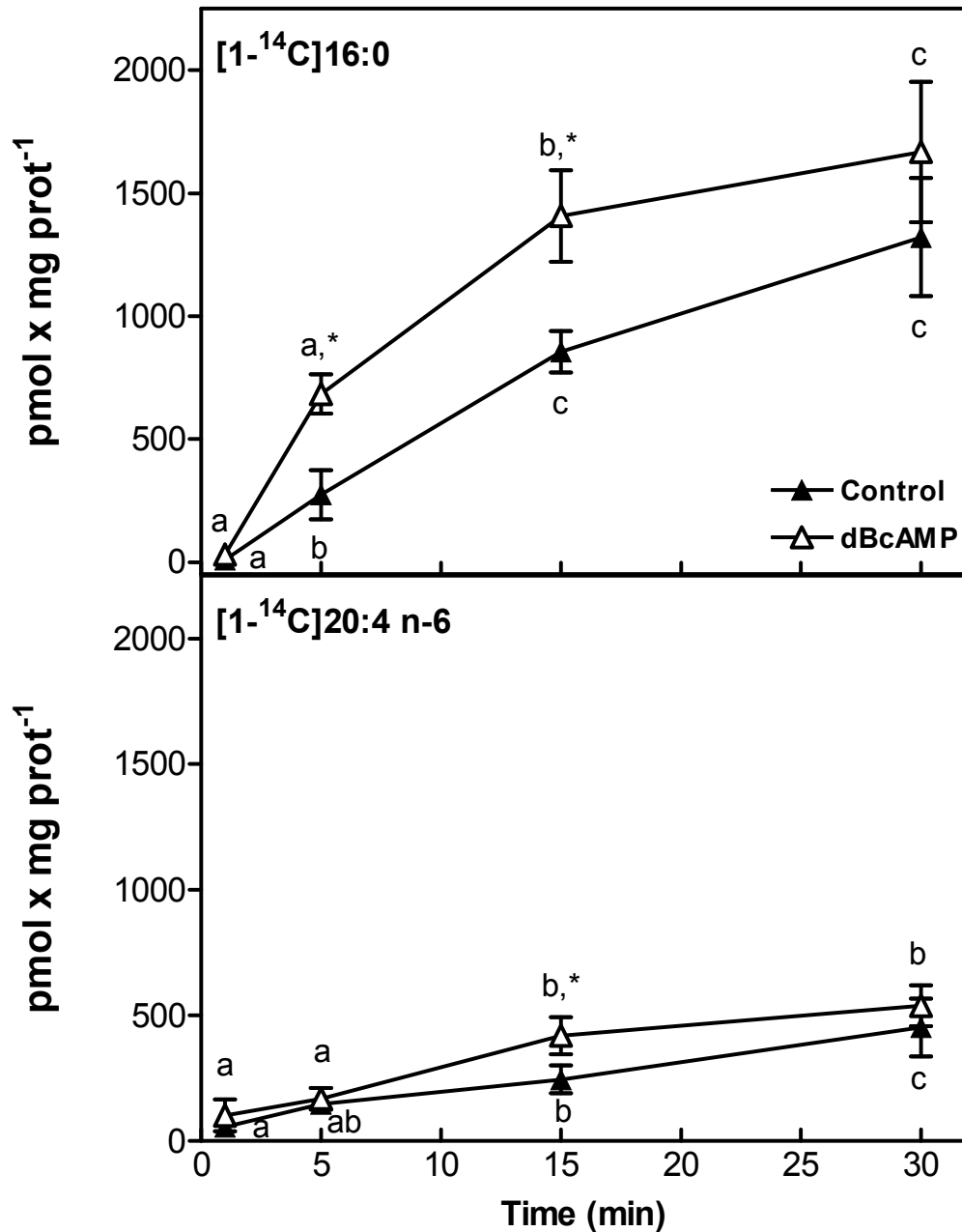
Figure 7. Effect of dBcAMP treatment on tracer incorporation into neutral lipids in dBcAMP treated and untreated astrocytes. The extent of esterification of [1-^{14}C]16:0 (upper panel) and [1-^{14}C]20:4n-6 (lower panel) for untreated (Control, filled-triangle) and treated (dBcAMP, unfilled-triangle) astrocytes from 1 to 30 minutes. Unesterified free fatty acids were not included in the neutral lipid mass. Values represent means ±

standard deviation (n=5). The asterisk indicates a statistically significant difference from untreated (control) to treated (dBcAMP) astrocytes while lettering denotes statistically significant differences within groups using a one-way ANOVA and a Tukey-Kramer *post hoc* test ($p < 0.05$). Reproduced with permission.
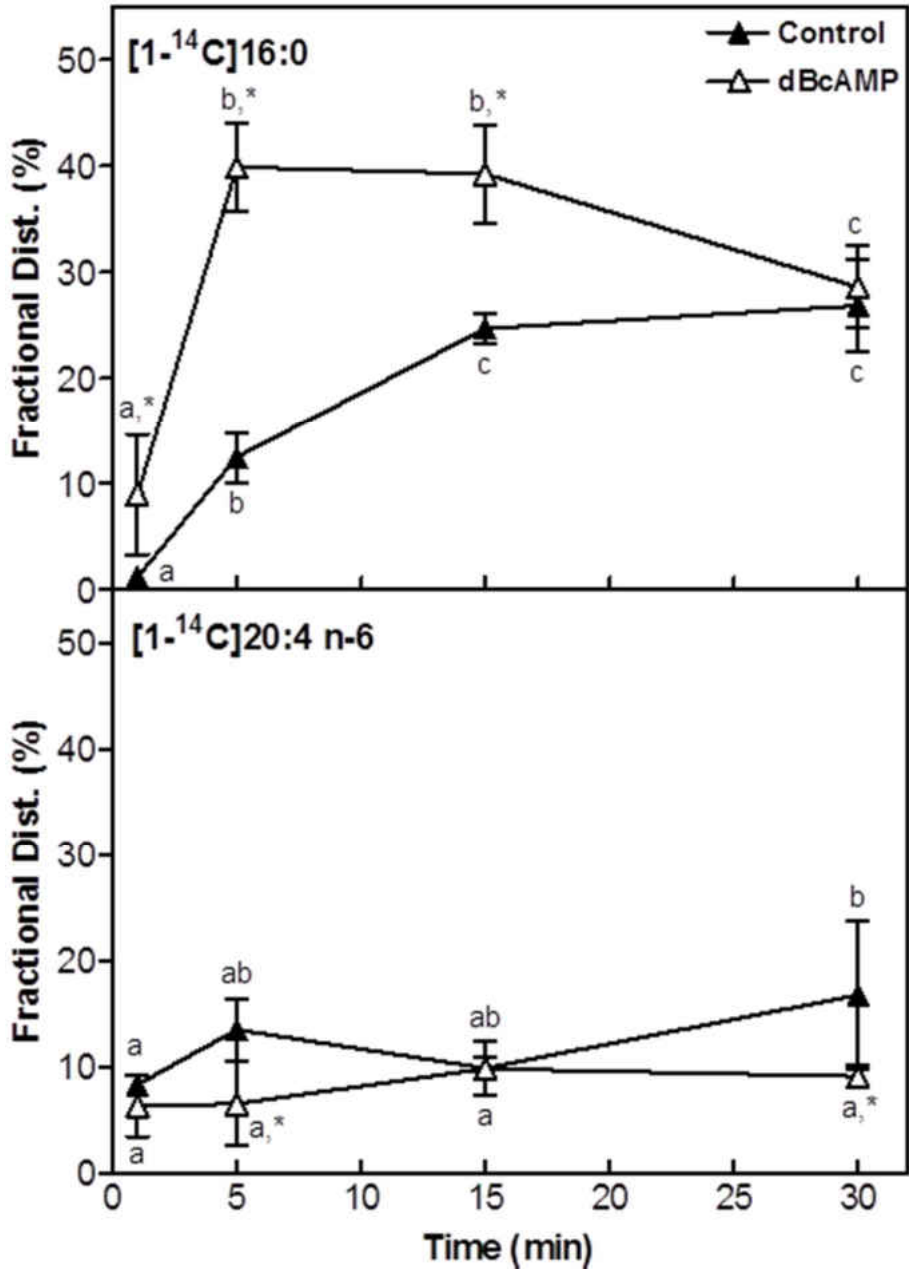
Figure 8. Fractional distribution of tracer into neutral lipid fraction in dBcAMP treated and untreated astrocytes. The Fractional Distribution of $[1\text{-}^{14}\text{C}]16{:}0$ (upper panel) and $[1\text{-}^{14}\text{C}]20{:}4\text{n-6}$ (lower panel) for untreated (Control, filled-triangle) and treated (dBcAMP, unfilled-triangle) astrocytes from 1 to 30 minutes. Values represent means ± standard deviation (n=5). The asterisk indicates a statistically significant difference from untreated

(control) to treated (dBcAMP) astrocytes while lettering denotes statistically significant

differences within groups using a one-way ANOVA and a Tukey-Kramer *post hoc* test (p

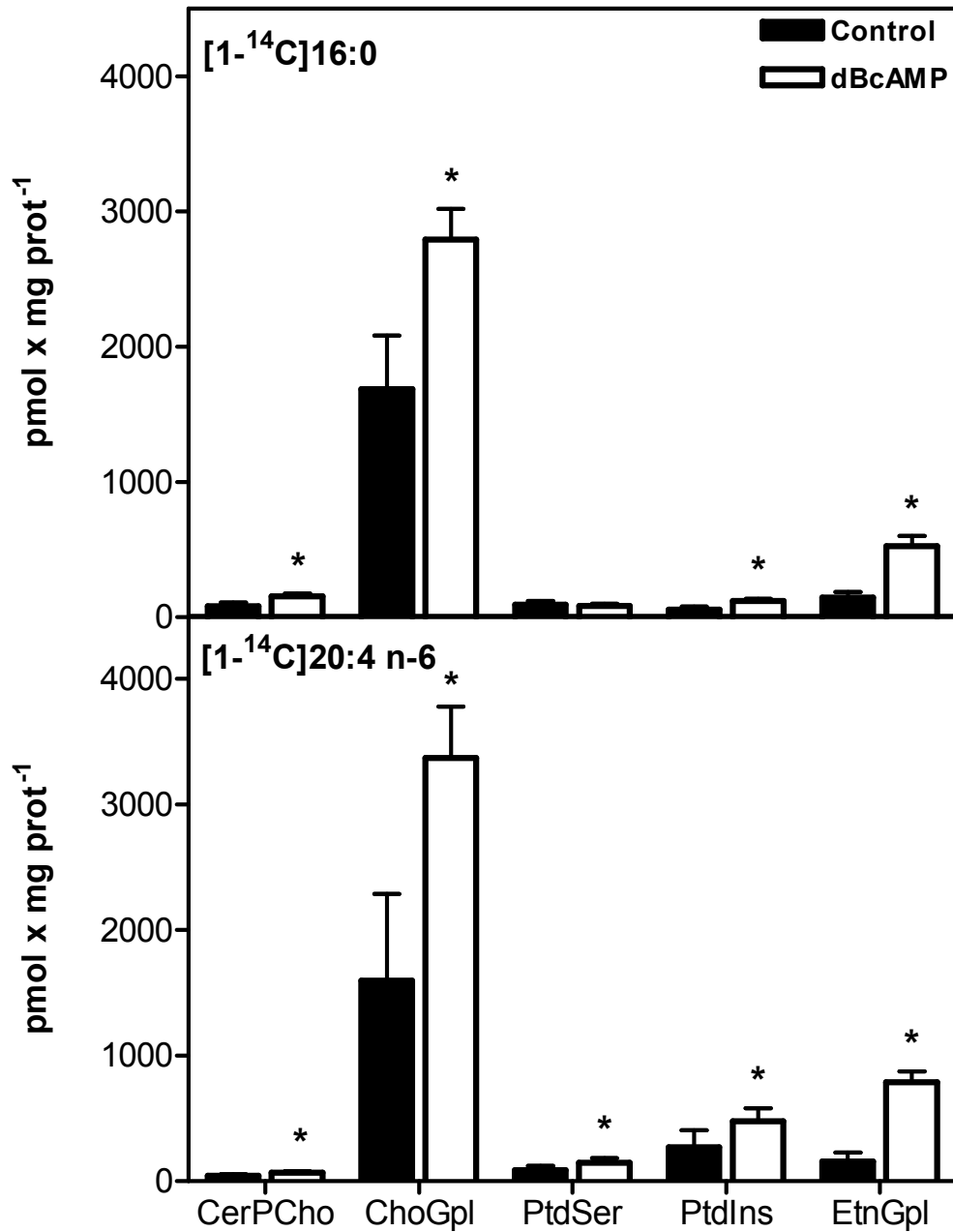< 0.05). Reproduced with permission.
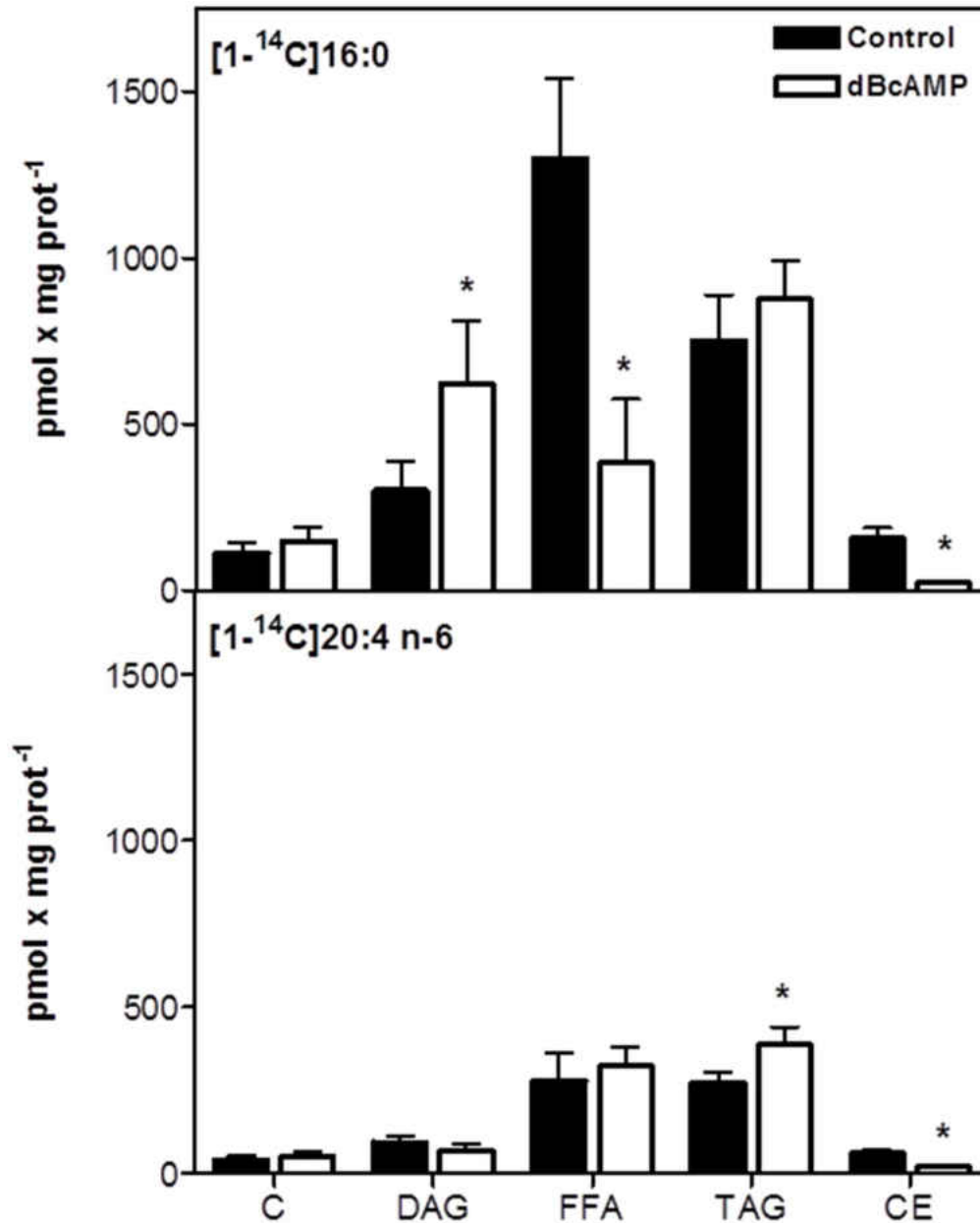
Figure 9. Tracer esterification into individual neutral lipids in dBcAMP treated and

untreated astrocytes. The extent of esterification of [1-^{14}C]16:0 (upper panel) and [1-

^{14}C]20:4n-6 (lower panel) for untreated (Control, filled) and treated (dBcAMP, unfilled) astrocytes from 30 minutes. Values represent means ± standard deviation (n=5). The asterisk indicates a statistically significant difference from untreated (control) astrocytes using Student's *t*-test ($p < 0.05$). Reproduced with permission.

Neutral lipid fractions were differentially altered by dBcAMP treatment

Although differences between groups in esterification of tracers into the neutral lipid pool was limited, we separated the neutral lipid fraction into individual neutral lipid classes to determine if dBcAMP treatment had an effect on targeting the tracers to individual neutral lipid classes. Unlike [1-^{14}C]20:4n-6, targeting of [1-^{14}C]16:0 for esterification into neutral lipids was significantly increased in diacylglycerol (DAG) (Fig. 9). Both tracers however, had a similar reduction of esterification into CE (Fig. 9) in dBcAMP treated astrocytes. Overall, treatment enhanced [1-^{14}C]16:0 targeting to neutral lipids to a greater extent than for [1-^{14}C]20:4n-6. Interestingly, the amount of [1-^{14}C]16:0 found in the FFA pool was greater than that of [1-^{14}C]20:4n-6 in non-treated cultures, suggesting a slower overall rate of [1-^{14}C]16:0 esterification as compared to [1-^{14}C]20:4n-6 in non-treated cultures. However, after dBcAMP treatment, esterification of [1-^{14}C]16:0 free fatty acids was decreased to a similar level as [1-^{14}C]20:4n-6 tracer (Fig. 9). Both tracers had a limited degree of carbon recycling as noted by the limited radioactivity in cholesterol (Fig. 9).

mRNA expression of key enzymes associated with Acyl-CoA metabolism is modulated by dBcAMP

Quantitative real-time PCR was used to evaluate the expression of *Acsl-1*, *-3*, *-4*, *-5*, and *-6* versions 1-4, which activate fatty acids for metabolism by addition of a CoA to

the carboxylic acid of the fatty acid.   We also evaluated gene expression of Acyl-CoA

thioesterase (*Acot7*), which hydrolyzes acyl-CoA esters to their non-esterified FFA and

CoASH. In addition, because Snca facilitates Acsl activity toward [1-^{14}C]20:4n-6

(Golovko *et al.* 2005) and its expression impacts astrocyte fatty acid uptake (Castagnet

et al. 2005), we determined *Snca* expression. In dBcAMP treated astrocytes there was

a significant 4.8-fold increase in gene-expression of *Acsl3* (Fig. 10B) and a significant

1.3-fold increase in *Acsl4* (Fig. 10A) gene expression. Both Acsl3 and Acsl4 prefer

20:4n-6 as a substrate (Van Horn *et al.* 2005; Kang *et al.* 1997). This increase in gene

expression is consistent with increased uptake and trafficking of [1-^{14}C]20:4n-6 in

dBcAMP treated astrocytes.   Acsl3 and -6 are the predominant isoforms found in mouse

brain, there were also minor, but significant changes in expression of *Acsl6_v1* and 6_*v3*

between groups (Fig. 11). *Acsl5,* which predominately prefers 16:0 as a substrate, was

reduced by 43% (Fig. 11), although 16:0 uptake was unchanged and esterification was

increased suggesting the substantial increase in *Acsl3* expression has more of an effect

on 16:0 regardless of substrate preference*. Acsl6_v1* was reduced by 25%, while

Acsl6_v3 was increased 1.2-fold in dBcAMP treated astrocytes. *Acot7* gene-expression

was reduced by 23% (Fig. 10A), consistent with decreased presence of tracer found in

FFA pools. Because FABP can affect fatty acid uptake and trafficking, we examined the

impact of dBcAMP treatment on astrocytes expression of *Fabp3, -5,* and *-7*. Expression

of *Fabp7,* the major FABP in astrocytes, was reduced 45%, while *Fabp5* expression was

reduced 24%, but it is expressed 60-fold less in astrocytes than *Fabp7* (Fig. 12). The

expression of *Fabp3* was unchanged, and it is expressed nearly 200-fold less than

Fabp7 in astrocytes. This suggests that changes in *Fabp* do not account for the

increased uptake of 20:4n-6 or the increased esterification of 20:4n-6 or 16:0 into

phospholipids. Interestingly, *Snca* gene expression was also reduced by 47% in

dBcAMP treated astrocytes (Fig. 13). Collectively, these results demonstrate that

dBcAMP increased expression of *Acsl3, Acsl4, and Acsl6v_3* while *Acsl5, Acsl6_v1, and*

Acot7 were reduced. These changes in *Acsl* expression is consistent with the changes

observed in fatty acid uptake and trafficking.
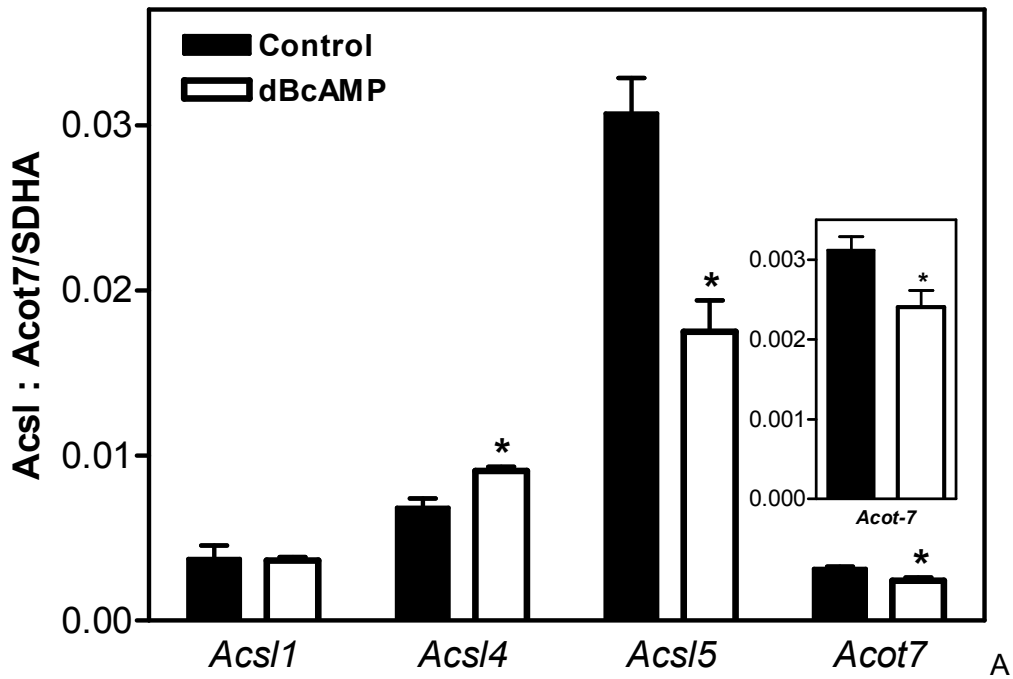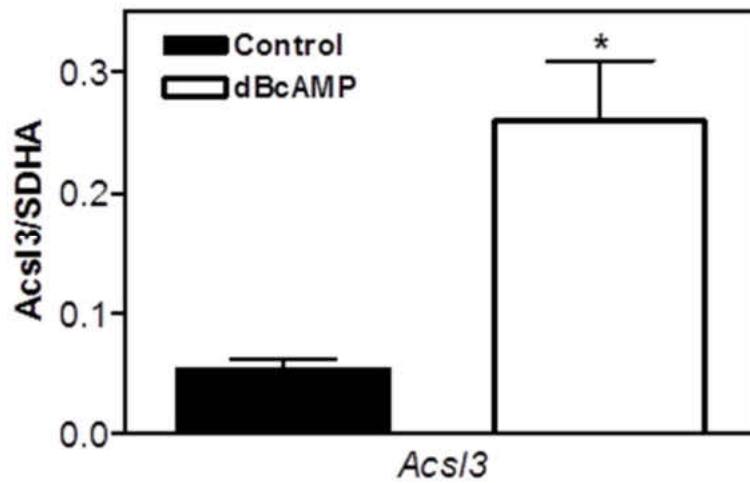
Figure 10. Effect of dBcAMP treatment on expression of Acsl1, -4, -5 and Acot7 (A) and Acsl3 (B) in astrocytes. RNA was extracted, cDNA was synthesized, and qRT-PCR used to determine mRNA expression levels. Values represent means ± standard deviation for untreated (Control, filled) and treated (dBcAMP, unfilled) astrocytes. The asterisk indicates a statistically significant difference from untreated (control) astrocytes using Student's t-test ($p < 0.05$). Reproduced with permission.
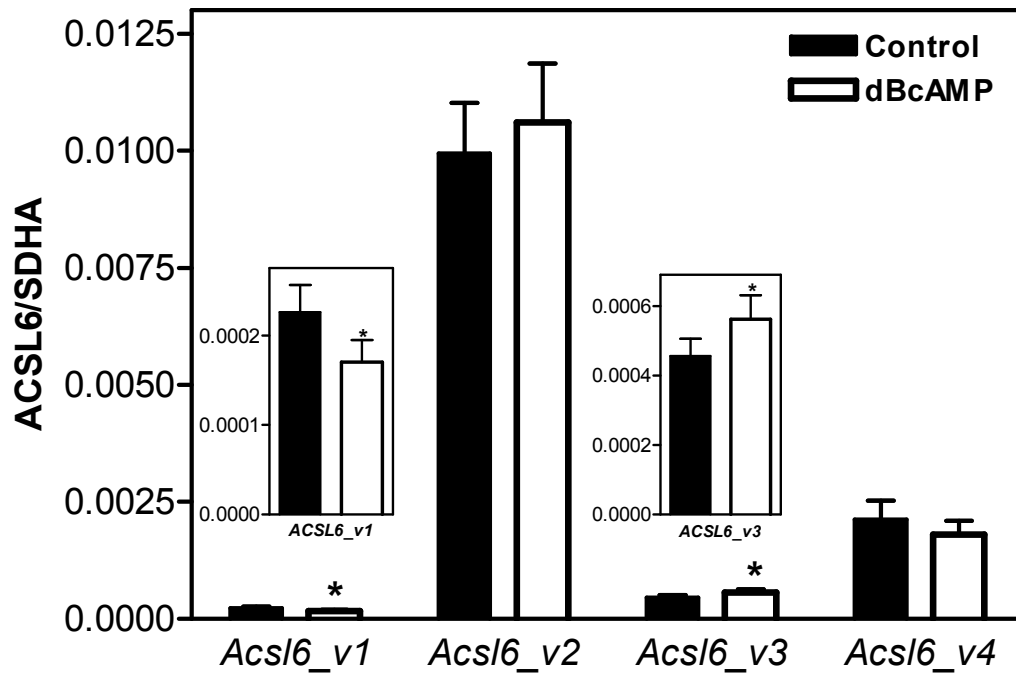
Figure 11. Effect of dBcAMP treatment on expression of Acsl6 versions 1-4 in astrocytes. RNA was extracted, cDNA was synthesized, and qRT-PCR used to determine mRNA expression levels. Values represent means ± standard deviation for untreated (Control, filled) and treated (dBcAMP, unfilled) astrocytes. The asterisk indicates a statistically significant difference from untreated (control) astrocytes using Student's *t*-test ($p < 0.05$). Reproduced with permission.
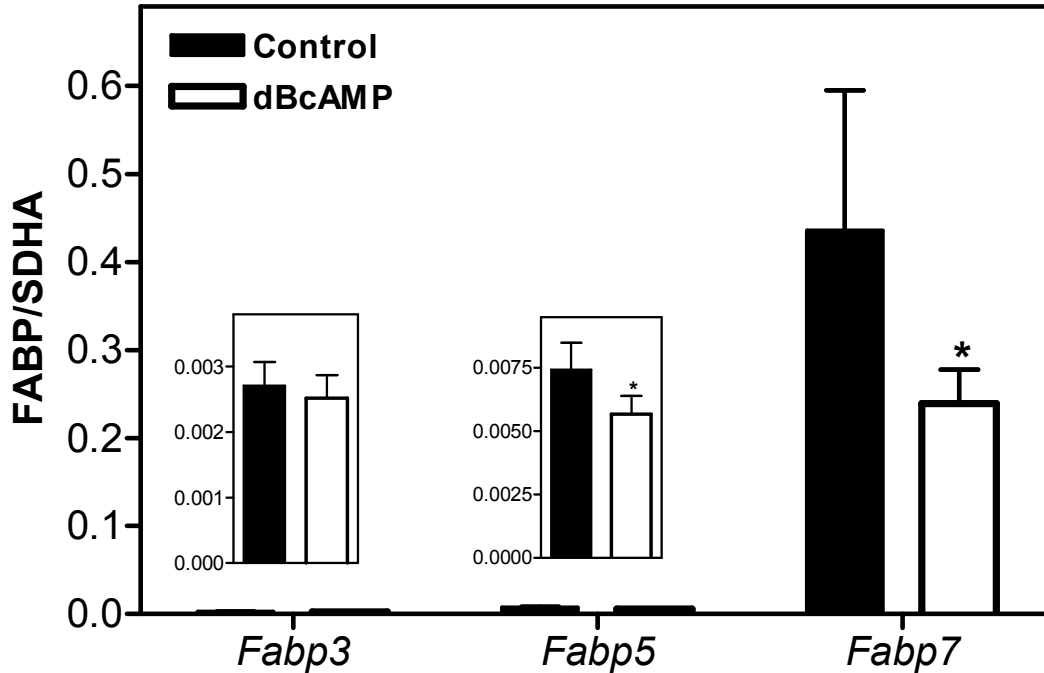
Figure 12. Effect of dBcAMP treatment on expression of Fabp3, -5, and -7 in astrocytes. RNA was extracted, cDNA was synthesized, and qRT-PCR used to determine mRNA expression levels. Values represent means ± standard deviation for untreated (Control, filled) and treated (dBcAMP, unfilled) astrocytes. The asterisk indicates a statistically significant difference from untreated (control) astrocytes using Student's t-test ($p < 0.05$). Reproduced with permission.
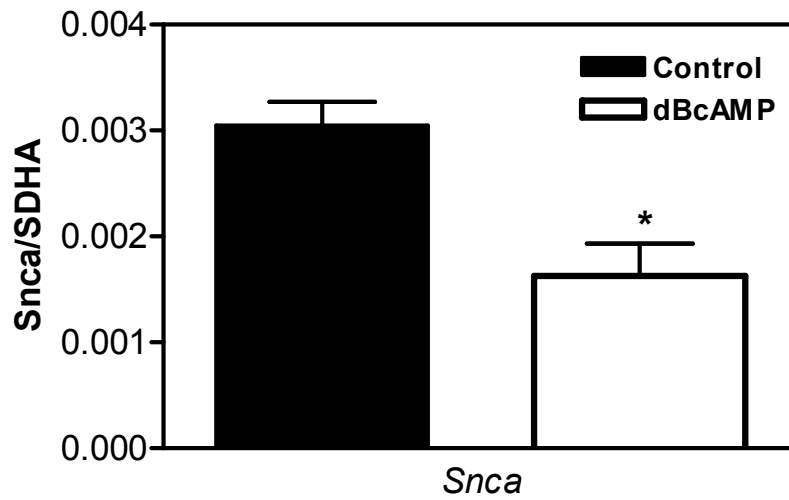
Figure 13. Effect of dBcAMP treatment on expression of *Snca* in astrocytes. RNA was extracted, cDNA was synthesized, and qRT-PCR used to determine mRNA expression levels. Values represent means ± standard deviation for untreated (Control, filled) and treated (dBcAMP, unfilled) astrocytes. The asterisk indicates a statistically significant difference from untreated (control) astrocytes using Student's *t*-test ($p < 0.05$). Reproduced with permission.

DISCUSSION

Astrocytes are highly versatile support cells in the CNS. Protoplasmic astrocytes send out end-feet that establish connections between neurons, endothelial cells comprising the blood-brain barrier, and glial cells. These interactions are vital in the homeostatic functions of the brain, particularly having an active role in neurotransmitter uptake and degradation, glucose uptake and storage, and fatty acid synthesis and export via apolipoproteins. Furthermore, they play a role in neuronal electric excitability and synaptic transmission via signal transduction by induced calcium release. After injury however, alterations in astrocytic morphology and functional state occur as a result of gliosis. This phenotypic shift to a reactive astrocyte is expected to have a distinct and active role during neurodegeneration and CNS remodeling. In our model, astrocytes treated with dBcAMP are found to shift from normal astrocytes into large, stellate, multiprocessed cells with an enlarged nuclear size consistent with reactive astrocytes.

Astrocytes control cerebral blood flow (Koehler *et al.* 2009) and are vital in 20:4n-6 metabolism. Radiolabeling studies in dBcAMP treated astrocytes show increased elongation and desaturation of, linoleic acid (18:2n-6) to 20:4n-6, demonstrating that astrocytes are fully capable of producing 20:4n-6 (Williard *et al.* 2002). In C6 glioma cells, dBcAMP treatment enhances 18:2n-6 uptake 1.8-fold and results in a corresponding increase in 18:2n-6 elongation and desaturation to 20:4n-6 (Robert *et al.* 1983). Furthermore, co-culturing endothelial cells (Bernoud *et al.* 1998) or neurons (Moore *et al.* 1991) with astrocytes result in a dramatic increase in 20:4n-6 formation

from 18:2n-6 in these cells. Interestingly, astrocytes cultured alone with 18:2n-6 will release less 20:4n-6 into the medium then when co-cultured with endothelial cells (Bernoud *et al.* 1998). This suggests that astrocytes actively sense their surrounding fatty acid levels and will release 20:4n-6 as needed. Herein, we demonstrate that a phenotypic shift towards reactive-like astrocytes elicited by dBcAMP treatment selectively increased the uptake of both 20:4n-6 and enhanced esterification of 20:4n-6 and 16:0 into phospholipids. In addition, incorporation of 20:4n-6 and 16:0 into EtnGpl was increased ~4-fold suggesting dBcAMP treatment has a selective effect on EtnGpl metabolism. Overall, dBcAMP administration results in a fatty acid specific increase in total uptake and a general increase in lipid metabolism.

A critical driving force for fatty acid uptake is the activation of fatty acids by Acsl to form the acyl-CoA that is then esterified into phospholipids. The rapid incorporation of fatty acids into phospholipids in dBcAMP treated astrocytes is consistent with dBcAMP treatment (1 day) increasing total phospholipid levels by 20% (Murphy *et al.* 1997). Although we did not measure phospholipid mass herein, our results indicate that dBcAMP treatment of astrocytes results in increased uptake into the cells (Fig. 1) and increased targeting of 20:4n-6 to the phospholipid fraction (Fig. 2,3,8). To delineate the contribution of long chain acyl-CoA synthetases in this observed increase in dBcAMP astrocytes, we determined mRNA expression of these key lipid enzymes. There are five long chain acyl-CoA synthetase isoforms in humans and rodents (de Jong *et al.* 2007; Watkins *et al.* 2007). These isoforms differ in their substrate preferences, regulation, enzyme kinetics, alternative splicing and location. Of these 5 isoforms, Acsl-3 and-6 are prominently found in the brain (Fujino *et al.* 1996; Cao *et al.* 2000; Kee *et al.* 2003; Van Horn *et al.* 2005; Mashek *et al.* 2006).   Acsl-6 is alternatively spliced into four variants

45

Acsl6_v1-4 in mouse (Kee *et al.* 2003; Lee *et al.* 2005a) and two variants Acsl6_v1 and

-2 in rats (Van Horn *et al.* 2005). Although fatty acid binding affinity has not been shown

in mouse, Van Horn *et. al.* demonstrated that rat Acsl6 splice variant 1 prefers linoleic

and alpha-linolenic acids, precursors for 20:4n-6 and docosahexaenoic acid (22:6n-3) ,

respectively, while Acsl6 variant 2 preferentially binds 22:6n-3. This difference in splice

variant affinity demonstrates an important link between Acsl levels and a role in

selectively enhancing fatty acid uptake and metabolism.

This supposition is supported by Acsl isoforms being capable of altering the

synthesis, oxidation of cellular lipids (Muoio *et al.* 2000; Igal and Coleman 1996; Igal *et

al.* 1997), and acyl-CoA trafficking to specific metabolic pools (Coleman *et al.* 2002).

Interestingly, Acsl4 has a high affinity for 20:4n-6 in both mouse and rat (Kang *et al.*

1997; Van Horn *et al.* 2005), which has been suggested to play a critical role in

phospholipid reacylation (Muoio *et al.* 2000; Igal *et al.* 1997). Our results show dBcAMP

treated astrocytes had increased 20:4n-6 esterification into phospholipids, specifically

ChoGpl, PtdSer, PtdIns, and EtnGpl (Fig. 5), accompanied by a 1.3-fold increase in

Acsl4 expression (Fig. 10A), suggesting that Acsl4 is the major driver in 20:4n-6 uptake.

Notably, a limited degree of tracer was found in neutral lipids, suggesting that the

increased 20:4n-6 taken up was mainly targeted specifically to phospholipid formation

(Fig. 7,8,9).

We also observed minor changes in *Acsl6* variant expression. In PC12 cells,

Acsl6 level increases total cellular phospholipids but only marginally increases 20:4n-6

uptake (Marszalek *et al.* 2005). We observed only relatively small, but significant

changes, in *Acsl6_v1* and *Acsl6_v3* expression (Fig. 11). Furthermore, Acsl6 have

varying affinities for polyunsaturated fatty acids (Van Horn *et al.* 2005) and when

knocked down in mouse brain reduces 20:4n-6-CoA formation (Kee *et al.* 2003),

suggesting they may play a role in trafficking of 20:4n-6 into specific lipid classes.

The treated astrocytes did not have increased uptake of 16:0 (Fig. 1), but did

exhibit increased mass of [1-^{14}C]16:0 targeted to phospholipids (Fig. 4) due to increased

FFA esterification after dBcAMP treatment (Fig. 9). Similar to *Acsl4*, *Acsl3* is also highly

expressed in brain (Van Horn *et al.* 2005) and is inhibited by Triacin C (Lewin *et al.*

2001), a competitive inhibitor of several Acsl. Triacin C inhibition of Acsl3 does not alter

fatty acid oxidation, but reduces triacylglycerol synthesis (Muoio *et al.* 2000). The

endoplasmic reticulum localization of Acsl3 (Poppelreuther *et al.* 2012) suggests it has a

role in lipid reacylation. Because *Acsl3* expression is significantly increased (Fig. 10B) in

dBcAMP treated astrocytes we believe it plays a role in enhanced esterification of both

16:0 and 20:4n-6 into phospholipid pools. Interestingly, Acsl3 increases uptake of both

18:1 (oleic acid) and 20:4n-6 in COS cells (Poppelreuther *et al.* 2012), which is

consistent with our observations. This coupled with varying kinetic properties based

upon fatty acid, including a lower V_{max} of Acsl3 and -4 for 16:0 (Van Horn *et al.* 2005),

may also account for the lack of increased 16:0 uptake into dBcAMP treated astrocytes.

While *Acsl5,* which prefers saturated fatty acids as a substrate (Van Horn *et al.* 2005),

was reduced 43%, we did not see a corresponding reduction in 16:0 uptake. This

suggests that any influence that this change in Ac*sl5* expression may have had on 16:0

uptake was masked by the significant increase in *Acsl3* expression.

FABP3 selectively facilitates brain 20:4n-6 uptake and trafficking (Murphy *et al.*

2005). Because 20:4n-6 uptake is increased in dBcAMP treated astrocytes, alterations

in expression of *Fabp3* could be a potential mechanism for the increase in dBcAMP-

treated astrocyte 20:4n-6 uptake. However, *Fabp3* expression was unchanged and was

expressed at negligible levels in dBcAMP treated astrocytes (Fig. 12) as compared to *Fabp7*. This suggests that the increased expression of *Acsl3* and *Acsl4* had a major role in the increased 20:4n-6 uptake and esterification. This supposition is consistent with the decreased expression of *Fabp7* and *Fabp5* observed in the dBcAMP treated astrocytes, as a reduction in the expression of these FABP is not consistent with an increase in 20:4n-6 uptake. Although FABP7 may significantly impact 22:6n-3 uptake and trafficking, it poorly binds to 16:0 (Balendiran *et al.* 2000), further supporting our hypothesis that increased *Acsl* activity differentially impact fatty acid uptake in dBcAMP treated astrocytes.

In astrocytes, *Snca* ablation reduces 16:0 and 20:4n-6 uptake and reduced targeting to phospholipids pools which enhance trafficking to neutral lipid pools (Castagnet *et al.* 2005). Herein, we report a significant decrease in *Snca* expression after dBcAMP treatment but with an increase in 20:4n-6 uptake suggesting that enhanced *Acsl* expression may have a more robust effect on fatty acid metabolism than Snca. This is important because Snca has a major role in brain 20:4n-6 metabolism (Golovko *et al.* 2006a). Therefore, further study on the effect of dBcAMP treatment on the mRNA expression and protein levels of Snca are required to determine its association with changes in uptake and incorporation.

In summary, dBcAMP treatment of astrocytes impacted both 16:0 and 20:4n-6 astrocytic metabolism. However, this treatment increased cellular fatty acid uptake of only 20:4n-6, suggesting that during dBcAMP treatment, astrocytes had an increased need for 20:4n-6, which is supported by the increased initial rate of incorporation into phospholipids. Because 16:0 and 20:4n-6 were highly esterified with dBcAMP treatment, we hypothesize there is a metabolic FA-CoA pool targeted specifically for

phospholipids by dBcAMP treatment via increased acyl-CoA synthetase expression, especially *Acsl3* and *-4*, and resulted in an overall increase in phospholipid incorporation. These results are important because they are the first to demonstrate the preferential increase in 20:4n-6 uptake and increased esterification of both 20:4n-6 and 16:0 coincide with increased expression of acyl-CoA synthetases in a model of reactive astrocytes.

CHAPTER III

INTRODUCTION

Microglia, Snca, and Inflammation

 Microglia are known as the resident immune cell of the central nervous system that play a vital role in immune response and maintenance in the brain (Kabba *et al.* 2017; Kim and de Vellis 2005). Microglia reactivity and activation are suggested as an early defense mechanism for the CNS following pathological events (Subramaniam and Federoff 2017; Kreutzberg 1996; von Bernhardi *et al.* 2015). During activation microglia show a phenotypic shift, proliferation, chemotaxis towards areas of damage or infection, and release potent mediators such as PGE_2 or TNFα (Park *et al.* 2008; Fischer and Reichmann 2001; Babcock *et al.* 2013; Fan *et al.* 2017; Levi *et al.* 1998). Microglia are vital in phagocytosis of apoptotic cells and removal of debris as well as bacteria from the brain (Kaur *et al.* 2004; Hughes *et al.* 2010; Ulvestad *et al.* 1994; Fincher *et al.* 1996). Interestingly, depending on phenotype microglia have cytotoxic or neuroprotective effects (Franco and Fernández-Suárez 2015).

 Microglia express vital components of the endocannabinoid (eCB) system including receptors, ligands, and metabolic enzymes (Mecha *et al.* 2016). The endocannabinoid receptor 1 (CB1r) was first cloned in 1990 (Matsuda *et al.* 1990) and is found throughout the nervous system (Herkenham *et al.* 1990), immune system, adipose, liver, muscle, kidney, reproductive system, and lungs (Pagotto *et al.* 2006a; Pagotto *et al.* 2006b). This system plays a vital role in analgesia, synaptic plasticity (learning and memory), appetite, immune function and several other physiological

events (Hohmann *et al.* 1995; Di Marzo and Deutsch 1998; Cravatt *et al.* 2001; Brenowitz and Regehr 2005; Kishimoto 2006; Pagotto *et al.* 2006a). The CB1r belong to the GPCR family (Mukhopadhyay and Howlett 2001; Herkenham *et al.* 1990) and are the most highly expressed GPCR in the brain (Devane *et al.* 1988; Herkenham *et al.* 1990). CB2r, which shares 44% homology, was first cloned several years later in 1993 (Munro *et al.* 1993) and is more prevalent in immune cells (Galiègue *et al.* 1995). CB1 and -2 receptors are highly expressed in both murine and human macrophages (Carlisle *et al.* 2002; Chiurchiù *et al.* 2015). The CB2r is regulated during pathological insult and CB2r stimulation inhibits microglia reactivity and promotes a neuroprotective phenotype. eCB are bioactive lipids which play a role in lipid signal transduction events and increased levels coincide with or shortly follow immune function and eCB metabolism enzymes are modulated in response to inflammatory stimuli.

There are two prominent arachidonic acid containing eCB N-arachidonyl ethanolamine (anandamide) and 2-arachidonyl glycerol (2-AG). In this section we will be focusing on 2-AG as that is the most prevalent endogenous CNS agonist of CB2r (Di Marzo *et al.* 1998; Bisogno *et al.* 1999). In general, 2-AG is synthesized from membrane phospholipids and released on demand in response to stimuli (Di Marzo and Deutsch 1998). Some data suggests that at least part of the eCB pool may be stored before release (Alger and Kim 2011), suggesting that eCB may be accumulated and trafficked before release. However, the notion of preformed 2-AG pools is still debated (Hashimotodani *et al.* 2013).

2-AG biosynthesis follows one of two pathways. One pathway is the result of either α- or β-diacylglycerol lipase, a calcium-sensitive *sn*-1 selective lipase that cleaves the *sn*-1 position of *sn*-2-arachidonate containing diacylglycerol. The *sn*-2-arachidonate containing diacylglycerol is derived primarily from hydrolysis of membrane phospholipids

by phospholipase C, (PLC) (Bisogno *et al.* 2003). The other less prevalent pathway is the hydrolysis of arachidonic acid containing lysophosphatidic acid by a phosphatase (Nakane *et al.* 2002; Higgs and Glomset 1994). This is important because Snca increases PLC activation which drives the generation of DAG (Narayanan *et al.* 2005). To inactivate 2-AG, two steps are required. First 2-AG must be taken up into a cell followed by hydrolysis. It can be hydrolyzed by fatty acid amide hydrolase or in most cases (85%), monoacylglycerol lipase or cleaved by α/β serine hydrolase domain-containing proteins 6 & 12 (Blankman *et al.* 2007). 2-AG may also be metabolized into highly bioactive signaling molecules as it is a substrate for COX (Straiker *et al.* 2011; Richie-Jannetta *et al.* 2010), LOX (Kozak *et al.* 2002; Kozak and Marnett 2002), and cytochrome P450 and phosphorylation to produce lysophosphatidic acid (Bektas *et al.* 2005). Without a doubt eCB play a major role in the homeostasis of the nervous system and pharmacologically increasing levels of eCB shows some resistance to neurodegenerative disease.

The presence of reactive microglia are a hallmark of Parkinson's disease (Subramaniam and Federoff 2017; Kim and de Vellis 2005). With increased Parkinson's progression there is a consistent increase in CD68 stained microglia (Croisier *et al.* 2005). This reactivity is widespread and not limited to the substantia nigra where the death of dopaminergic neurons is the result of Parkinsonian pathology. In MPTP-induced Parkinson's disease there is a substantial shift of microglia to a reactive phenotype and this activation is maintained for several years (Barcia *et al.* 2004; McGeer *et al.* 2003). This suggests that microglial activation and maintenance of its reactive phenotype is important in disease progression.

Lipopolysaccharide (LPS) and interlukin-1β increase α and β-*Snca* mRNA expression and protein levels in human astrocytes and macrophages suggesting a role

in inflammation (Tanji *et al.* 2001; Tanji *et al.* 2002). Interestingly, stimulation by purified Snca protein is able to induce a phenotypic shift to a reactive state and induces increased cytokine secretion in microglia (Zhang *et al.* 2005; Klegeris *et al.* 2008). Similarly, microglia and macrophages become activated by stimulation of either monomeric or fibrillary aggregates of Snca (Zhang *et al.* 2005; Wilms *et al.* 2009; Lee *et al.* 2009). Our lab has previously hypothesized that either extra or intra cellular Snca modulates microglia activity (Austin *et al.* 2011; Rojanathammanee *et al.* 2011; Floden *et al.* 2005). To further support the idea that Snca plays an important role in proinflammatory lipid-dependent signaling events we determined if *Snca* expression has an impact on 2-AG levels following LPS treatment.

Lipid mediated signaling pathways are important in microglia activation and *Snca* expression modulates microglia activation state. PLD_2 is required for activation of macrophages in response to LPS and TNFα. We and others have determined Snca tonically inhibits PLD and therefore Snca plays a role in PLD mediated microglia activation (Austin *et al.* 2011; Jenco *et al.* 1998; Ahn *et al.* 2008; Payton *et al.* 2004; Outeiro and Lindquist 2003). Increased expression of *Snca* has been found following stimulation (Milner and Campbell 2003) and microglia of *Snca* gene-ablated mice are phenotypically different from wildtype (Austin *et al.* 2006) suggesting Snca plays a pivotal role in activation. Microglia from gene-ablated mice demonstrate a hyper-reactive, ramified, vacuolar morphology with an increased cytokine secretory phenotype compared to wild type and exacerbated reactive phenotype following LPS treatment, but with a significantly decreased phagocytic ability (Austin *et al.* 2006). Microglia activation markers CD68, β1 integrin and α tubulin are increased in *Snca* deficient microglia and are further exacerbated with LPS treatment (Austin *et al.* 2006). *Snca* deficient microglia release increased levels of proinflammatory cytokines TNFα and IL-6 (Austin *et al.* 2006;

Austin *et al.* 2011). In BV-2 cells over-expressing wild type and mutant forms of Snca, there is no change in PLD1/2, PLA_2, or COX-1 protein levels, but COX-2 protein levels are significantly increased (Rojanathammanee *et al.* 2011). This suggests that Snca selectively regulates protein expression and that the effect of Snca on PLD activity is not a result of decreased protein levels. BV-2 cells expressing *Snca* and its mutants showed a similar reduction as primary *Snca* gene-ablated microglia in phagocytic ability and interestingly BV-2 cells over expressing *Snca* are not neurotoxic to neurons (Rojanathammanee *et al.* 2011). These data suggest a fundamental role for intercellular Snca in regulation of microglia phenotypic shift and Snca's important role in the inflammatory response.

Herein, we determine if Snca plays a role in 2-AG release from whole brain and microglia following LPS stimulation. We utilized a *Snca* gene-ablated and *Snca* knock-in mouse model and primary postnatal microglia from these wild type and *Snca* gene-ablated mice. *Snca* deficient mice have elevated basal levels of 2-AG that was exacerbated by LPS stimulation. *Snca* knock-in mice had variable 2-AG levels that were within the wildtype and *Snca* deficient mice levels. However, *Snca* expression was not changed during the 3 hour LPS stimulation in wildtype mice. Inversely in wild type primary microglia there was a significant reduction of 2-AG following LPS stimulation after 12 hours of stimulation. This reduction remains prevalent at 18 hours and was accompanied by a reduction in *Snca* expression. When expressed as % control enhanced eicosanoid production follows this same timeline. Interestingly, *Snca* deficient microglia show a delayed reduction of 2-AG, requiring 24 hours of LPS treatment to be significantly reduced. However, their basal eicosanoid production is exacerbated as compared to wildtype. This data suggests that Snca plays an important role in early 2-

54

AG lipid mediated signaling which may have downstream effects on microglia phenotype

and phagocytic ability.

MATERIALS AND METHODS

Mice

  This study was conducted in accordance with the National Institutes of Health Guidelines for the Care and Use of Laboratory Animals and under an animal protocol approved by the University of North Dakota IACUC (Protocol 0708-1c). The wild type mice used for the protocol were the 129/SvEv strain, *Snca* gene-ablated mice generated by gene-targeted deletion of *Snca,* or *Snca* knock-in mutant (A30P and A53T) or human (hSnca) on the 129/SvEv background (Cabin *et al.* 2002). Male mice were age matched ~10 months old and were given standard laboratory chow and water *ad libitum*.

LPS treatment and tissue collection

  Previously published data showed no difference in blood brain barrier permeability between single does and divided doses of LPS (Jangula and Murphy 2013), we used a single dose of lipopolysaccharide (LPS) derived from *E. coli* 055:B5 J (Sigma cat# L2880) dissolved in phosphate buffered saline (0.25 mg/mL). Mice were injected with LPS (1 mg/kg) intraperitoneally (i.p.). Whole brain was removed, flash frozen in liquid nitrogen, and then pulverized into a homogeneous powder under liquid nitrogen conditions.

Cells

  Mouse glia were isolated from brains of 1 day old 129/SvEv mice under an approved protocol by the University of North Dakota (Grand Forks, ND) Animal Care and Use Committee (UND protocol #1106-1C). To obtain astrocytes, cortices were triturated

in Dulbecco's modified Eagle's medium (DMEM) to separate cells, filtered through 80 μm Nylon mesh, and resuspended in DMEM containing 10% fetal bovine serum (FBS).   Astrocytes were cultured in DMEM containing 10% FBS, 3.7 g/L bicarbonate, 2 mM glutamine, 100 μg/mL penicillin/streptomycin, and 5 mM HEPES at pH 7.4 in a water jacketed incubator at 37°C in 5% CO_2 atmosphere.   Astrocytes were expanded by subculturing on T-75 flasks (4:1) by loosening the adherent cells with 0.25% trypsin. The third passage (3:1) was plated on 100 mm polystyrene cell culture plates prior to treatment with dBcAMP.

To obtain microglia, cortices were collected into dissection buffer containing 1 mM EDTA, 1 mM EGTA, 1 mg/mL glucose in phosphate buffered saline and mechanically separated with forceps. Two volumes of 0.25% trypsin was added and the tissue was incubated for 15 mins. Following incubation trypsin was inhibited with the addition of microglia media containing DMEM:Hams F12 (1:1) medium 10% FBS, 5% Horse serum, 3.7 g/L bicarbonate, 2 mM glutamine, 100 μg/mL penicillin/streptomycin, and 5 mM HEPES at pH 7.4. Cells were triturated to break up tissue and filtered through 80 μm Nylon mesh and resuspend in microglia medium in T-75 flasks. Medium was changed after 48 hours and then again after one week. Microglia were collected between days 10 -14 by shaking flasks for 45 mins at 200 rpm on an orbital shaker and plated on 6-well polystyrene cell culture plates in half conditioned media and half new media at ~250,000 cells per well. Microglia are allowed to reattach and equilibrate for 24 h before LPS treatment (50 ng/mL) in microglia medium.

Mass Spectrometry Lipid Extraction

To homogenized brain tissue samples, analytes were extracted from the tissues using a two-phase extraction method. Homogenized tissue was added directly to a

Tenbroeck homogenizer containing 100 ng of 2-arachidonyl glycerol-d_5 and 100 pg prostaglandin E2-d_4 standards in 1 mL of saline. To the Tenbroeck homogenizer 1 mL of acetone was added followed by homogenization of tissue. Once tissue was homogenized, the extract was removed using a silanized Pasture pipette, saved in a silanized screw top test tube and then the homogenizer was washed with 1 mL of acetone and the wash added to the initial extract. Then protein residue was pelleted by centrifugation at 3,250 x g for 15 min at 4 °C and the supernatant was moved to a new silanized tube.

For microglia medium, analytes were extracted from the medium using a two-phase extraction method. Microglia medium (1 mL) was added directly to a silanized test tube containing 1 ng of 2-arachidonyl glycerol-d_5 and 100 pg prostaglandin E2-d_4 standards in 2 mL acetone. After protein removal (brain samples only) 2 mL of hexane was added to the extract, vortexed, and centrifuged at centrifugation at 3,250 xg for 15 min at 4 °C. The upper phase containing 2-arachidonyl glycerol (2-AG) was transferred to a new silanized tube for later quantification. The extract was washed two more times with 2 mL of hexane and the upper phase saved. To the lower phase containing eicosanoids, 30 µL of 2 M formic acid and 2 mL chloroform containing 0.005% BHT was added, vortexed and centrifuged. The bottom chloroform phase containing eicosanoids was removed and placed in a new silanized tube. To the chloroform phase, 200 µL of methanol was added and the sample was evaporated under N_2 (g). The sample was then transferred to a silanized micro insert using 150 µL of chloroform/methanol (9:1 by vol.). The tube containing extract was washed with 150 µL of chloroform/methanol (9:1 by vol.) and added to the micro insert. and dried down under N_2 (g). The sample was then redisolved in methanol/water (1:1 by vol.) and proceeded to LC-MS analysis. The

hexane phase containing 2-arachidonyl glycerol and arachidonyl ethanolamide was dried down under N_2 (g) and 1 mL of acetonitrile was used to resuspend the analytes. 20 μL of the sample was mixed with 20 μL of water in a silanized micro insert and used for analysis by LC-MS.

Liquid Chromatography-Mass Spectrometry (LC-MS) analysis

The above extracts prepared for analysis of 2-AG, AEA, and eicosanoids were then analyzed by LC- MS as previously described (Brose *et al.* 2016; Brose and Golovko 2013). 2-AG was resolved using a Waters ACUITY UPLC HSS T3 column (1.8 μM, 100 Å pore diameter, 2.1 x 150 mm, Waters, Milford, MA) with an ACUITY UPLC HSS T3 precolumn (1.8 μM, 100 Å pore diameter, 2.1 x 150 mm, Waters, Milford, MA) at a temperature of 55°C. The LC system was configured with a Waters Acuity UPLC pump and autosampler set at 8°C. The LC eluent was analyzed using a triple quadrupole mass spectrometer (Xevo TQ-S, Waters) with electrospray ionization operated in positive ion mode. The capillary voltage was 2.35 kV and the cone voltage was 30V. The desolvation temperature was 550°C with a source temperature of 150°C. The desolvation gas flow was 1000 L/hr, the cone gas flow was 150 L/hr, and the nebulizer gas was at 7.0 Bar. MassLynx V4.1 software (Waters) was used for instrument control, data acquisition and sample analysis. The 2-AG and eicosanoids were quantified, using 2-AG-d_8 and PGE$_2$-d_4 as the internal standard, respectively. The analytes were monitored in multiple reaction monitoring mode using 12 V for collision energy and the following mass transition for analytes and their internal standards: 2-AG 379.3/287.7 and 2-AG-d_8 387.5/294.4, PGE$_2$ 351.2/189.5 and PGE$_2$$d_4$ 355.2/275.5.

Quantitative real-time PCR

RNA was extracted from microglia using the Qiagen RNeasy Kit and quantified on an Epoch spectrophotometer system (BioTek, Winooski, VT, USA). Optical density was used to verify RNA concentration at 260 nm and genomic DNA contamination by 260/280 nm ratio. Then 100 ng to 1 µg of total RNA was used for first strand synthesis using the SuperScript III First-Strand Synthesis System primed with random hexamers (Life Technologies, NY, USA). cDNA was quantified using a Bio Rad CFX96 real-time PCR detection system using Power SYBR green master mix (Life Technologies, NY, USA). Primers used for *Snca* and *Sdha* are shown in Table 2. Samples were pre-denatured (95°C for 10 m) then a polymerase-activation program (45 cycles of 95°C for 15 s, 55°C for 30 s, and 72°C for 30 s) was followed by post-annealing at 72°C for 120 s. Then a melting temperature (T_m) curve program (60-95°C ramp at 0.5°C/s) was used to identify *a*mplification contaminants. A common threshold of fluorescence was set and using the absolute standard curve method, the number of cycles (Ct) was used to determine absolute number of copies of target gene cDNA. Endogenous control succinate dehydrogenase complex, subunit A, (flavoprotein) *Sdha*, was used to normalize target gene copy number found by qRT-PCR, resulting in a ratio of target gene to endogenous control gene.

Isoform	Forward Primer	Reverse Primer
Sdha	CCTACCCGATCACATACTGTG	AGTTGTCCTCTTCCATGTTCC
Snca	GCCCTTGCCTCTTTCATTG	GTCCTTTCATGAACACATCCATG

Table 2. Primer sequences used for microglia qRT-PCR

Statistics

      Statistical analysis was done using Instat® statistical program (Graphpad, San Diego, CA). Multiple comparisons were assessed using a one-way ANOVA and a Tukey-Kramer *post hoc* test, with $p < 0.05$ considered to be significant. Where appropriate (Fig. 6, 9, 10, 11, and 12) Student's two-tailed *t*-test was used to determine significance between treatment groups, with $p < 0.05$ considered to be significant. Each time point contains samples from five (n=5) individually treated separate cell cultures. For analysis of gene-expression, mice n=5 and microglia n=3.

RESULTS

Microwave irradiation is crucial in determining basal 2-arachidonyl glycerol levels in mouse brain.

Because 2-AG levels may be impacted by post-mortem delay and because we have found that microwave irradiation limits changes in lipid release during post-mortem delay (Murphy 2010), I determined the impact of post-mortem delay on 2-AG levels. Non-microwave irradiated brains had significantly higher 2-AG levels than microwave irradiated brains (Figure 14). There was no significant difference in 2-AG levels between mice expressing different forms of *Snca* that were not microwave irradiated before removal of brain that was dependent on the form of *Snca* expression. However, there were several differences between microwave irradiated brains. *Snca* gene-ablated mice have significantly increased basal 2-AG levels (39.2 ng/gww) compared to wild type mice (7.5 ng/gww) (Figure 14). Interestingly, the human *Snca* knock-in mice have some reduction of 2-AG levels (24.0 ng/gww) when compared to *Snca* gene-ablated mice (Figure 14), but *hSnca* does not fully reduce basal 2-AG levels to wild type concentrations. There is a similar observation for both A30P (13.1 ng/gww) and A53T (19.1 ng/gww) mutant *Snca* knock-in mice having concentrations between the wild type and *Snca* gene-ablated mice (Figure 14). This suggests that the addition of human or mutant Snca restores some function with regards to basal 2-AG levels. Importantly, there was a significant 240-fold increase in wild type mouse brain 2-AG levels in the brains of mice not microwave irradiated vs microwave irradiated (Figure 14). Therefore,

removal of brain from cranial vault without heating the brain *in situ* prior to removal

results in a substantial significant increase in 2-AG levels.
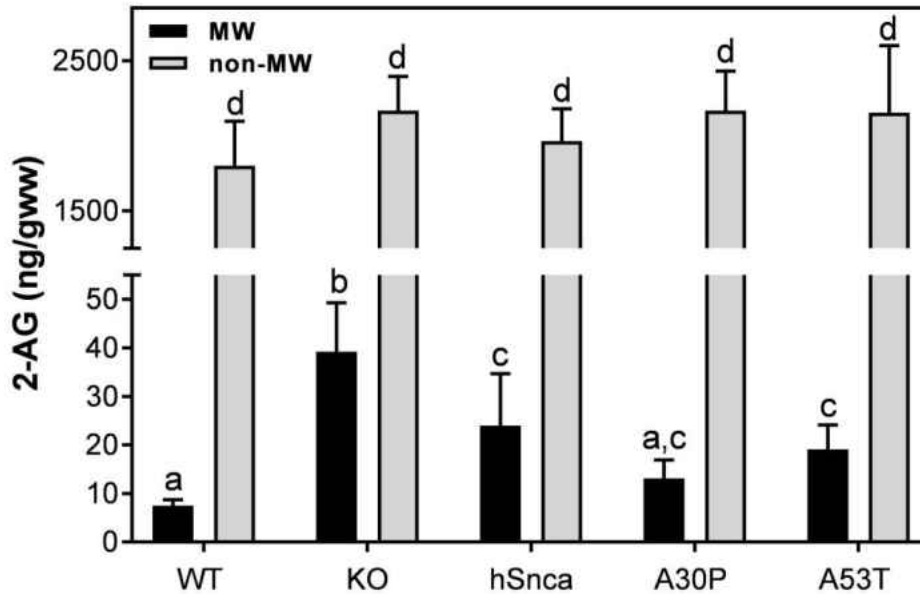
Figure 14. 2-AG levels in microwaved vs non-microwaved mouse brain. 2-AG levels in

WT, KO, hSnca, A30P, A53T mice microwave irradiation (black) and not-microwave

irradiated (gray). Values represent means ± standard deviation (n=4-6). Lettering

denotes statistically significant differences between groups using a one-way ANOVA and

a Tukey-Kramer *post hoc* test ($p < 0.05$).

Snca gene-ablated mice have exacerbated 2-AG levels from LPS treatment.

Because we found a significant difference between basal 2-AG levels we

determined how LPS treatment will affect 2-AG levels differently in mice. We found no

significant difference of basal levels of *Snca* expression in wildtype mice or after 3 hours

of LPS treatment (Figure 15). Because LPS treatment does not affect *Snca* level

expression in wild type mice, this suggests that 2-AG level changes in LPS treated mice

is not a result of differences in *Snca* expression.
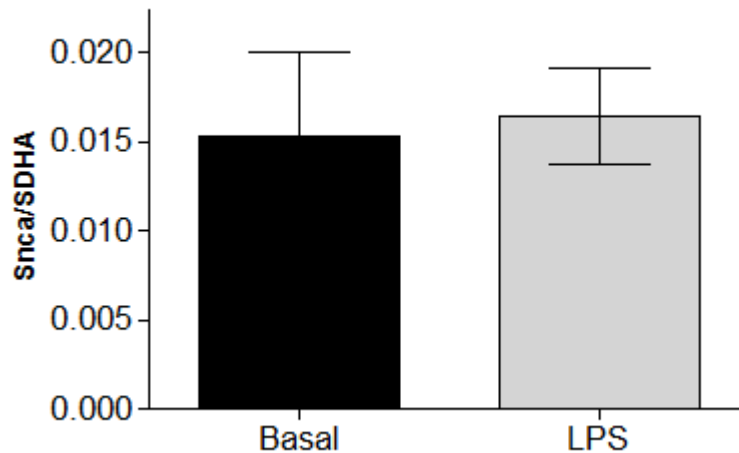
Figure 15. *Snca* expression in brains of wild type mice treated with LPS. *Snca*

expression levels in wild type mice following 3 hour LPS (1mg/kg, i.p.) treatment. Values

represent means ± standard deviation (n=5). The asterisk indicates a statistically

significant difference from untreated mice using Student's *t*-test ($p < 0.05$).

We did however, find a significant 1.4-fold increase in 2-AG levels of wild type mice after

3 hour LPS treatment (Figure 16). This significant difference was also found in *Snca*

gene-ablated mice. However, LPS treatment of *Snca* gene-ablated mice resulted in a

1.7-fold increase of 2-AG levels. Interestingly, basal 2-AG levels in *Snca* gene-ablated

mice were significantly increased 1.24-fold over wildtype levels (Figure 16). This

indicates that *Snca* gene-ablated mice have higher basal levels of 2-AG and that LPS

treatment causes a significantly higher increase of 2-AG as compared to the increased

observed in wild type mice.
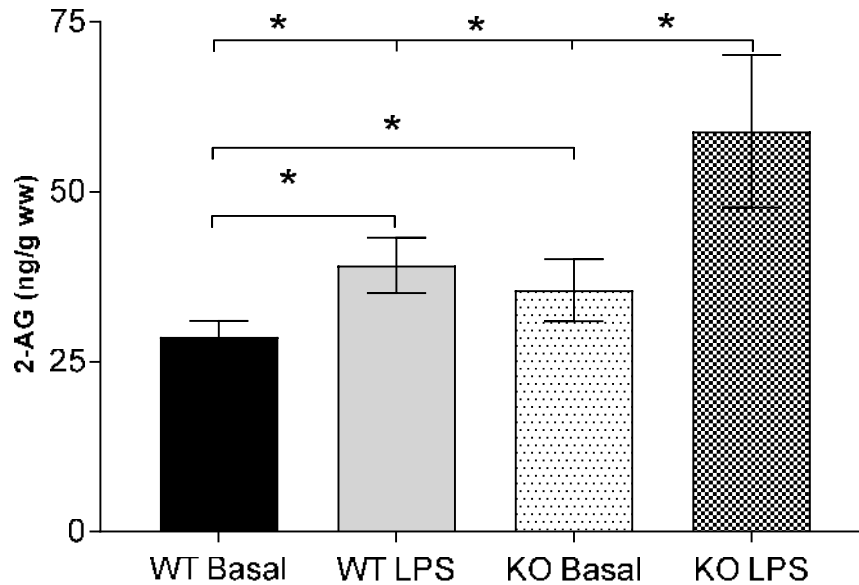
Figure 16. Brain 2-AG levels in wild type and *Snca* gene-ablated mice basal and treated

with LPS. 2-AG levels in wild type and *Snca* gene-ablated (KO) mice following 3 hour

PBS (basal) or LPS (1mg/kg, i.p.) treatment. Values represent means ± standard

deviation (n=5). The asterisk indicates a statistically significant difference from groups

using Student's *t*-test ($p < 0.05$).

LPS treatment in immortalized mouse microglia increases 2-AG levels

Because 2-AG is an important signaling molecule in microglia macrophage phenotype

we determined if LPS (50 ng/mL) treatment affects 2-AG and prostaglandin levels. In

BV-2 (C57BL/6 mouse brain microglia immortalized cells) an 18 hour LPS treatment

resulted in a significant 2.8-fold increase in 2-AG levels (Figure 17).

65
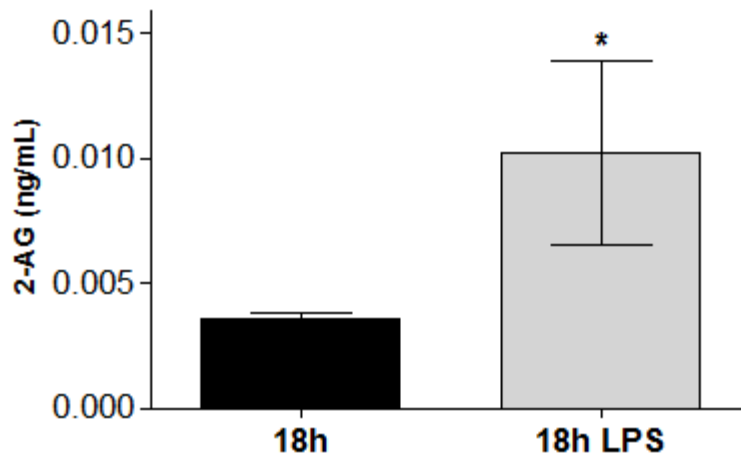
Figure 17. 2-AG levels in BV-2 microglia medium treated with LPS. 2-AG levels in BV-2

immortalized mouse microglia following 18 hours of LPS (50 ng/ml) treatment or no

treatment (basal control). Values represent means ± standard deviation (n=5). The

asterisk indicates a statistically significant difference from control using Student's *t*-test

($p < 0.05$).

After 18 hours of LPS treatment eicosanoid levels were also determined. Prostaglandin

E_2 (PGE$_2$), prostaglandin D_2 (PGD$_2$), prostaglandin $F_{2\alpha}$ (PGF$_{2\alpha}$) were significantly

increased while thromboxane B_2 (TXB$_2$) and 6-keto prostaglandin $F_{1\alpha}$ (6-ketoPGF$_{1\alpha}$)

were unchanged (Figure 18). The massive increase in PGE$_2$ and PGD$_2$, 10-fold and 168-

fold, respectively, suggests that there is a substantial microglia reaction phenotype as

expected with LPS treatment.
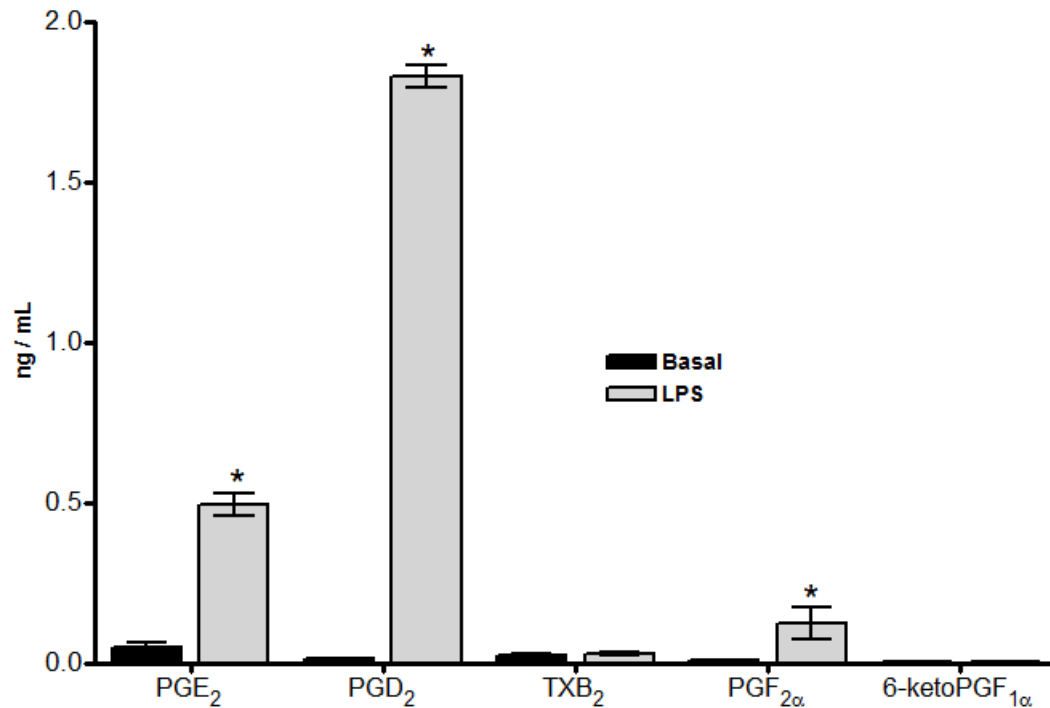
Figure 18. Prostaglandin levels in BV-2 microglia medium treated with LPS.
Prostaglandin levels in medium of BV-2 immortalized mouse microglia following 18
hours of LPS (50 ng/ml) treatment or no treatment (control). Values represent means ±
standard deviation (n=5). The asterisk indicates a statistically significant difference from
control using Student's *t*-test ($p < 0.05$).

BV-2 cells were very effective at showing a significant reaction to LPS however, we and
others (Kim *et al.* 2009) have found that BV-2 cells do not express *Snca* at a level high
enough to quantify by RT-qPCR or protein levels quantifiable by Western blotting.
Because of the lack of *Snca* expression another model would have to be utilized to
determine if *Snca* expression affects 2-AG levels.

Primary Snca gene-ablated microglia have reduced basal 2-AG levels.

Because BV-2 cells did not express *Snca*, we chose to use a model that naturally contains Snca instead of transfecting BV-2 cells which may negatively perturb the BV-2 system. Therefore, primary wild type and *Snca* gene-ablated (KO) microglia were used. Unlike mouse brain, primary gene-ablated microglia had a 59% reduction in basal levels of 2-AG released in the medium (Figure 19). This suggests that in unstimulated primary microglia, *Snca* gene-ablation has a significant effect on 2-AG levels. Our previously published data determined that *Snca* gene-ablated microglia have higher basal total prostaglandin release into the medium partially due to increased phospholipase D_2 (PLD_2) and cyclooxygenase-2 (COX-2) levels (Austin *et al.* 2011).
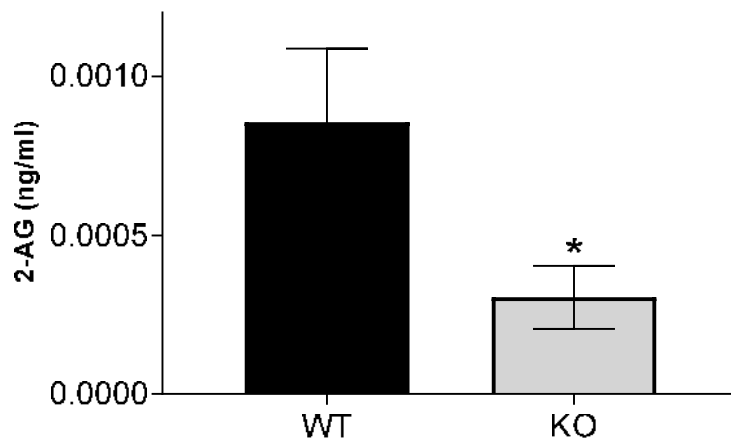
Figure 19. Basal 2-AG levels in medium of wild type and *Snca* gene-ablated primary microglia. Values represent means ± standard deviation (n=5). The asterisk indicates a statistically significant difference from control using Student's *t*-test ($p < 0.05$).

Primary microglia had reduced 2-AG levels but increased eicosanoid production after LPS treatment.

Because we are interested in Snca effect on inflammation we treated primary microglia at several time points with LPS to induce a reactive phenotype. After 6 hours of LPS treatment there was no significant difference in 2-AG levels in the medium (Figure 20).
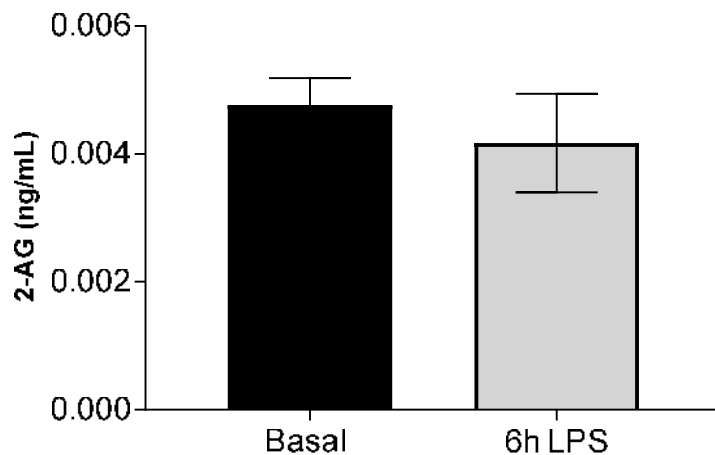
Figure 20. 2-AG levels in medium of primary microglia after 6 h of LPS treatment. 2-AG levels in medium of primary mouse microglia following 6 hours of LPS (50 ng/ml) treatment or no treatment (basal control). Values represent means ± standard deviation (n=3).

There was also no significant difference in *Snca* expression levels after 6 hours of LPS treatment in wild type microglia (Figure 21). here was however, an 80% decrease in TXB$_2$ and a significant 2.8-fold increase in PGD$_2$ released into the medium of wild type microglia (Figure 22). This data suggests that while small changes occured in released

eicosanoids, 6 hours of LPS treatment does not affect either *Snca* expression or alter

the amount of 2-AG levels released into the medium, but does impact PGD_2 synthesis
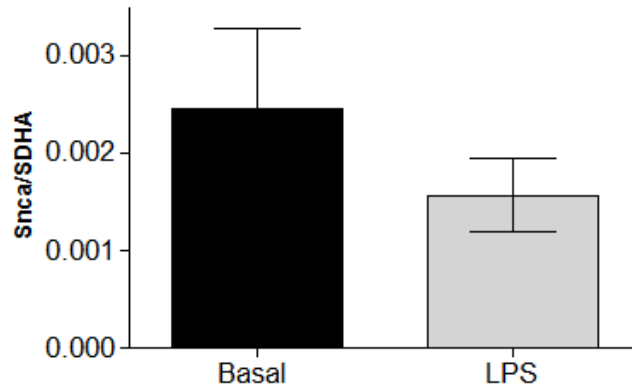
Figure 21. *Snca* expression in primary microglia with 6 h LPS treatment. *Snca*

expression levels in primary microglia following 6 hour LPS (1mg/kg, i.p.) treatment.

Values represent means ± standard deviation (n=3).

A
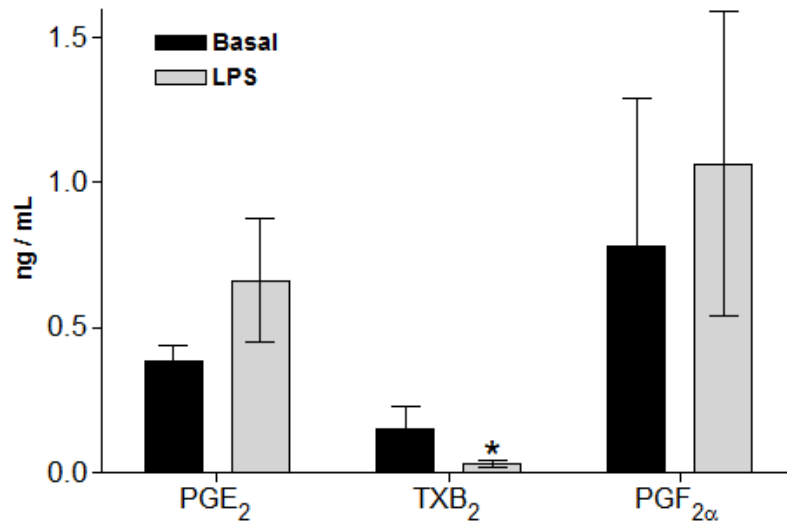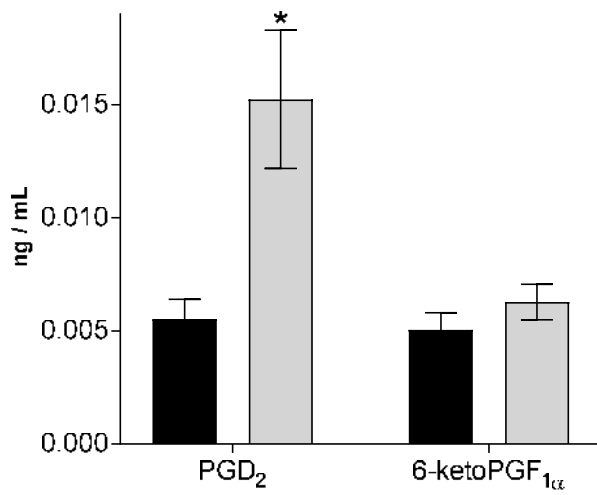
B continued

Figure 22. Prostaglandin levels in medium of primary microglia treated with LPS 6 h.

Prostaglandin levels in medium of primary mouse microglia following 6 hours of LPS (50

ng/ml) treatment or no treatment (control). Values represent means ± standard deviation

(n=3). The asterisk indicates a statistically significant difference from control using

Student's *t*-test (*p* < 0.05).

However, after 18 hours of LPS treatment there was a significant 59% reduction in 2-AG

levels in medium of wild type microglia (Figure 23). Concomitantly, there was a

significant albeit small reduction (17%) in *Snca* expression in wild type microglia (Figure

24).
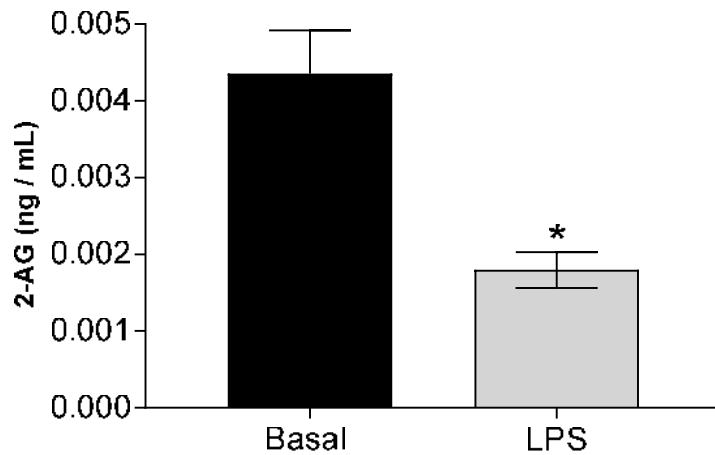
Figure 23. 2-AG levels in medium of primary microglia after 18 h LPS treatment. 2-AG

levels in medium of primary mouse microglia following 18 hours of LPS (50 ng/ml)

treatment or no treatment (basal control). Values represent means ± standard deviation

(n=3). The asterisk indicates a statistically significant difference from control using

Student's *t*-test (*p* < 0.05).
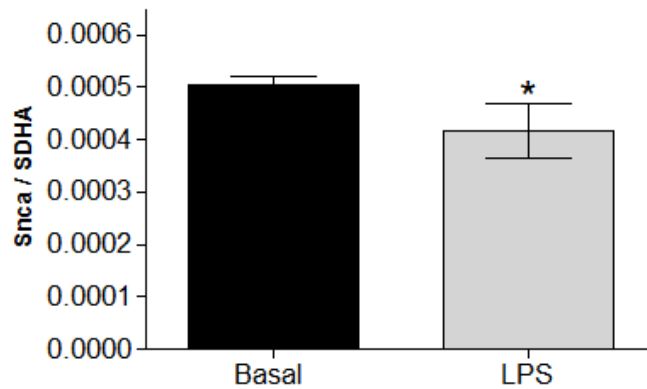
Figure 24. *Snca* expression in primary microglia with 18 h LPS treatment. *Snca* expression levels in primary microglia following 18 hour LPS (1mg/kg, i.p.) treatment. Values represent means ± standard deviation (n=3). The asterisk indicates a statistically significant difference from basal control using Student's *t*-test ($p < 0.05$).

After 18 hours of LPS treatment there was a large increase in several eicosanoids in the medium of primary wild type microglia similar to those found in BV-2 cells treated for 18 hours with LPS. PGD_2 was increased 138-fold, $PGF_{2\alpha}$ was increased 23-fold, TXB_2 was increased 7.8-fold, and PGE_2 was increased 173-fold in medium of LPS treated primary microglia (Figure 25).

A

B continued
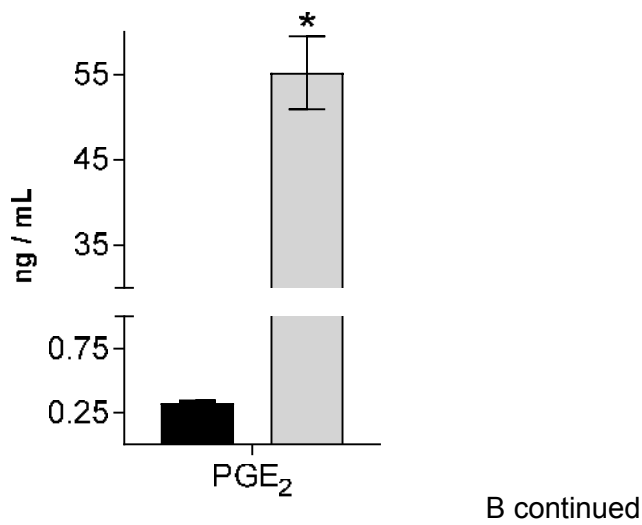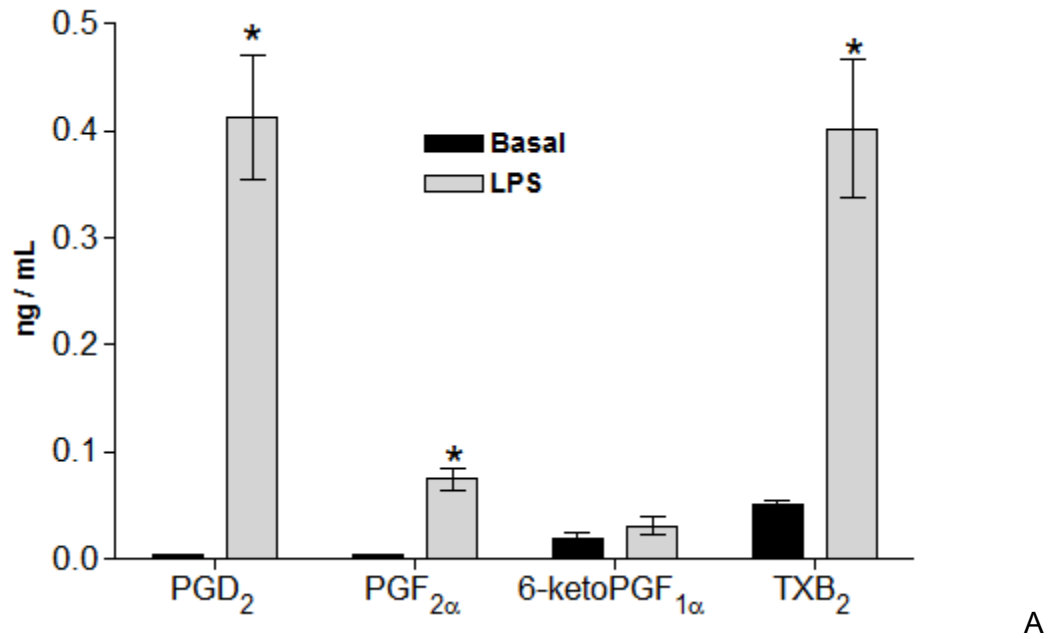
Figure 25. Prostaglandin levels in medium of primary microglia treated with LPS 18 h. Prostaglandin levels in medium of primary mouse microglia following 18 hours of LPS (50 ng/ml) treatment or no treatment (control). Values represent means ± standard deviation (n=3). The asterisk indicates a statistically significant difference from control using Student's t-test ($p < 0.05$).

2-AG levels and Snca expression are reduced at the same time point after LPS treatment.

To determine if *Snca* expression and 2-AG levels change over time of LPS treatment, we examined *Snca* expression at several different time points and expressed data as percent control. We found that after 12 hours of treatment there was a significant reduction in released 2-AG levels vs control (Figure 26). This significant reduction was similar to what we found in *Snca* gene expression after 12 hours of LPS treatment (Figure 27).
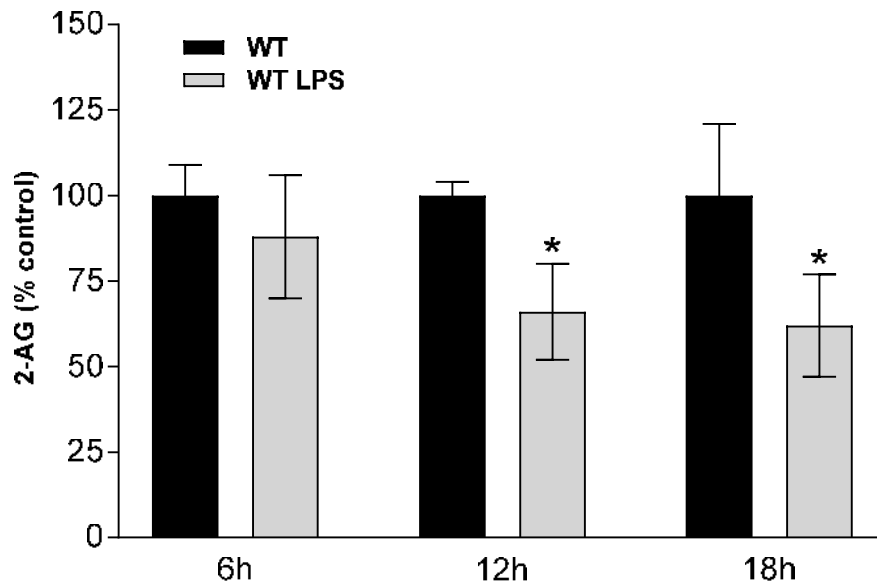
Figure 26. 2-AG levels in medium of primary microglia time response following LPS treatment. 2-AG levels expressed as % control in medium of primary mouse microglia following 6, 12, or 18 hours of LPS (50 ng/ml) treatment. Values represent means ± standard deviation (n=3). The asterisk indicates a statistically significant difference from control using Student's *t*-test ($p < 0.05$).

Similarly, *Snca* gene expression was reduced after 12 hours of LPS treatment in wild type primary microglia (Figure 27). These data suggests that both 2-AG released into medium and *Snca* expression is reduced concomitantly in primary microglia after 12 hours of LPS treatment.
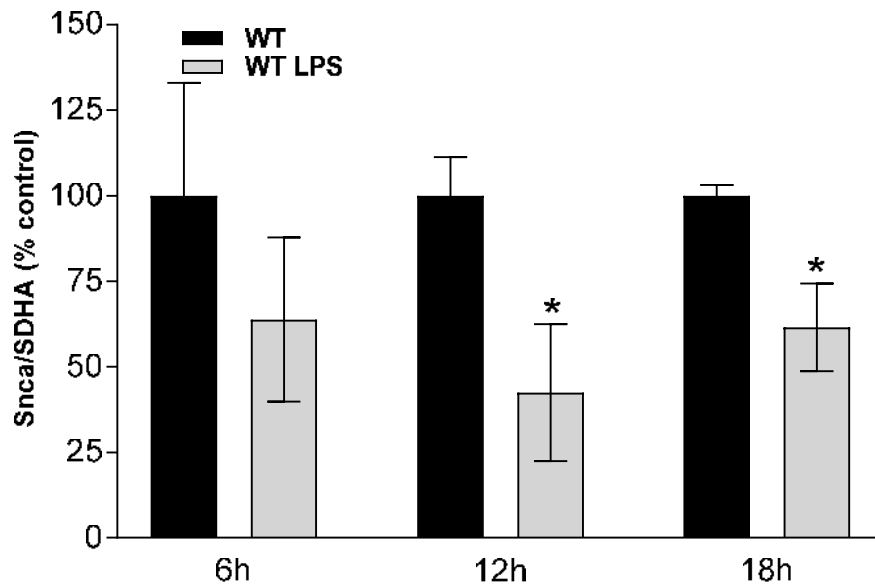
Figure 27. *Snca* expression in primary microglia time response following LPS treatment. *Snca* expression levels expressed as % control in primary microglia following 6, 12, or 18 hour of LPS (1mg/kg, i.p.) treatment. Values represent means ± standard deviation (n=3). The asterisk indicates a statistically significant difference from basal control using Student's *t*-test ($p < 0.05$).

Primary Snca gene-ablated microglia have reduced 2-AG levels but increased eicosanoid production after LPS treatment.

Because *Snca* expression was significantly reduced concomitantly with 2-AG levels in wild type mice following LPS treatment it suggests that *Snca* expression may impact 2-

AG and eicosanoid synthesis sin microglia. To test this hypothesis, we treated *Snca* gene-ablated primary microglia with LPS. A significant reduction of 2-AG occurred at 24 hours of LPS treatment in microglia from gene-ablated mice (Figure 28), whereas for wild type microglia, this reduction occurred at 12 hours (Figure 26).
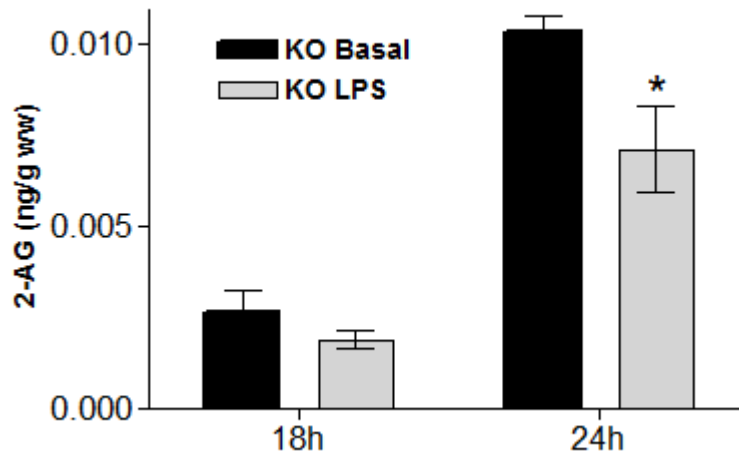
Figure 28. 2-AG levels in medium of *Snca* gene-ablated primary microglia after 18 or 24 h of LPS treatment. 2-AG levels in medium of primary mouse microglia following 18 or 24 hours of LPS (50 ng/ml) treatment or no treatment (basal control). Values represent means ± standard deviation (n=3). The asterisk indicates a statistically significant difference from control using Student's *t*-test ($p < 0.05$).

Interestingly, at 24 hours of LPS treatment there were significant differences in eicosanoids however, several were differentially modulated. PGE_2, PGD_2 and TXB_2 were increased following LPS treatment in a manner similar to wild type microglia

(Figure 29). However, PGF$_{2\alpha}$ was significantly reduced in *Snca* gene-ablated microglia, but in wild type microglia there was a significant increase after 18 hours of LPS treatment. 6-ketoPGF$_{1\alpha}$ was significantly reduced in *Snca* gene-ablated mice, but not in wild type mice.

A

B continued
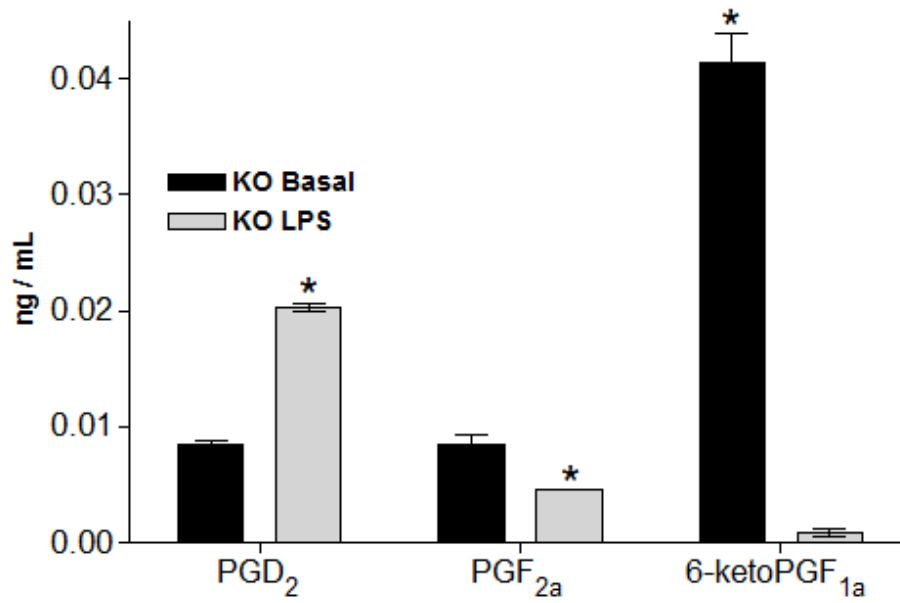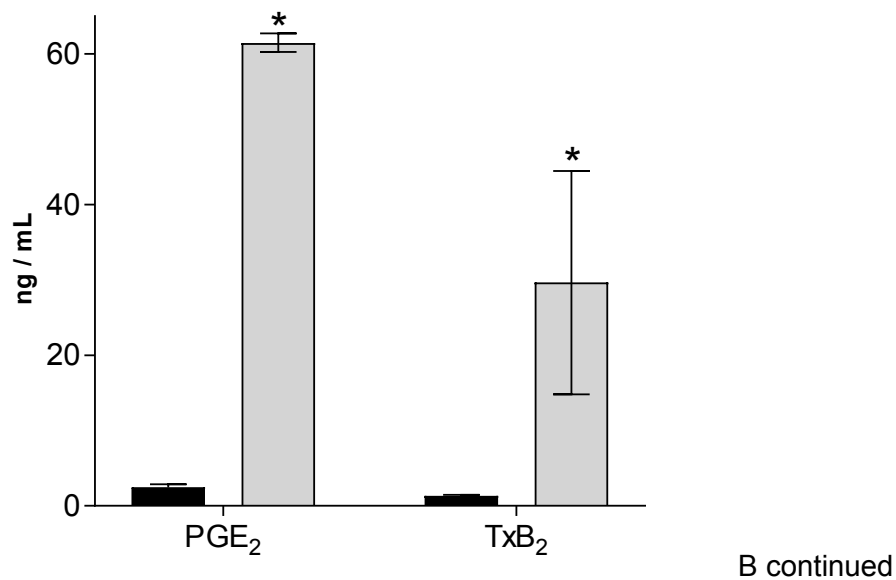
Figure 29. Prostaglandin levels in medium of primary *Snca* gene-ablated microglia treated with of LPS 24 h. Prostaglandin levels in medium of primary mouse microglia following 24 hours of LPS (50 ng/ml) treatment or no treatment (control). Values represent means ± standard deviation (n=3). The asterisk indicates a statistically significant difference from control using Student's *t*-test ($p < 0.05$).

To determine the inflammatory state of the microglia we looked at combined eicosanoid levels in medium of wild type basal (Ctr), wild type LPS treated (WT), and *Snca* gene-ablated LPS treated (KO) primary microglia. Interestingly, there was not a significant change in WT microglia combined eicosanoid release between 6 and 12 hours of LPS treatment which was unexpected (Figure 30). There was however, a drastic increase in combined eicosanoids between 12 and 18 hours of LPS treatment in wild type microglia. *Snca* gene-ablated microglia with LPS treatment had exacerbated combined eicosanoid levels as compared to wild type, suggesting a more inflammatory phenotype. These data together suggests a role of Snca in modulating both 2-AG levels and eicosanoids

79

as a result of LPS treatment and subsequent inflammatory phenotype of microglia. This

conclusion is supported by the correlation between a decrease in *Snca* expression in

wild type microglia and an increase in total prostaglandin production.
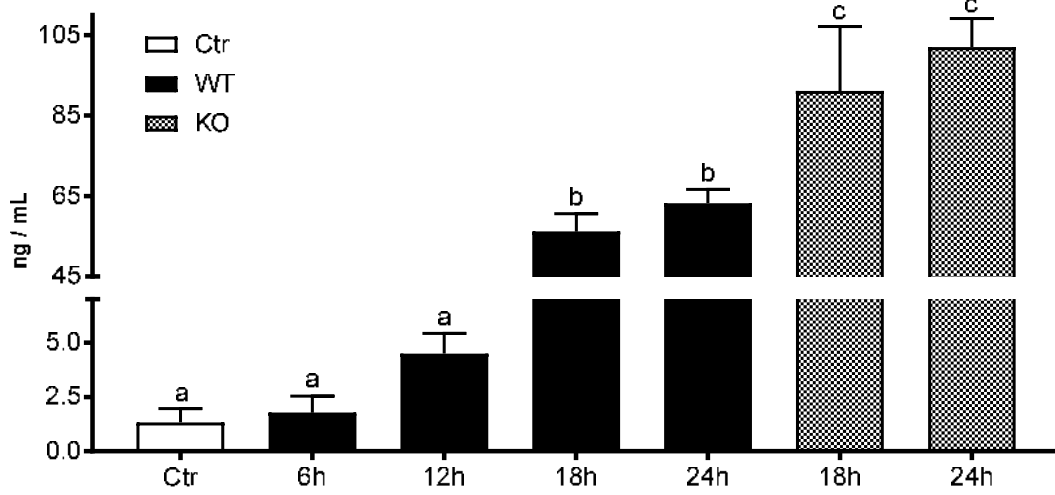
Figure 30. Combined prostaglandin level time response in medium of wild type and

Snca gene-ablated primary microglia treated with LPS. Total prostaglandin time

response in medium of wild type and *Snca* gene-ablated primary mouse microglia

following LPS (50 ng/ml) treatment or no treatment (control). Values represent means ±

standard deviation (n=3). Lettering change denotes statistically significant differences

between groups using a one-way ANOVA and a Tukey-Kramer *post hoc* test ($p < 0.05$).

DISCUSSION

I determined if alterations in *Snca* expression resulted in changes in 2-AG release during LPS treatment, examining this role in whole brain and in microglia isolated from the brains of wild type and *Snca* deficient mice. I have focused on identifying changes that result from the absence of Snca to determine if its normal physiologic role is as a molecular switch in microglia, shifting microglia biochemical phenotype. The role of Snca in lipid mediated signal transduction is well established and the results presented here suggest that Snca has a role or at least a concomitant gene expression reduction in microglia with increasing time of LPS stimulation. In wild type microglia there was a concomitant reduction in 2-AG release into the medium following LPS treatment in a time-dependent manner (Figures 26, 27). Furthermore, *Snca* deficient microglia showed a similar reduction in 2-AG release but revealed a delayed response to LPS stimulation. Interestingly, *Snca* expression in whole brain was not changed following 3 hour stimulation with LPS but *Snca* deficient mice had increased basal 2-AG synthesis that was further increased by LPS treatment.

Snca has a crucial role in brain lipid metabolism and significantly alters the brains inflammatory state (Golovko *et al.* 2005; Golovko *et al.* 2006a; Perrin *et al.* 2000; Trexler and Rhoades 2009; Bodner *et al.* 2010; Ramakrishnan *et al.* 2006; Barceló-Coblijn *et al.* 2007; Murphy *et al.* 2008; Golovko *et al.* 2006b). The role of Snca in arachidonate recycling (Golovko *et al.* 2006a) and the increase in PG synthesis following ischemia (Golovko and Murphy 2008) is consistent with the decreased 2-AG level and increased eicosanoid, especially PGE_2 and PGD_2, synthesis observed in microglia

81

following LPS treatment. While, others have shown that overexpression of Snca is toxic to neurons (Zhou *et al.* 2000; Shavali *et al.* 2008; Lee *et al.* 2001), over expressing wild type and mutant *Snca* in BV-2 cells does not increase neurotoxicity or promote cell death in BV-2 cells when cell viability was examined by activity of lactate dehydrogenase (Rojanathammanee *et al.* 2011). This suggests intracellular Snca does not intrinsically induce phenotypic change through cell toxicity but may regulate microglia activation by inducing 2-AG levels. Furthermore, it is postulated that decreasing basal microglia Snca levels in pathologic events such as PD may in fact have a negative impact on the brains inflammation state by increasing microglia reactivity (Austin *et al.* 2011).

Because 2-AG levels may have an impact on microglia phenotype we determined 2-AG levels in wild type, gene-ablated, and knock-in animals. Microwave irradiation is crucial for determining basal 2-AG levels in mouse brain (Brose *et al.* 2016). Non-microwave irradiated brain suggests a 200-fold higher basal level as compared to microwaved brain thus microwave irradiation is required to determine basal 2-AG levels in mouse brain. *Snca* gene-ablated mice have significantly higher basal levels of 2-AG vs. wild type mice, which is consistent with the role of Snca in increasing PLC activity (Austin *et al.* 2011). Interestingly, *Snca* gene-ablated mice expressing *hSnca* or mutant *Snca* had only a partial reduction in 2-AG levels to basal wild type levels. Although data from previous experiments linking Snca to Acsl activity for its impact on arachidonic acid metabolism suggests Snca mutants will act like the null (Golovko *et al.* 2006a), the 2-AG data in whole brain suggests that there may be a differential effect that is dependent on the Snca mutation and that some activity is restored by the presence of *hSnca* and by the *Snca* mutant knock-ins albeit not in its function in arachidonate Acsl mediated metabolism. This indicates that not all functions of Snca in the mutant forms function as

the null. Others have suggested that mutations of Snca will lead to unique microglia phenotypes which may explain our results (Kim *et al.* 2009; Rojanathammanee *et al.* 2011).

While *Snca* expression is unaffected by 3 hour LPS treatment in wild type mice, there is a significant increase of 2-AG levels over basal levels in wild type brain. This increase in whole brain 2-AG levels is exacerbated in *Snca* deficient mice suggesting that Snca has a role in brain 2-AG levels during inflammation, but it was unexpected that in the absence of *Snca* 2-AG would be elevated. Furthermore, there was not a significant difference between basal 2-AG levels in *Snca* deficient mice and LPS stimulated wild type mice, again suggesting that in *Snca* deficient mice 2-AG synthesis is already at a stimulated level. It is interesting to note that 2-AG alone can drive microglia to an alternative phenotype *in vitro* (Mecha *et al.* 2015) and may indicate a role in the alternative phenotype as we have seen in *Snca* deficient microglia. Our findings demonstrate decreased 2-AG levels from LPS treatment that resulted in a reduction in *Snca* expression that may result in a reduction in recycling arachidonic acid having an effect on 2-AG biosynthesis. The reduction in arachidonic acid recycling in the whole brain may not only alter free arachidonic acid but arachidonic acid containing DAG as well, but this possible mechanism needs to be further elucidated.

Because *Snca* gene-ablated mice had increased basal brain 2-AG levels and we expected to find reduction due to reduced microglia phagocytic ability, we determined 2-AG levels in primary microglia. Following LPS stimulation, there was a concomitant reduction in released 2-AG levels and *Snca* expression after 12 hours. This suggest that 2-AG levels are altered possibly as an effect of reduced *Snca* expression in LPS stimulated wild type primary microglia. Interestingly, 2-AG levels are not altered until 24 hours after LPS stimulation in *Snca* deficient primary microglia. This suggests that *Snca*

deficient primary microglia have altered 2-AG synthesis or degradation. A reduction in

CB2r stimulation results in an increase of microglia reactivity (Carlisle *et al.* 2002),

migration (Walter *et al.* 2003) and CB2r stimulation in microglia is neuroprotective in an

MPTP induced Parkinson's disease (Chung *et al.* 2016). We see a decrease in 2-AG

that is the natural ligand for CB2r and due to this decrease may result in this reactive

phenotype.

Our previously published data determined that although *Snca* deficient microglia

have increased PLD_2 expression to possibly compensate for reduced phagocytic ability

there is still a loss of phagocytic function (Austin *et al.* 2011). 2-AG regulates microglia

motility as CB2r is localized to the leading edge of activated microglia and stimulation by

2-AG results in extracellular signal-regulated kinase 1/2 activation (Walter *et al.* 2003).

This is important because the basal reduction found in *Snca* gene-ablated microglia as

well as the reduction of *Snca* in microglia following LPS stimulation may be a cause for

reduced microglia phagocytic ability. This is coupled with a significantly exacerbated

prostaglandin profile, where PGE_2 is significantly increased over wild type microglia at

the same time of LPS stimulation. Others have shown that PGE_2 stimulates COX-2 but

not COX-1 and PGE_2 limits certain types of phagocytosis (Li *et al.* 2015; Keene *et al.*

2010; Nagano *et al.* 2010; Medeiros *et al.* 2009; Brock *et al.* 2008; Stachowska *et al.*

2007). *Snca* ablation i*n vivo* increases palmitic acid turnover in choline

glycerophospholipids suggesting Snca has a role in inhibiting PLD activity (Golovko *et al.*

2006a). In conjunction with PLD_2 tonic inhibition by Snca there may be some interplay

as phosphatidic acid can be metabolized into 2-AG. Our data supports the hypothesis

that *Snca* expression is linked to 2-AG release in primary microglia and may contribute

to regulating the phagocytic phenotype *in vivo*. However, further study is needed to

elucidate the discrepancy between basal brain 2-AG levels of *Snca* deficient mice and

the greater response to LPS-stimulation of the *Snca* deficient brain with regards to 2-AG formation. However, our data clearly support the hypothesis that *Snca* expression has a significant role in microglial phenotype, supporting previous work demonstrating an enhanced inflammatory response and a reduced phagocytic response in LPS treated microglia from *Snca* deficient brains.

Our data shows that decreasing *Snca* expression may in fact have a negative outcome in CNS inflammatory diseases such as Parkinson's disease. Reduced ARA recycling and increased eicosanoid synthesis following ischemia is consistent with increased basal secretion of eicosanoids in *Snca* deficient microglia. Therefore, reducing *Snca* expression may result in an increased inflammatory state of the microglia. Furthermore, overexpression of *Snca* and *Snca* mutants in BV-2 cells did not result in increased neurotoxic secretion (Rojanathammanee *et al.* 2011) suggesting that basal levels of intracellular Snca may play a neuroprotective role acting as a molecular switch in microglia, helping to enable the phenotypic shift from a proinflammatory to phagocytic phenotype.

CHAPTER IV

INTRODUCTION

Impact of alpha-synuclein on fatty acid metabolism during inflammatory response.

Snca ablation reduces palmitic acid (PAM, 16:0) and arachidonic acid (ARA, 20:4n-6) uptake in mouse astrocyte cultures and in whole brain *in vivo*, consistent with a role in brain lipid metabolism. Although PAM incorporation and turnover is reduced in most phospholipids by *Snca* ablation, there is a marked increase in PAM incorporation and turnover in choline glycerophospholipids (ChoGpl). This is consistent with the tonic inhibition of phospholipase D2 (PLD2) by Snca, because PLD2 selectively metabolizes ChoGpl. Snca is also critical for ARA incorporation and turnover in brain phospholipids due to a reduction in ARA-CoA formation. In microsomes from *Snca* ablated mice, ER-localized Acsl activity towards ARA is decreased, but activity is restored by the addition of physiological levels of either wildtype mouse or human Snca (hSnca). However, addition of mutant forms of Snca (A53T and A30P) did not restore activity, suggesting that mutant Snca functions similarly to the null. Although Snca has a robust impact on lipid metabolism, lipid mediated signal transduction, and in neuroinflammation, it is unknown if LPS treatment, inducing a neuroinflammatory response, in *Snca* gene-ablated mice will have a similar impact on ARA metabolism in the intact animal. Because mutant Snca does not restore selective ARA-CoA Acsl activity and Snca ablation results in enhanced PLD2 activity, our central hypothesis is that *Snca* gene-ablated mice will have an increased neuroinflammatory response due to reduced

ARA recycling and lack of PLD2 activity inhibition when compared to wild-type mice. These studies will elucidate a fundamental function of Snca *in vivo*.

We propose a set of well-defined experiments using steady state kinetics of radiolabeled fatty acid tracers to extend our studies of the role of Snca in lipid metabolism and inflammation *in vivo* in SV/129 wild-type and *Snca* gene-ablated mice. Our long-term goal is to understand the action of Snca on fatty acid metabolism as well as its role in the inflammatory response. The objective of this study is to elucidate the function *in vivo* of Snca in ARA metabolism using fatty acid radiotracers to study the role of Snca in the inflammatory response induced by LPS treatment. We believe Snca has a key role in fatty acid uptake and trafficking and our goal is elucidate its biological role in downstream neuroinflammatory regulation via its influence on ARA metabolism, offering insight into the pathophysiology of neuroinflammation.

Recent studies suggest Snca has a role in brain fatty acid metabolism. Snca was thought to be a fatty acid binding protein (FABP) due to similar protein homology and structure (Sharon *et al.* 2001), but its binding constants for fatty acids and its impact on lipid metabolism is clearly different from classical FABP (Murphy *et al.* 2005; Barceló-Coblijn *et al.* 2007). However, like FABP (Murphy *et al.* 2005), Snca increases Acsl activity, but is specific to ARA,(Golovko *et al.* 2006a). Furthermore, *Snca* deficiency results in decreased PAM and ARA uptake, incorporation rate and fractional turnover in phospholipids(Golovko *et al.* 2005; Golovko *et al.* 2006a). However, PAM incorporation into choline glycerophospholipids (ChoGpl), a preferred substrate for PLD2, is increased, while its incorporation and turnover into other major phospholipids is reduced (Golovko *et al.* 2005). This is significant because it known that Snca tonically inhibits PLD2 activity (Jenco *et al.* 1998; Outeiro and Lindquist 2003), which we have shown is critical in enhancing neuroinflammatory response in *Snca* deficient microglia (Austin *et al.* 2006;

Austin *et al.* 2011). Similarly, prostaglandin formation is increased following LPS treatment or global ischemia as a result of dysfunctional ARA metabolism (Golovko and Murphy 2008). Although Snca function has been studied in lipid metabolism, the function Snca under inflammatory conditions in lipid metabolism is poorly understood. While we have demonstrated previously the enhanced inflammatory response via ARA metabolites in *Snca* ablated mice, how ARA metabolism is perturbed *in vivo* is unknown. This work is significant because it will identify key roles of Snca in modulation of neuroinflammatory response.

Snca facilitates PAM and ARA uptake in astrocytes (Castagnet *et al.* 2005) and brain (Golovko *et al.* 2005; Golovko *et al.* 2006a), but it also has a role in brain neutral lipid metabolism (Barceló-Coblijn *et al.* 2007). Using a steady-state kinetic model, it is demonstrated that *Snca* deficiency reduces ARA incorporation and turnover in brain phospholipids (Golovko *et al.* 2006a). This reduced ARA metabolism in *Snca* deficient brain is the result of decreased Acsl activity, which is restored *in vitro* by adding physiological levels of Snca (Golovko *et al.* 2006a). However, mutant forms of Snca fail to restore this activity. Further, while we have identified a link between *Snca* deficiency and enhanced PLD2 activity using PAM kinetic analysis and studies in microglia cultures, the importance of Snca in the process is unknown. This work links Snca to dysfunction in ARA metabolism resulting in an enhanced inflammatory response. This is a major departure from the traditional ideas regarding Snca biology and will offer a better fundamental understanding of how *Snca* ablation can modulate lipid mediated signal transduction associated with neuroinflammation.

In this chapter, I determined the role of Snca in ARA uptake and trafficking in brain and liver following 3 hours of LPS treatment. In the absence of Snca, there is a

significant increase in the uptake of ARA into brain during LPS induced

neuroinflammation. Targeting to organic (lipid pools) and aqueous (β-oxidation)

fractions are increased during LPS-treatment, indicating more tracer is entering the *Snca*

deficient brain. However, fractional distribution into organic or aqueous fractions is not

affected. Incorporation into phospholipid pools in the *Snca* deficient mouse is increased,

consistent with the increase in the organic fraction. Consistent with the enhanced

incorporation into phospholipids, ARA trafficking into phosphatidylinositol and choline

glycerophospholipids are increased. We also found decreased targeting of ARA into

diacylglycerol suggests either an increase in DAG formation in brain of wild-type mice by

phospholipase C or greater utilization of DAG for phospholipid synthesis in brain of *Snca*

gene-ablated mice and may contribute to the increase in 2-AG levels found in whole

brain. These data suggest that during lipopolysaccharide-induced neuroinflammation

where ARA release is enhanced, Snca has a crucial role in maintaining ARA metabolism

into specific phospholipid pools utilized in lipid-mediated signaling.

MATERIALS AND METHODS

Mice

This study was conducted in accordance with the National Institutes of Health Guidelines for the Care and Use of Laboratory Animals and under an animal protocol approved by the University of North Dakota IACUC (Protocol 0708-1c). The wild type mice used for the protocol were the 129/SvEv strain and the *Snca* gene-ablated mice were generated by gene-targeted deletion of *Snca* (Cabin *et al.* 2002). Male mice were age matched ~10 months old and were given standard laboratory chow and water *ad libitum*.

Surgery, LPS treatment and Fatty Acid Infusion

Samples were collected from age matched (~9 month-old) SV/129 wild type or *Snca* gene-ablated male mice (National Institute of Cancer, Frederick, MD) under an approved protocol by the University of North Dakota (Grand Forks, ND) Animal Care and Use Committee (protocol 0110-1). During catheter insertion mice were anesthetized with (1-3%) isoflurane and polyethylene10 catheters were inserted into the right femoral vein and artery. Because previously published data showed no difference in blood brain barrier permeability between single does and divided doses of LPS (Jangula and Murphy 2013), we used a single dose of lipopolysaccharide (LPS) derived from *E. coli* 055:B5 J (Sigma cat# L2880) dissolved in phosphate buffered saline (0.25 mg/mL). Mice were injected with LPS (1 mg/kg) dose intraperitoneally (i.p.) post-surgery. Mice were allowed to recover from anesthesia for three hours following surgery to allow equilibration of metabolism following anesthesia (Murphy *et al.* 2004; Murphy *et al.* 2000b). At 3 h post

LPS injection, mice were infused with 170 µCi/kg [1-^{14}C]20:4n-6 at a rate of 50 µl/min for 10 min to achieve steady state plasma radioactivity. Blood was collected at set intervals and plasma separated to assess intravascular radioactivity and confirm steady state plasma radioactivity. Mice were then euthanized at 10 min with pentobarbital (i.v.) and immediately subjected to head focused microwave irradiation to heat denature enzymes *in situ* (Golovko *et al.* 2005; Murphy 2010). Whole brain, liver, and heart were removed, flash frozen in liquid nitrogen, and then pulverized into a homogeneous powder under liquid nitrogen conditions. Plasmas as well as whole blood, because of the contribution of residual blood to tissue radioactivity, was extracted using a two-phase extraction method (Folch *et al.* 1957) as previously described (Murphy *et al.* 2008). Residual blood in liver, heart, and brain was estimated to be 17, 22, and 2%, respectively, based upon previously published data (Smith 1970; Regoeczi and Taylor 1978; Rosenberger *et al.* 2002; Rosenberger *et al.* 2003).

Tissue Lipid Extraction

Following pulverization, lipids were extracted from the tissues using a two-phase extraction method (Folch *et al.* 1957). Powdered tissue was kept on dry ice until added to a tared Tenbroeck homogenizer, to determine the mass (g ww) of the tissue added. To the Tenbroeck homogenizer 17 vol. of chloroform and methanol (2:1, by vol) was added. Once tissue was homogenized, the extract was removed, saved and then the homogenizer was washed with 3 vol. of chloroform and methanol (2:1, by vol) and the rinse added to the initial extract. The tissue residue was saved for protein quantification. After homogenization, 4 vol of 0.9% KCl was added to extract, mixed by vortexing, and allowed to separate into two phases overnight at -20°C under a $N_{2(g)}$ atmosphere. The following morning, the top phase was removed and saved. To the lower phase, 4 vol. of

chloroform, methanol, and water (3:48:47, by vol) was added, the sample vortexed, chilled, and subjected to centrifugation to facilitate phase separation. The upper phase was removed and combined with the previous upper phase to determine aqueous fraction radioactivity using liquid scintillation counting (LSC). The lower phase was dried down with N_2 (g) and dissolved in hexane:2-propanol (3:2, by vol) and a portion used to determine organic radioactivity using LSC. The unused portion was stored under $N_{2(g)}$ atmosphere at -80°C in hexane:2-propanol (3:2, by vol).

Lipid Separation by Thin Layer Chromatography

Extracted lipids were separated using thin layer chromatography (TLC) on heat-activated (110°C) Whatman silica gel-60 plates. Neutral lipids were separated into individual classes using petroleum either, diethyl ether, and acetic acid (75:25:1.3, by vol.) (Marcheselli V.L. et. al. 1988). Phospholipids were separated into individual classes using chloroform, methanol, acetic acid, and water (50:37.5:3:2, by vol.) (Jolly *et al.* 1997). Lipids were visualized using iodine (phospholipids) or 6-(p-toluidino)-2-naphthalenesulfonic acid (TNS) (neutral lipids) and identified using commercially available standards (Avanti, Polar Lipids, Alabaster, AL). Once lipids were visualized, the silica was scraped into glass scintillation vials and 0.5 mL ddH$_2$O was added to facilitate desorption of lipids from the silica. Then 10 mL of Scintiverse BD cocktail (Fisher Scientific, Pittsburg, PA, USA) was added and samples were mixed by vortexing and then allowed to settle for one hour. Samples were counted on a Beckman LS 6500 liquid scintillation counter equipped with low-level detection software (Fullerton, CA, USA).

PCR

Snca gene-ablation (neomycin-resistance gene- NeoR) and wild type Snca

expression was determined using PCR. Briefly, 20mg of brain tissue from infused mice

was extracted to obtain crude gDNA. Primers were chosen for Snca forward

(5'GGGTATTGATGGCTGCATCAGAG3'), Snca Reverse

(5'CACCAGCCTATCCAGGTTGAGTTC3'), NeoR (5'GATTGCACGCAGGTTCTCCG3'),

NeoR (5'CCAACGCTATGTCCTGATAG3') amplification (Integrated DNA Technologies,

Coralville, IA, USA). Following extraction, GoTaq mastermix (Promega, Madison, WI)

was utilized with 1 μL each of forward and reverse primers (10 μM) to perform PCR.

Samples were denatured at 95°C for 3 min, followed by 35 cycles of 30 sec at 95°C, 30

sec at 54°C, and 1 min at 72°C, and ending with 5 min extension at 72°C. Samples

were then resolved on a 1% agarose gel containing 50 ug of ethidium bromide and

visualized on a ChemiDoc XRS+ UV light box (BioRad, Hercules, CA). Image analysis

was completed with Quantity One software (BioRad, Hercules, CA).

Protein Quantification

Protein content in the tissue residue was quantified using a modified dye-binding

assay utilizing bovine serum albumin as a standard (Bradford 1976). The tissue residue

was dried of residual solvent and then subject to hydrolysis with 0.2 KOH at 65°C

overnight (Murphy and Horrocks 1993). Samples were then mixed with dye binding

reagent and allowed to equilibrate for 10 min prior to reading on a spectrophotometer at

595 nm.

Statistics

Statistical analysis was done using Instat® statistical program (Graphpad, San

Diego, CA). Multiple comparisons were assessed using a one-way ANOVA with a

Tukey-Kramer *post hoc* test, with p < 0.05 considered as significant, n=10-11. A two-

tailed Student's *t*-test was used to determine significance between treatment groups,

with *p* < 0.05 considered to be significant, n=10-11.

RESULTS

Plasma curves of [1-^{14}C]20:4n-6 infused into wild type and Snca gene-ablated mice are not different between groups

Because fatty acids are infused into animals based on weight it is important to quantify how much tracer reaches plasma and that animals are reaching a steady state concentration. Plasma is tested at several time points throughout the tracer infusion. These data indicate that wild type and *Snca* gene-ablated mice received equal quantities of infused radiotracer (Figure 31). To further quantify infused radiotracer, plasma curves were integrated to determine area under the curve. There were was no difference found between area under the curve of wild type (1634 +/- 263) or *Snca* gene-ablated (1436 +/- 336) mice (table 3). These data indicate that groups received equal quantities of infused radiotracer.
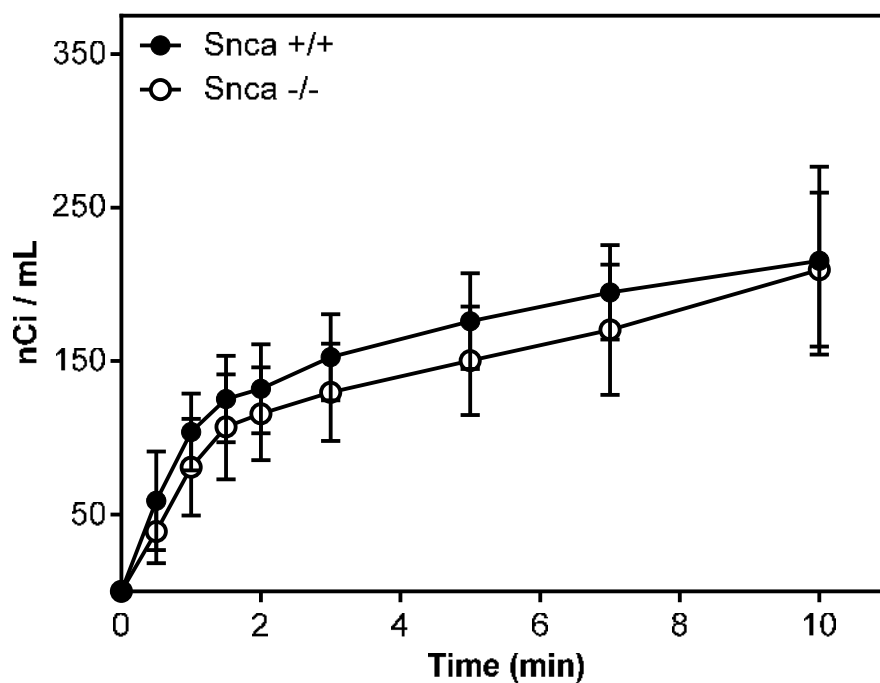
Figure 31. [1-14C]20:4n-6 tracer in plasma during 10 minute infusion. Organic plasma curve of infused wild type (Snca +/+ filled circle) or *Snca* gene-ablated (Snca -/- unfilled circle) mice over 10 minute infusion. Values represent means ± standard deviation (n=10-11).

Plasma Curve (Area Under Curve)

Snca +/+	1634 ± 263
Snca -/-	1436 ± 336

Table 3. Integrated plasma curve area. Integrated area under plasma curve of wild type (Snca +/+) or *Snca* gene-ablated (Snca -/-) mice. Values represent means ± standard deviation (n=10-11).

PCR of brain tissue of wild type and Snca gene-ablated mice

Because previous data has shown that *Snca* deficient mice have reduced [1-^{14}C]20:4n-6

uptake and incorporation into phospholipid pools, we confirmed the groups used in this

experiment by genotyping of the brain tissue. Due to the required time and effort of

mouse surgery and infusion only 3 – 4 mice may be infused per day and therefore

several groups of mice are required. To confirm our samples were not mislabeled, all

mice were genotyped but one mouse per surgery group is shown (Figure 32). As

expected, WT mouse brain expressed *Snca* while *Snca* gene-ablated mice did not

produce any bands corresponding to genomic *Snca* (Figure 32A). Inversely, the marker

gene after *Snca* gene-ablation, neomycin resistance gene (NeoR), was only expressed

in *Snca* gene-ablated mice (KO) (Figure 32B).
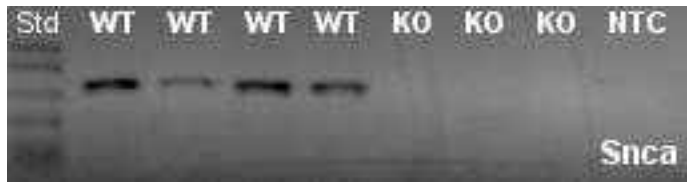
A

B

Figure 32. Tissue genotyping by PCR of mouse brain. An example of mouse *Snca*

gDNA expression in wild type (WT) or *Snca* gene-ablated mice (A). An example of

mouse NeoR gDNA expression in wild type (WT) or *Snca* gene-ablated mice (B).

Snca gene-ablation reduces [1-^{14}C]20:4n-6 uptake but not metabolic targeting into brain

Following brain lipid extraction, radioactivity in organic and aqueous fractions was

determined. In *Snca* gene-ablated mice there was a significant increase in both organic

and aqueous fractions as compared to wild type mice (Figure 33). As expected there

was also a significant increase in the total (organic and aqueous fractions combined)

radioactivity. These data indicate more [1-^{14}C]20:4n-6 tracer enters into both the organic

fraction, primarily representing incorporation into lipid pools, and into the aqueous

fraction, representing products of β-oxidation. Interestingly, there was no difference in

the fractional distribution of organic or aqueous fractions (Figure 34) suggesting

distribution into metabolic pools was not affected by *Snca* gene-ablation.
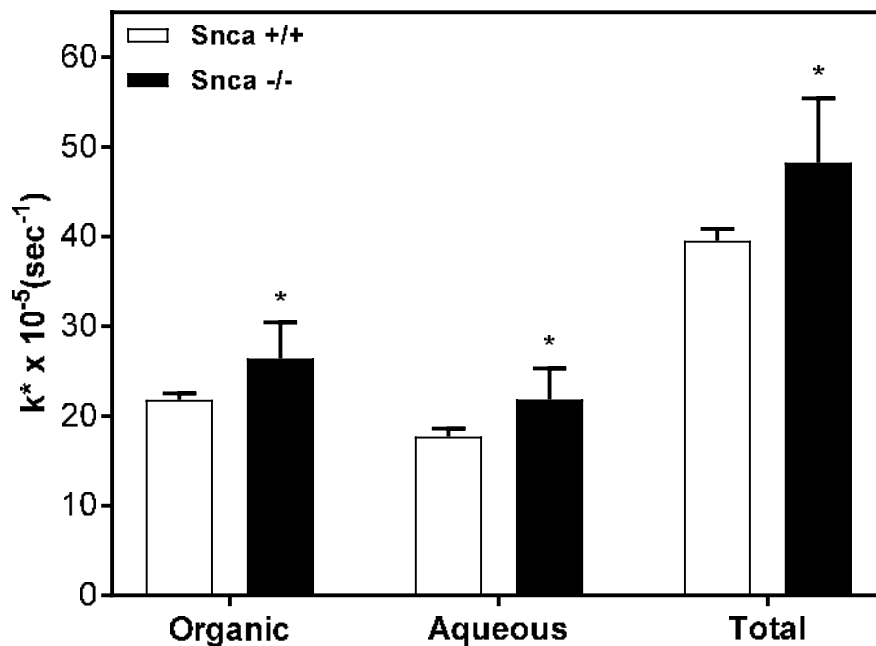
Figure 33. [1-14C]20:4n-6 incorporation into organic and aqueous brain fraction in wild

type or *Snca* gene-ablated mice. The extent of [1-^{14}C]20:4n-6 organic and aqueous

fraction incorporation into brain of wild type (Snca +/+) or *Snca* gene-ablated (Snca -/-)

mice following 3 h LPS (i.p. 1 mg/kg) treatment. Values represent means ± standard

deviation (n=10-11). The asterisk indicates a statistically significant difference from wild

type (control) mice using Student's *t*-test ($p < 0.05$).
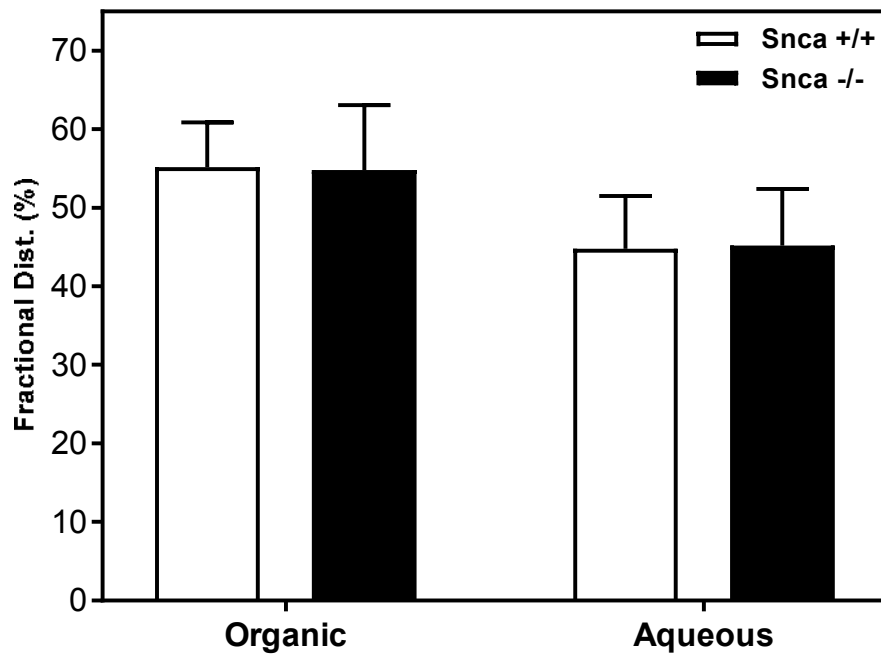
Figure 34. [1-14C]20:4n-6 fractional distribution into brain fraction in wild type or *Snca*

gene-ablated mice. The extent of [1-^{14}C]20:4n-6 organic and aqueous fractional

distribution into brain of wild type (Snca +/+) or *Snca* gene-ablated (Snca -/-) mice

following 3 h LPS (i.p. 1 mg/kg) treatment. Values represent means ± standard

deviation (n=10-11).

[1-¹⁴C]20:4n-6 uptake and metabolic targeting in liver are not different between groups

Because liver does not express *Snca* (Golovko *et al.* 2005) we used liver as a negative control. Consistent with previously published data, *Snca* gene-ablation does not affect uptake or metabolic targeting of [1-¹⁴C]20:4n-6 in the liver (Figure 35 and 36).
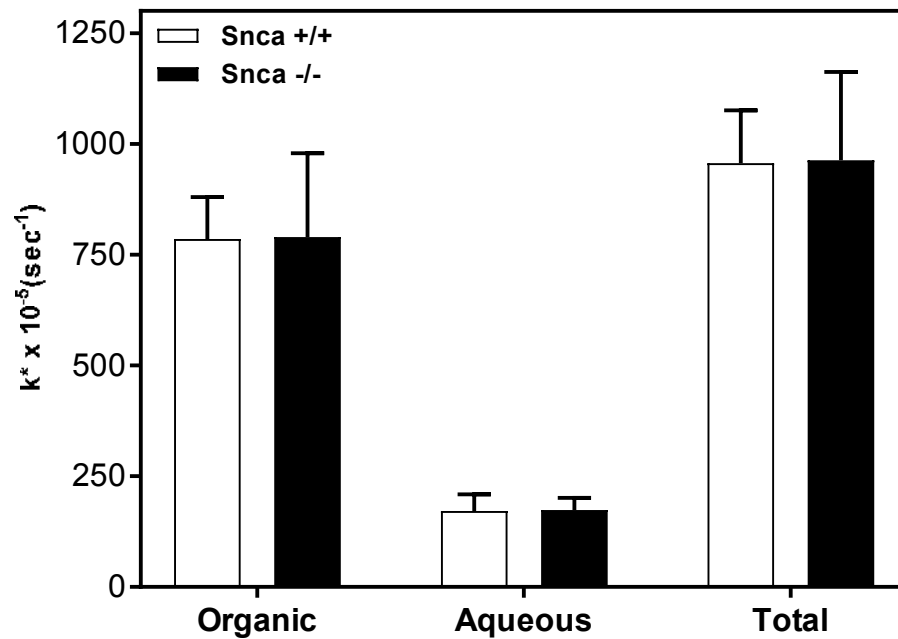
Figure 35. [1-14C]20:4n-6 incorporation into organic and aqueous liver fraction in wild type or *Snca* gene-ablated mice. The extent of [1-¹⁴C]20:4n-6 organic and aqueous fraction incorporation into liver of wild type (Snca +/+) or *Snca* gene-ablated (Snca -/-) mice following 3 h LPS (i.p. 1 mg/kg) treatment. Values represent means ± standard deviation (n=10-11).
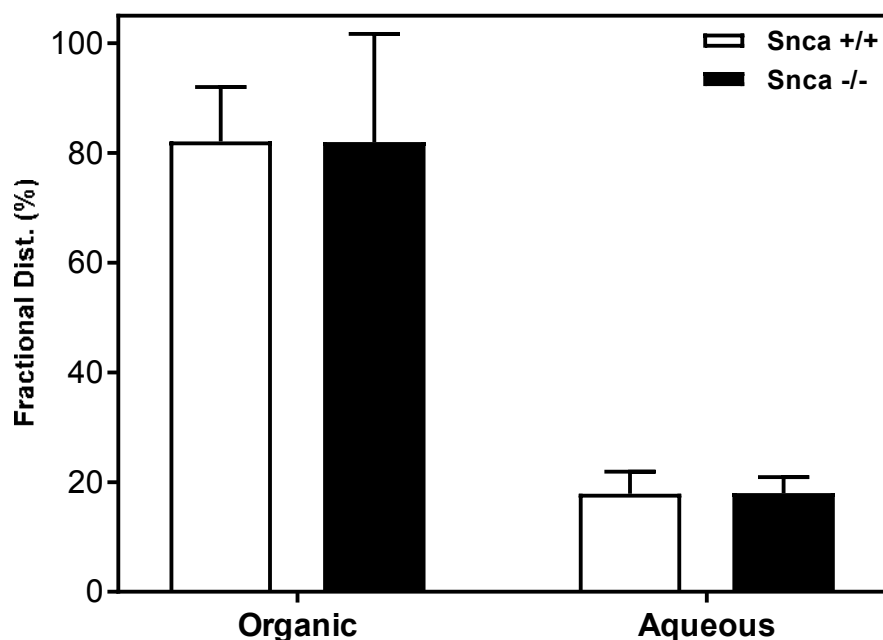
Figure 36. [1-14C]20:4n-6 fractional distribution into liver fraction in wild type or *Snca* gene-ablated mice. The extent of [1-^{14}C]20:4n-6 organic and aqueous fractional distribution into liver of wild type (Snca +/+) or *Snca* gene-ablated (Snca -/-) mice following 3 h LPS (i.p. 1 mg/kg) treatment. Values represent means ± standard deviation (n=10-11).

Total uptake into phospholipids and neutral lipids of [1-^{14}C]20:4n-6 is altered between groups in brain but not liver

After determining organic and aqueous fraction radioactivity, the organic fraction is separated by column chromatography into neutral lipid and phospholipid pools. In the brain there is a significant 1.4-fold increase in targeting into the phospholipid pool, but no change in neutral lipids of *Snca* gene-ablated mice (Figure 37). Targeting to neutral lipids and phospholipids is not significantly altered in liver (Figure 38), which is consistent with the lack of any difference in the total organic fraction between groups.

These data suggest that the increase in brain organic fraction is esterified into the

phospholipid pool.

Figure 37. [1-14C]20:4n-6 incorporation into brain neutral or phospholipids in wild type or

Snca gene-ablated mice. The extent of [1-^{14}C]20:4n-6 incorporation into brain neutral

and phospholipids of wild type (Snca +/+) or *Snca* gene-ablated (Snca -/-) mice following

3h LPS (i.p. 1mg/kg) treatment. Values represent means ± standard deviation (n=10-

11). The asterisk indicates a statistically significant difference from wild type (control)

mice using Student's *t*-test ($p < 0.05$).
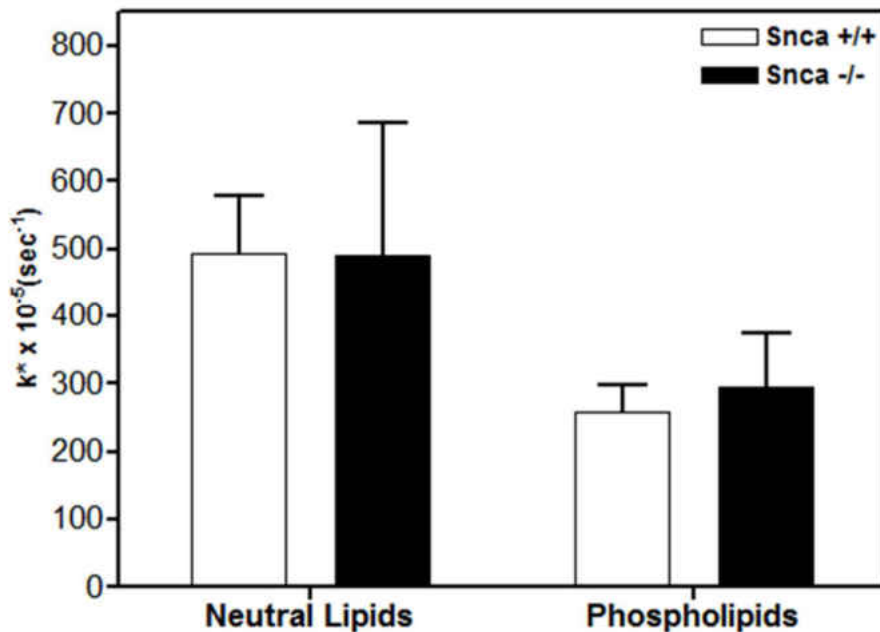
Figure 38. [1-14C]20:4n-6 incorporation into liver neutral or phospholipids in wild type or

Snca gene-ablated mice. The extent of [1-^{14}C]20:4n-6 incorporation into liver neutral

and phospholipids of wild type (Snca +/+) or *Snca* gene-ablated (Snca -/-) mice following

3 h LPS (i.p. 1 mg/kg) treatment. Values represent means ± standard deviation (n=10-

11).

Esterification of [1-^{14}C]20:4n-6 into neutral lipid and phospholipid fractions were altered by Snca gene-ablation in brain

Snca gene-ablated mice had significantly increased radioactivity in the

phosphatidylinositol (PtdIns) and the choline glycerophospholipids (ChoGpl) in the brain,

which is consistent with the enhanced incorporation into brain phospholipids (Table 5).

Enhanced incorporation into PtdIns is noteworthy as it is a vital phospholipid involved

with PLC-mediated signal transduction and for 2-AG formation. The increase of [1-

^{14}C]20:4n-6 into ChoGpl, a storage phospholipid for 20:4n-6 in the brain, suggests that there is increased ChoGpl turnover during LPS induced inflammation and subsequent increased incorporation of tracer in *Snca* gene-ablated mice. Consistent with previous data, *Snca* ablation increases phospholipase D activity causing increased turnover of ChoGpl, a PLD substrate (Golovko *et al.* 2006a). *Snca* gene-ablation reduced diacylglycerol by 75% (Table 5), which could result from either a reduction in DAG formation by phospholipase C or a greater utilization of DAG for phospholipid synthesis, consistent with the increased phospholipid fraction.

	$k^* \times 10^{-5}$ (sec^{-1})				Fractional Dist. (%)				
	WT		KO		WT		KO		
	Mean	STD	Mean	STD	Mean	STD	Mean	STD	
DAG	0.22	0.23	0.06	0.10 *	5.3	5.6	1.0	1.8	*
FFA	3.40	1.20	4.58	2.17 ns	84.0	29.7	84.3	40.0	ns
TAG	0.45	0.37	0.80	0.52 ns	11.2	9.1	14.7	9.5	ns
Ptd$_2$Gro	0.09	0.12	0.06	0.09 ns	0.8	1.0	0.4	0.7	ns
EtnGpl	0.97	0.46	1.11	0.54 ns	8.5	4.0	7.8	3.8	ns
PtdIns	3.67	0.67	4.85	1.02 *	32.2	5.9	34.0	7.1	ns
PtdSer	0.32	0.31	0.49	0.43 ns	2.8	2.7	3.4	3.0	ns
ChoGpl	6.35	0.76	7.78	1.11 *	55.7	6.7	54.5	7.8	ns

* denotes significance $p < 0.05$ Student's unpaired, two-tailed t-test

Table 5. [1-^{14}C]20:4n-6 incorporation into individual brain neutral or phospholipids in wild type or *Snca* gene-ablated mice. The extent of [1-^{14}C]20:4n-6 incorporation into brain neutral lipids or esterification into phospholipids of wild type (Snca +/+) or *Snca* gene-ablated (Snca -/-) mice following 3 h LPS (i.p. 1 mg/kg) treatment. Values represent

means ± standard deviation (n=10-11). The asterisk indicates a statistically significant

difference from wild type (control) mice using Student's *t*-test (*p* < 0.05).

Esterification of [1-^{14}C]20:4n-6 into neutral lipid fractions were altered by Snca gene-ablation but not into phospholipids in liver

Following separation of neutral lipids and phospholipids, samples are further separated

into individual lipid fractions. Tracer entering into free fatty acid and diacylglycerol pools

is significantly increased in *Snca* gene-ablated mice. Similar to previously published

results, *Snca* gene-ablation had no impact on tracer incorporation into liver

phospholipids.

	$k^* \times 10^{-5}$ (sec^{-1})					Fractional Dist. (%)				
	WT		KO			WT		KO		
	Mean	STD	Mean	STD		Mean	STD	Mean	STD	
Chol	10.4	2.2	13.6	3.8	ns	2.2	0.1	2.8	0.8	ns
DAG	12.9	2.3	19.2	5.0	*	2.8	0.5	3.9	1.0	*
FFA	33.0	12.0	51.6	18.0	*	7.1	2.6	10.6	3.7	ns
TAG	406.7	48.8	399.9	152.7	ns	87.6	10.5	82.2	31.4	ns
CE	1.6	0.5	2.0	0.8	ns	0.3	0.1	0.4	0.2	ns
Ptd$_2$Gro	8.5	5.6	11.8	7.7	ns	4.0	2.6	5.4	3.5	ns
PtdOH	7.0	2.6	4.7	1.8	ns	3.3	1.2	2.1	0.8	ns
EtnGpl	23.4	10.2	23.6	12.8	ns	10.9	4.8	10.7	5.8	ns
PtdIns	18.5	7.0	18.1	9.6	ns	8.6	3.3	8.2	4.3	ns
PtdSer	135.3	56.7	136.0	62.1	ns	1.6	0.7	3.5	2.8	ns
ChoGpl	135.3	56.7	136.0	62.1	ns	63.3	26.5	61.7	28.2	ns
CerPCho	3.1	1.3	3.4	2.0	ns	1.5	0.6	1.5	0.9	ns
lysoPtdCho	14.6	8.0	15.3	8.9	ns	6.8	3.7	6.9	4.0	ns

* denotes significance p < 0.05 Student's unpaired, two-tailed t-test
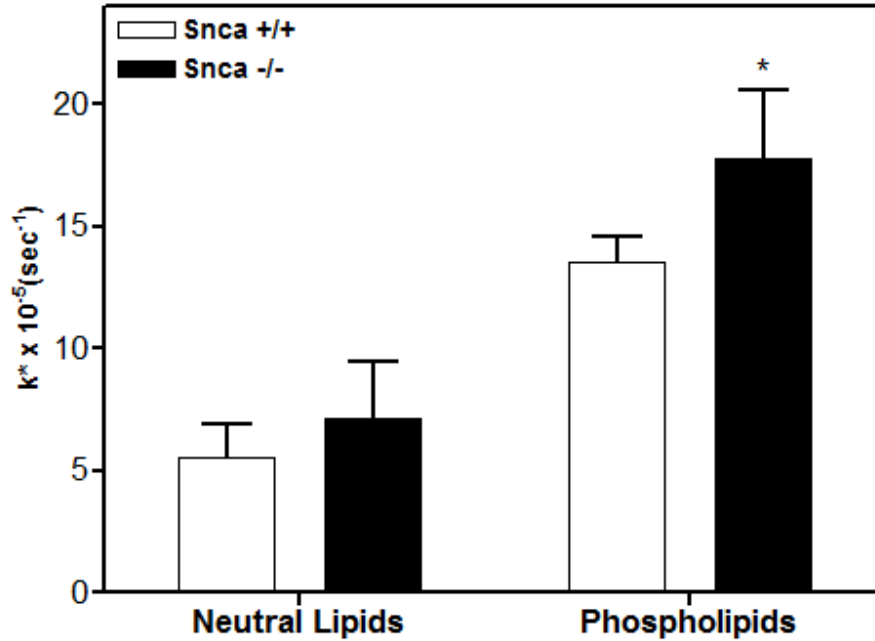
Table 5. [1-^{14}C]20:4n-6 incorporation into individual liver neutral or phospholipids in wild type or *Snca* gene-ablated mice. The extent of [1-^{14}C]20:4n-6 incorporation into liver neutral lipids or esterification into phospholipids of wild type (Snca +/+) or *Snca* gene-ablated (Snca -/-) mice following 3 h LPS (i.p. 1 mg/kg) treatment. Values represent means ± standard deviation (n=10-11). The asterisk indicates a statistically significant difference from wild type (control) mice using Student's *t*-test ($p < 0.05$).

DISCUSSION

In this study, we applied a well-defined radiotracer steady-state kinetic model to determine fatty acid uptake and turnover to determine if *Snca* ablation altered ARA metabolism during neuroinflammation. *Snca* expression is known to affect brain fatty acid uptake and trafficking into specific lipid pools, including increased ARA uptake and incorporation by modulating ER-localized Acsl activity (Golovko *et al.* 2006a). Incubation with wildtype, but not mutant forms of Snca protein restores Acsl activity to produce ARA-CoA in microsomes isolated from *Snca* ablated mice (Golovko *et al.* 2006a). Similarly, dysfunctional ARA metabolism in *Snca* ablated mice results in increased prostaglandin biosynthesis (Golovko and Murphy 2008) suggesting a pivotal role of Snca in the inflammatory response.

Snca has a role in the inflammatory response of microglia via modulation of lipid mediated signaling pathways (Austin *et al.* 2006). Snca inhibits PLD activity in yeast (Outeiro and Lindquist 2003) as well as in animal studies (Jenco *et al.* 1998). PLD activity is essential for activation of microglia required for inflammatory response including expression of key cytokines such as IL-1 and TNF-α (Austin *et al.* 2006; Austin *et al.* 2011). Butanol treatment attenuated PLD-mediated generation of increased cytokine secretion observed in *Snca* ablated microglia (Austin *et al.* 2011) suggesting Snca has a direct effect on inflammation via PLD2 pathway. Hence, Snca is known to affect ARA metabolism producing inflammatory metabolites as well as PLD2 activity modulation, key players in lipid mediated signal transduction. In microglia, *Snca* deficiency results in a basally reactive phenotype and secretory phenotype that was

exacerbated following LPS stimulation (Rojanathammanee *et al.* 2011). Because Snca increases eicosanoid synthesis and lipid mediated signaling, it is important to asses if Snca modulates ARA metabolism in the presence of inflammatory response.

In the absence of *Snca* expression, brain ARA uptake as well as targeting to organic and aqueous fractions are increased during LPS stimulation (Figure 33), indicating more tracer is entering the *Snca* deficient brain. However, metabolic distribution into organic or aqueous fractions is unaffected (Figure 34). These results are consistent with the increased ARA uptake and trafficking to organic fractions of dBcAMP stimulated astrocytes (Figure 1), which also had reduced *Snca* expression (Figure 13). This is in contrast to ARA uptake and targeting into unstimulated *Snca* deficient mice, where ARA uptake and targeting into brain organic fraction is reduced while the aqueous fraction remained unchanged (Golovko *et al.* 2006a). This previous study in unstimulated mice is consistent with other studies that observed a decrease in the uptake and trafficking of 16:0 in *Snca* deficient unstimulated mouse brain (Golovko *et al.* 2005)and astrocytes (Castagnet *et al.* 2005). Under inflammatory conditions, the lack of *Snca* enhances ARA uptake and trafficking into fractions associated with lipid-mediated signaling consistent with inflammatory response.

The incorporation into total phospholipids is increased in *Snca* gene-ablated mice, suggesting enhanced phospholipid pool targeting (Figure 37). This is consistent with increased targeting into phospholipids in dBcAMP treated astrocytes (Figure 4) due to selective increased *Acsl* expression (Figure 10,11). However, due to decreased Acsl activity in *Snca* deficient mouse brain that is not subjected to inflammation, other mechanisms are anticipated. FABP bind and chaperon fatty acids which facilitates uptake and targeting as well as affecting phospholipid metabolism (Binas *et al.* 1999; Murphy *et al.* 2000a; Murphy *et al.* 2005). The brain has detectable protein levels of

FABP3, FABP5, and FABP7 (Owada and Kondo 2003; Owada *et al.* 1996; Owada 2008; Veerkamp and Zimmerman). FABP3 is expressed in the brain primarily in neurons, with the highest expression in cortical layers, in hippocampus, and in dentate gyrus (Owada *et al.* 1996; Sellner *et al.* 1995). FABP3 has a binding preference for *n-6* fatty acids (Hanhoff *et al.* 2002), suggesting that this protein may be involved in the increased uptake and trafficking of ARA in brain (Murphy *et al.* 2005). Further study is needed to elucidate the mechanism by which ARA uptake and trafficking into phospholipids is regulated in the brain following LPS stimulation.

In the absence of *Snca*, there is a reduction in brain unesterified free fatty acid mass (Sharon *et al.* 2003). While we did not determine free fatty acid mass we found a significant increase in free fatty acid incorporation into stimulated *Snca* deficient liver but brain incorporation was not changed suggesting Snca has a role in free fatty acid trafficking at least in liver during the inflammatory response. There was no change in incorporation into liver phospholipids which is consistent with previously published data (Golovko *et al.* 2006a). Because Snca protein is not detected in the liver (Golovko *et al.* 2005), the increase in diacylglycerol and free fatty acid incorporation is possibly a result of lipid alteration in systemic metabolism and requires further study.

Snca gene-ablated mice had significantly increased ARA trafficking into phosphatidylinositol and choline glycerophospholipids in the brain and is consistent with the enhanced incorporation into brain phospholipids (Table5). Both PtdIns and ChoGpl contain high amounts of ARA. Increased trafficking into PtdIns may have a significant impact on PLC mediated signaling events and may account for the increased 2-AG formation in LPS treated *Snca* deficient brain (Figure 14). The increase of ARA incorporation into ChoGpl, the initial storage phospholipid for ARA in the brain, suggests that there is increased ChoGpl turnover during LPS induced inflammation and

subsequent increased incorporation of tracer in *Snca* gene-ablated mice. Consistent with

previous data, *Snca* ablation increases phospholipase D activity causing increased

turnover of ChoGpl, a PLD substrate (Golovko *et al.* 2006a). Snca tonically inhibits PLD

and in *Snca* deficient microglia there is enhanced PLD activity and increased ARA

metabolism (Austin *et al.* 2006). In brain, *Snca* gene-ablation reduced diacylglycerol

which could result from either a reduction in diacylglycerol formation by PLC or a greater

utilization of diacylglycerol for phospholipid synthesis, consistent with the increased

phospholipid fraction. This is important because ARA is the major polyunsaturated

fatty acid at the *sn*-2 position in EtnGpl and ChoGpl (Svennerholm 1968; Murphy 1984;

López *et al.* 1995).

In summary, these data suggest that during LPS-induced neuroinflammation

where ARA release is enhanced, Snca has a critical role in maintaining ARA metabolism

and trafficking and suggests that Snca affects lipid-mediated signaling events. This work

links Snca to dysfunction in ARA metabolism resulting in an enhanced inflammatory

response. Interestingly, when ARA metabolism is enhanced, in *Snca* deficient mice

there is an opposite effect on uptake and trafficking of ARA when compared to *Snca*

deficient mice at basal levels. Further study is required to determine the mechanism

behind this differential affect in ARA metabolism following LPS stimulation. This work

supports current data suggesting that Snca plays a significant role in maintaining ARA

homeostasis of the brain under neuroinflammatory conditions and further study on the

role of Snca on lipid metabolism in the brain is required.

CONCLUDING REMARKS

I have used several model systems including primary cultured astrocytes and microglia, *Snca* deficient and mutant knock-in mice, and a steady state-kinetic mouse model to determine the role of Snca lipid-mediated signal transduction during neuroinflammation. Herein, we have determined several major roles of Snca during inflammation:

(i) Astrocytes play a vital role in brain lipid metabolism. Therefore, we determined the impact of dBcAMP treatment on radiolabeled ARA and 16:0 uptake and metabolism in primary cultured murine cortical astrocytes. In dBcAMP treated astrocytes, total ARA uptake was increased 1.9-fold compared to control, while total 16:0 uptake was unaffected. dBcAMP treatment increased expression of *Acsl*3 (4.8-fold) and *Acsl*4 (1.3-fold), which preferentially use ARA and are highly expressed in astrocytes, consistent with the increase in ARA uptake. However, expression of *Fabp*5 and *Fabp*7 were significantly reduced by 25% and 45%, respectively. *Acot7* (20%) was also reduced, suggesting dBcAMP treatment favors acyl-CoA formation. dBcAMP treatment enhanced ARA (2.2-fold) and 16:0 (1.6-fold) esterification into total phospholipids, but the greater esterification of ARA is consistent with the observed uptake through increased *Acsl*, but not *Fabp* expression. Although total 16:0 uptake was not affected, there was a dramatic decrease in 16:0 in the free fatty acid pool as esterification into the phospholipid pool was increased, which is consistent with the increase in *Acsl3* and *Acsl4* expression. In summary, our data demonstrates that dBcAMP treatment increases ARA uptake in astrocytes and this increase appears to

111

be due to increased expression of *Acsl3* and *Acsl4* coupled with a reduction in *Acot7* expression all of which occurs in the presence of reduced *Snca* expression.

(ii) *Snca* deficient mice have higher basal brain 2-AG levels compared to wildtype and LPS stimulation further exacerbated 2-AG synthesis. Microglia isolated from *Snca* gene-ablated mice have reduced phagocytic ability (Austin *et al.* 2006), while having elevated levels of proinflammatory cytokines and eicosanoids. Because 2-AG, a ligand of CB2 receptors, has an important role in microglia motility (Walter *et al.* 2003), we examined its association with *Snca* expression. We treated *Snca* gene-ablated mice with LPS, which increased brain 2-AG levels compared to control mice. In control mice, brain *Snca* expression was unchanged 3 hours after LPS-treatment, although eicosanoid levels were significantly elevated. Interestingly, *Snca* deficient mice had higher basal brain 2-AG levels compared to control. The increase in basal and LPS-stimulated 2-AG levels in *Snca* deficient mice could result from multiple pathways and/or cell types and may be inherently linked to the observed increase in ARA incorporation into PtdIns during inflammation in brains of *Snca* gene-ablated mice.

(iii) In microglia from control mice, LPS-treatment reduced 2-AG levels in the medium at 12h to 24h but not at 6h when compared with non-stimulated microglia. Concomitantly, *Snca* expression was reduced at 12h to 24h but not 6h after LPS-stimulation. In *Snca* gene-ablated mice, LPS-treatment also reduced 2-AG levels in the medium compared to non-treated *Snca* deficient microglia, but was delayed to 24h and was not reduced to the same extent as control. Our data supports the hypothesis that *Snca* expression is linked to 2-AG release in primary microglia and may contribute to regulating the phagocytic phenotype *in vivo*. However, further study is needed to elucidate the increase in basal brain 2-AG levels of *Snca* deficient mice and the greater response to LPS-stimulation.

(iv) Using *Snca* gene-ablated mice, we determined the impact of Snca on brain ARA metabolism during LPS-induced inflammatory response *in vivo* using an established steady-state kinetic model. In liver, no significant differences were observed in ARA uptake or incorporation into lipid pools between groups. In *Snca* deficient mouse brain, there was a significant 1.3-fold increase in ARA uptake. This indicated more ARA entering the *Snca* deficient brain from plasma. In the organic fraction, there was a significant 1.4-fold increase into total phospholipids in KO mice, accounted for by increased incorporation into choline glycerophospholipids and phosphatidylinositol. In neutral lipid pools, ARA incorporation into diacylglycerols was reduced 75% in KO mice. Hence, under inflammatory conditions where ARA release is enhanced, Snca has a crucial role in maintaining ARA metabolism, and in the absence of Snca results in increased uptake and incorporation into lipid pools associated with enhanced lipid-mediated signaling during neuroinflammatory response.

These data suggest that under inflammatory conditions where ARA release is enhanced, Snca has a crucial role in modulating ARA metabolism, and the absence of Snca results in increased uptake and incorporation into lipid pools associated with enhanced lipid-mediated signaling during neuroinflammatory response. This work supports current data suggesting that Snca plays a significant role in maintaining homeostasis of the brain under neuroinflammatory conditions and further study on Snca mechanistic action is warranted.

APPENDICIES

Abbreviations

16:0, PAM, palmitic acid

18:2n-6, LNA, linoleic acid

20:4n-6, ARA, arachidonic acid

22:6n-3, DHA, docosahexaenoic acid

2-AG, 2-arachidonyl glycerol

6-ketoPGF$_{1\alpha}$, 6-keto Prostaglandin F$_{1\alpha}$

Acot7, Acyl-CoA thioesterase

Acsl, long-chain acyl-CoA synthetase

ApoE, apolipoprotein E

Cer<u>P</u>Cho, sphingomyelin

ChoGpl, choline glycerophospholipids

CNS, Central Nervous System

COX-1/2, Cyclooxygenase – 1/2

DAG, diacylglycerol(s)

dBcAMP, dibutyryl-cAMP

Endocannabinoid receptor (1/2) eCB1r

Endocannabinoid, eCB

EtnGpl, ethanolamine glycerophospholipids

FABP3, (Heart)- fatty acid binding protein 3

FABP5, (Epidermal)- fatty acid binding protein 5

FABP7, (Brain)- fatty acid binding protein 7

FFA, free fatty acids

GPCR, G protein coupled receptor

hSnca, Human α-synuclein

IL-1, Interluken-1

IL-6, Interluken-6

KO, Snca gene ablated

LDLR, low-density lipoprotein receptors

LPS, lipopolysaccharide

MPTP, 1-methyl-4-phenyl-1,2,3,6-tetrahydropyridine

NeoR, Neomycin resistance gene

PD, Parkinson's Disease

PGD_2, Prostaglandin D_2

PGE_2, Prostaglandin E_2

$PGF_{2\alpha}$, Prostaglandin $F_{2\alpha}$

PLA_2, Phospholipase A_2

PLC, Phospholipase C

PLD, Phospholipase D

PtdSer, phosphatidylserine

PtdIns, Phosphatidylinositol

PUFA, polyunsaturated fatty acids

SDHA, succinate dehydrogenase complex, subunit A, (flavoprotein)

Snca, α-synuclein

TAG, triacylglycerol(s)

TNF-α, Tumor necrosis facto

WT, Wild type

Copyright permission

REFERENCES

Adamczyk A., Solecka J., Strosznajder J. B. (2005) Expression of alpha-synuclein in different brain parts of adult and aged rats. *J. Physiol. Pharmacol.* **56**, 29–37.

Ahn B.-H., Rhim H., Kim S. Y., Sung Y.-M., Lee M.-Y., Choi J.-Y., Wolozin B., et al. (2002) α-Synuclein Interacts with Phospholipase D Isozymes and Inhibits Pervanadate-induced Phospholipase D Activation in Human Embryonic Kidney-293 Cells. *J. Biol. Chem.* **277**, 12334–12342.

Ahn K., McKinney M. K., Cravatt B. F. (2008) Enzymatic Pathways That Regulate Endocannabinoid Signaling in the Nervous System. *Chem. Rev.* **108**, 1687–1707.

Alger B. E., Kim J. (2011) Supply and demand for endocannabinoids. *Trends Neurosci.* **34**, 304–315.

Allen G. W., Liu J. W., León M. De (2000) Depletion of a fatty acid-binding protein impairs neurite outgrowth in PC12 cells. *Mol. Brain Res.* **76**, 315–324.

Austin S. A., Floden A. M., Murphy E. J., Combs C. K. (2006) Alpha-synuclein expression modulates microglial activation phenotype. *J. Neurosci.* **26**, 10558–63.

Austin S. A., Rojanathammanee L., Golovko M. Y., Murphy E. J., Combs C. K. (2011) Lack of alpha-synuclein modulates microglial phenotype in vitro. *Neurochem. Res.* **36**, 994–1004.

Babcock A. A., Wirenfeldt M., Finsen B. (2013) Quantification of Microglial Proliferation and Apoptosis by Flow Cytometry, in *Methods Mol. Biol.*, Vol. 1041, pp. 129–145.

Balendiran G. K., Schnutgen F., Scapin G., Borchers T., Xhong N., Lim K., Godbout R., Spener F., Sacchettini J. C. (2000) Crystal structure and thermodynamic analysis of

human brain fatty acid-binding protein. *J. Biol. Chem.* **275**, 27045–27054.

Barceló-Coblijn G., Golovko M. Y., Weinhofer I., Berger J., Murphy E. J. (2007) Brain neutral lipids mass is increased in α-synuclein gene-ablated mice. *J. Neurochem.* **101**, 132–141.

Barcia C., Bahillo A. S., Fernández-Villalba E., Bautista V., Poza Y Poza M., Fernández-Barreiro A., Hirsch E. C., Herrero M.-T. (2004) Evidence of active microglia in substantia nigra pars compacta of parkinsonian monkeys 1 year after MPTP exposure. *Glia* **46**, 402–409.

Beffert U., Stolt P. C., Herz J. (2004) Functions of lipoprotein receptors in neurons. *J. Lipid Res.* **45**, 403–409.

Bektas M., Payne S. G., Liu H., Goparaju S., Milstien S., Spiegel S. (2005) A novel acylglycerol kinase that produces lysophosphatidic acid modulates cross talk with EGFR in prostate cancer cells. *J. Cell Biol.* **169**, 801–811.

Bernhardi R. von, Eugenín-von Bernhardi L., Eugenín J. (2015) Microglial cell dysregulation in brain aging and neurodegeneration. *Front. Aging Neurosci.* **7**, 124.

Bernoud N., Fenart L., Bénistant C., Pageaux J. F., Dehouck M. P., Molière P., Lagarde M., Cecchelli R., Lecerf J. (1998) Astrocytes are mainly responsible for the polyunsaturated fatty acid enrichment in blood-brain barrier endothelial cells in vitro. *J. Lipid Res.* **39**, 1816–1824.

Bignami A., Dahl D. (1976) The astroglial response to stabbing. Immunofluorescence studies with antibodies to astrocytic specific protein (GFA) in mammalian and sub-mammalian vertebrates. *Neuropathol. Appl. Neurobiol.* **2**, 99–110.

Binas B., Danneberg H., McWhir J., Mullins L., Clark A. J. (1999) Requirement for the heart-type fatty acid binding protein in cardiac fatty acid utilization. *FASEB J.* **13**, 805–812.

Bisogno T., Berrendero F., Ambrosino G., Cebeira M., Ramos J. A., Fernandez-Ruiz J. J., Marzo V. Di (1999) Brain Regional Distribution of Endocannabinoids: Implications for Their Biosynthesis and Biological Function. *Biochem. Biophys. Res. Commun.* **256**, 377–380.

Bisogno T., Howell F., Williams G., Minassi A., Cascio M. G., Ligresti A., Matias I., et al. (2003) Cloning of the first sn1-DAG lipases points to the spatial and temporal regulation of endocannabinoid signaling in the brain. *J. Cell Biol.* **163**, 463–468.

Blankman J. L., Simon G. M., Cravatt B. F. (2007) A Comprehensive Profile of Brain Enzymes that Hydrolyze the Endocannabinoid 2-Arachidonoylglycerol. *Chem. Biol.* **14**, 1347–1356.

Bodner C. R., Maltsev A. S., Dobson C. M., Bax A. (2010) Differential phospholipid binding of alpha-synuclein variants implicated in Parkinson's disease revealed by solution NMR spectroscopy. *Biochemistry* **49**, 862–71.

Boyles J. K., Pitas R. E., Wilson E., Mahley R. W., Taylor J. M. (1985) Apolipoprotein E associated with astrocytic glia of the central nervous system and with nonmyelinating glia of the peripheral nervous system. *J. Clin. Invest.* **76**, 1501–1513.

Bradford M. M. (1976) A rapid and sensitive method for the quantitation of microgram quantities of protein utilizing the principle of protein-dye binding. *Anal. Biochem.* **72**, 248–254.

Brenowitz S. D., Regehr W. G. (2005) Associative Short-Term Synaptic Plasticity Mediated by Endocannabinoids. *Neuron* **45**, 419–431.

Brock T. G., Serezani C. H., Carstens J. K., Peters-Golden M., Aronoff D. M. (2008) Effects of prostaglandin E2 on the subcellular localization of Epac-1 and Rap1 proteins during Fcγ-receptor-mediated phagocytosis in alveolar macrophages. *Exp.*

Cell Res. **314**, 255–263.

Brose S. A., Golovko M. Y. (2013) Eicosanoid post-mortem induction in kidney tissue is prevented by microwave irradiation. *Prostaglandins. Leukot. Essent. Fatty Acids* **89**, 313–8.

Brose S. A., Golovko S. A., Golovko M. Y. (2016) Brain 2-Arachidonoylglycerol Levels Are Dramatically and Rapidly Increased Under Acute Ischemia-Injury Which Is Prevented by Microwave Irradiation. *Lipids* **51**, 487–495.

Bye N., Carron S., Han X., Agyapomaa D., Ng S. Y., Yan E., Rosenfeld J. V, Morganti-Kossmann M. C. (2011) Neurogenesis and glial proliferation are stimulated following diffuse traumatic brain injury in adult rats. *J. Neurosci. Res.* **89**, 986–1000.

Cabin D. E., Shimazu K., Murphy D., Cole N. B., Gottschalk W., McIlwain K. L., Orrison B., et al. (2002) Synaptic vesicle depletion correlates with attenuated synaptic responses to prolonged repetitive stimulation in mice lacking alpha-synuclein. *J. Neurosci.* **22**, 8797–807.

Cao Y., Murphy K. J., McIntyre T. M., Zimmerman G. A., Prescott S. M. (2000) Expression of fatty acid-CoA ligase 4 during development and in brain. *FEBS Lett.* **467**, 263–267.

Carlisle S. J., Marciano-Cabral F., Staab A., Ludwick C., Cabral G. A. (2002) Differential expression of the CB2 cannabinoid receptor by rodent macrophages and macrophage-like cells in relation to cell activation. *Int. Immunopharmacol.* **2**, 69–82.

Castagnet P. I., Golovko M. Y., Barceló-Coblijn G. C., Nussbaum R. L., Murphy E. J. (2005) Fatty acid incorporation is decreased in astrocytes cultured from α-synuclein gene-ablated mice. *J. Neurochem.* **94**, 839–849.

Chiurchiù V., Battistini L., Maccarrone M. (2015) Endocannabinoid signaling in innate and adaptive immunity. *Immunology* **144**, 352.

Chung Y. C., Shin W.-H., Baek J. Y., Cho E. J., Baik H. H., Kim S. R., Won S.-Y., Jin B. K. (2016) CB2 receptor activation prevents glial-derived neurotoxic mediator production, BBB leakage and peripheral immune cell infiltration and rescues dopamine neurons in the MPTP model of Parkinson's disease. *Exp. Mol. Med.* **48**, e205.

Ciesielski-Treska J., Ulrich G., Mensch C., Aunis D. (1984) Electrophoretic pattern and distribution of cytoskeletal proteins in flat-epitheloid and stellate process-bearing astrocytes in primary culture. *Neurochem. Int.* **6**, 533–543.

Coleman R. A., Lewin T. M., Horn C. G. Van, Gonzalez-Baró M. R. (2002) Do long-chain acyl-CoA synthetases regulate fatty acid entry into synthetic versus degradative pathways? *J. Nutr.* **132**, 2123–2126.

Cravatt B. F., Demarest K., Patricelli M. P., Bracey M. H., Giang D. K., Martin B. R., Lichtman A. H. (2001) Supersensitivity to anandamide and enhanced endogenous cannabinoid signaling in mice lacking fatty acid amide hydrolase. *Proc. Natl. Acad. Sci.* **98**, 9371–9376.

Croisier E., Moran L. B., Dexter D. T., Pearce R. K. B., Graeber M. B. (2005) Microglial inflammation in the parkinsonian substantia nigra: relationship to alpha-synuclein deposition. *J. Neuroinflammation* **2**, 14.

Csuka E., Hans V. H., Ammann E., Trentz O., Kossmann T., Morganti-Kossmann M. C. (2000) Cell activation and inflammatory response following traumatic axonal injury in the rat. *Neuroreport* **11**, 2587–2590.

DeMattos R. B., Brendza R. P., Heuser J. E., Kierson M., Cirrito J. R., Fryer J., Sullivan P. M., Fagan A. M., Han X., Holtzman D. M. (2001) Purification and characterization of astrocyte-secreted apolipoprotein E and J-containing lipoproteins from wild-type and human apoE transgenic mice. *Neurochem. Int.* **39**, 415–425.

Devane W. A., Dysarz F. A., Johnson M. R., Melvin L. S., Howlett A. C. (1988) Determination and characterization of a cannabinoid receptor in rat brain. *Mol. Pharmacol.* **34**, 605–13.

Dietschy J. M., Spady D. K., Stange E. F. (1983) Quantitative Importance of Different Organs for Cholesterol-Synthesis and Low-Density-Lipoprotein Degradation. *Biochem. Soc. Trans.* **11**, 639–641.

Dietschy J. M., Turley S. D. (2001) Cholesterol metabolism in the brain. *Curr. Opin. Lipidol.* **12**, 105–112.

Elshourbagy N. A., Liao W. S., Mahley R. W., Taylor J. M. (1985) Apolipoprotein E mRNA is abundant in the brain and adrenals, as well as in the liver, and is present in other peripheral tissues of rats and marmosets. *Proc. Natl. Acad. Sci. U. S. A.* **82**, 203–207.

Fan Y., Xie L., Chung C. Y. (2017) Signaling Pathways Controlling Microglia Chemotaxis. *Mol. Cells* **40**, 163–168.

Farrer M., Gwinn-Hardy K., Hutton M., Hardy J. (1999) The genetics of disorders with synuclein pathology and parkinsonism. *Hum. Mol. Genet.* **8**, 1901–5.

Fedoroff S., Ahmed I., Opas M., Kalnins V. I. (1987) Organization of microfilaments in astrocytes that form in the presence of dibutyryl cyclic AMP in cultures, and which are similar to reactive astrocytes in vivo. *Neuroscience* **22**, 255–266.

Fedoroff S., McAuley W. A., Houle J. D., Devon R. M. (1984) Astrocyte cell lineage. V. Similarity of astrocytes that form in the presence of dBcAMP in cultures to reactive astrocytes in vivo. *J. Neurosci. Res.* **12**, 14–27.

Feng L., Hatten M. E., Heintz N. (1994) Brain lipid-binding protein (BLBP): A novel signaling system in the developing mammalian CNS. *Neuron* **12**, 895–908.

Figueroa J. D., Serrano-Illan M., Licero J., Cordero K., Miranda J. D., Leon M. De (2016)

Fatty Acid Binding Protein 5 Modulates Docosahexaenoic Acid-Induced Recovery in Rats Undergoing Spinal Cord Injury. *J. Neurotrauma*, In Press.

Fincher E. F., Johannsen L., Kapás L., Takahashi S., Krueger J. M. (1996) Microglia digest Staphylococcus aureus into low molecular weight biologically active compounds. *Am. J. Physiol.* **271**, R149-56.

Fischer H. G., Reichmann G. (2001) Brain dendritic cells and macrophages/microglia in central nervous system inflammation. *J. Immunol.* **166**, 2717–26.

Floden A. M., Li S., Combs C. K. (2005) Beta-amyloid-stimulated microglia induce neuron death via synergistic stimulation of tumor necrosis factor alpha and NMDA receptors. *J. Neurosci.* **25**, 2566–75.

Folch J., Lees M., Sloane Stanley G. (1957) A simple method for the isolation and purification of total lipides from animal tissues. *J. Biol. Chem.* **226**, 497–509.

Franco R., Fernández-Suárez D. (2015) *Alternatively activated microglia and macrophages in the central nervous system*.

Fujino T., Kang M. J., Suzuki H., Iijima H., Yamamoto T. (1996) Molecular characterization and expression of rat acyl-CoA synthetase 3. *J. Biol. Chem.* **271**, 16748–16752.

Galiègue S., Mary S., Marchand J., Dussossoy D., Carrière D., Carayon P., Bouaboula M., Shire D., Fur G. Le, Casellas P. (1995) Expression of central and peripheral cannabinoid receptors in human immune tissues and leukocyte subpopulations. *Eur. J. Biochem.* **232**, 54–61.

Gispert S., Turco D. Del, Garrett L., Chen A., Bernard D. J., Hamm-Clement J., Korf H.-W., et al. (2003) Transgenic mice expressing mutant A53T human alpha-synuclein show neuronal dysfunction in the absence of aggregate formation. *Mol. Cell. Neurosci.* **24**, 419–29.

Goldman J. E., Abramson B. (1990) Cyclic AMP-induced shape changes of astrocytes are accompanied by rapid depolymerization of actin. *Brain Res.* **528**, 189–196.

Goldman J. E., Chiu F. C. (1984) Dibutyryl cyclic AMP causes intermediate filament accumulation and actin reorganization in astrocytes. *Brain Res.* **306**, 85–95.

Golovko M. Y., Faergeman N. J., Cole N. B., Castagnet P. I., Nussbaum R. L., Murphy E. J. (2005) Alpha-synuclein gene deletion decreases brain palmitate uptake and alters the palmitate metabolism in the absence of alpha-synuclein palmitate binding. *Biochemistry* **44**, 8251–8259.

Golovko M. Y., Murphy E. J. (2008) Brain prostaglandin formation is increased by alpha-synuclein gene-ablation during global ischemia. *Neurosci. Lett.* **432**, 243–247.

Golovko M. Y., Rosenberger T. A., Faergeman N. J., Feddersen S., Cole N. B., Pribill I., Berger J., Nussbaum R. L., Murphy E. J. (2006a) Acyl-CoA synthetase activity links wild-type but not mutant alpha-synuclein to brain arachidonate metabolism. *Biochemistry* **45**, 6956–6966.

Golovko M. Y., Rosenberger T. A., Feddersen S., Faergeman N. J., Murphy E. J. (2006b) α-Synuclein gene ablation increases docosahexaenoic acid incorporation and turnover in brain phospholipids. *J. Neurochem.* **101**, 201–211.

Hanaka S., Abe T., Itakura H., Matsumoto A. (2000) Gene expression related to cholesterol metabolism in mouse brain during development. *Brain Dev.* **22**, 321–326.

Hanhoff T., Lücke C., Spener F. (2002) Insights into binding of fatty acids by fatty acid binding proteins. *Mol. Cell. Biochem.* **239**, 45–54.

Hashimotodani Y., Ohno-Shosaku T., Tanimura A., Kita Y., Sano Y., Shimizu T., Marzo V. Di, Kano M. (2013) Acute inhibition of diacylglycerol lipase blocks endocannabinoid-mediated retrograde signalling: evidence for on-demand

biosynthesis of 2-arachidonoylglycerol. *J. Physiol.* **591**, 4765–76.

Hayashi H., Campenot R. B., Vance D. E., Vance J. E. (2004) Glial lipoproteins stimulate axon growth of central nervous system neurons in compartmented cultures. *J. Biol. Chem.* **279**, 14009–15.

Herkenham M., Lynn A. B., Litrle M. D., Johnsont M. R., Melvin L. S., Costa B. R. De, Riceo K. C. (1990) Cannabinoid receptor localization in brain. *Neurobiology* **87**, 1932–1936.

Hertz L. (1990) Dibutyryl cyclic AMP treatment of astrocytes in primary cultures as a substitute for normal morphogenic and "functiogenic" transmitter signals. *Adv. Exp. Med. Biol.* **265**, 227–243.

Higgs H. N., Glomset J. A. (1994) Identification of a phosphatidic acid-preferring phospholipase A1 from bovine brain and testis. *Proc. Natl. Acad. Sci. U. S. A.* **91**, 9574–8.

Hohmann A. G., Martin W. J., Tsou K., Walker J. M. (1995) Inhibition of noxious stimulus-evoked activity of spinal cord dorsal horn neurons by the cannabinoid WIN 55,212-2. *Life Sci.* **56**, 2111–8.

Horn C. G. Van, Caviglia J. M., Li L. O., Wang S., Granger D. A., Coleman R. A. (2005) Characterization of recombinant long-chain rat Acyl-CoA synthetase isoforms 3 and 6: Identification of a novel variant of isoform 6. *Biochemistry* **44**, 1635–1642.

Hughes M. M., Field R. H., Perry V. H., Murray C. L., Cunningham C. (2010) Microglia in the degenerating brain are capable of phagocytosis of beads and of apoptotic cells, but do not efficiently remove PrPSc, even upon LPS stimulation. *Glia* **58**, 2017–2030.

Igal R. A., Coleman R. A. (1996) Acylglycerol recycling from triacylglycerol to phospholipid, not lipase activity, is defective in neutral lipid storage disease

fibroblasts. *J. Biol. Chem.* **271**, 16644–16651.

Igal R. A., Wang P., Coleman R. A. (1997) Triacsin C blocks de novo synthesis of glycerolipids and cholesterol esters but not recycling of fatty acid into phospholipid: evidence for functionally separate pools of acyl-CoA. *Biochem. J.* **324**, 529–534.

Ignatius M. J., Shooter E. M., Pitas R. E., Mahley R. W. (1987) Lipoprotein uptake by neuronal growth cones in vitro. *Science* **236**, 959–962.

Iseki E., Marui W., Kosaka K., Akiyama H., Ueda K., Iwatsubo T. (1998) Degenerative terminals of the perforant pathway are human alpha-synuclein-immunoreactive in the hippocampus of patients with diffuse Lewy body disease. *Neurosci. Lett.* **258**, 81–4.

Jakes R., Spillantini M. G., Goedert M. (1994) Identification of two distinct synucleins from human brain. *FEBS Lett.* **345**, 27–32.

Jangula A., Murphy E. J. (2013) Lipopolysaccharide-induced blood brain barrier permeability is enhanced by alpha-synuclein expression. *Neurosci. Lett.* **551**, 23–7.

Jenco J. M., Rawlingson A., Daniels B., Morris A. J. (1998) Regulation of phospholipase D2: Selective inhibition of mammalian phospholipase D isoenzymes by alpha- and beta-synucleins. *Biochemistry* **37**, 4901–4909.

Jolly C. A., Hubbell T., Behnke W. D., Schroeder F. (1997) Fatty acid binding protein: stimulation of microsomal phosphatidic acid formation. *Arch. Biochem. Biophys.* **341**, 112–121.

Jolly C. A., Murphy E. J. (2002) Role of FABP in cellular phospholipid metabolism, in *Mamm. Fat. Acid Bind. Proteins Struct. Roles Cell Homeost.*, (Duttaroy A. K., Spener F., eds), pp. 327–342. Wiley-VCH Press.

Jones M., Keenan R. W., Horowitz P. (1982) Use of 6-p-toluidino-2-naphthalenesulfonic acid to quantitate lipids after thin-layer chromatography. *J. Chromatogr. A* **237**,

522–524.

Jong H. de, Neal A. C., Coleman R. A., Lewin T. M. (2007) Ontogeny of mRNA expression and activity of long-chain acyl-CoA synthetase (ACSL) isoforms in Mus musculus heart. *Biochim. Biophys. Acta* **1771**, 75–82.

Kabba J. A., Xu Y., Christian H., Ruan W., Chenai K., Xiang Y., Zhang L., Saavedra J. M., Pang T. (2017) Microglia: Housekeeper of the Central Nervous System. *Cell. Mol. Neurobiol.*

Kang M. J., Fujino T., Sasano H., Minekura H., Yabuki N., Nagura H., Iijima H., Yamamoto T. T. (1997) A novel arachidonate-preferring acyl-CoA synthetase is present in steroidogenic cells of the rat adrenal, ovary, and testis. *Proc. Natl. Acad. Sci. U. S. A.* **94**, 2880–2884.

Kaur C., Too H. F., Ling E. A. (2004) Phagocytosis of Escherichia coli by amoeboid microglial cells in the developing brain. *Acta Neuropathol.* **107**, 204–208.

Kee H. J., Koh J. T., Yang S. Y., Lee Z. H., Baik Y. H., Kim K. K. (2003) A novel murine long-chain acyl-CoA synthetase expressed in brain participates in neuronal cell proliferation. *Biochem. Biophys. Res. Commun.* **305**, 925–33.

Keene C. D., Chang R. C., Lopez-Yglesias A. H., Shalloway B. R., Sokal I., Li X., Reed P. J., et al. (2010) Suppressed accumulation of cerebral amyloid {beta} peptides in aged transgenic Alzheimer's disease mice by transplantation with wild-type or prostaglandin E2 receptor subtype 2-null bone marrow. *Am. J. Pathol.* **177**, 346–54.

Keller M., Seregi A., Hertting G., Jackisch R. (1987) Prostanoid formation in primary astroglial cell cultures: Ca(2+)-dependency and stimulation by A 23187, melittin and phospholipases A(2) and C. *Neurochem. Int.* **10**, 433–443.

Kim S., Cho S. H., Kim K. Y., Shin K. Y., Kim H. S., Park C. H., Chang K. A., Lee S. H., Cho D., Suh Y. H. (2009) a-Synuclein induces migration of BV-2 microglial cells by

up-regulation of CD44 and MT1-MMP. *J. Neurochem.* **109**, 1483–1496.

Kim S. U., Vellis J. de (2005) Microglia in health and disease. *J. Neurosci. Res.* **81**, 302–313.

Kishimoto Y. (2006) Endogenous Cannabinoid Signaling through the CB1 Receptor Is Essential for Cerebellum-Dependent Discrete Motor Learning. *J. Neurosci.* **26**, 8829–8837.

Klegeris A., Pelech S., Giasson B. I., Maguire J., Zhang H., McGeer E. G., McGeer P. L. (2008) Alpha-Synuclein activates stress signaling protein kinases in THP-1 cells and microglia. *Neurobiol. Aging* **29**, 739–752.

Koehler R. C., Roman R. J., Harder D. R. (2009) Astrocytes and the regulation of cerebral blood flow. *Trends Neurosci.* **32**, 160–169.

Kowal S. L., Dall T. M., Chakrabarti R., Storm M. V., Jain A. (2013) The current and projected economic burden of Parkinson's disease in the United States. *Mov. Disord.* **28**, 311–318.

Kozak K. R., Gupta R. A., Moody J. S., Ji C., Boeglin W. E., DuBois R. N., Brash A. R., Marnett L. J. (2002) 15-Lipoxygenase Metabolism of 2-Arachidonylglycerol. *J. Biol. Chem.* **277**, 23278–23286.

Kozak K. R., Marnett L. J. (2002) Oxidative metabolism of endocannabinoids. *Prostaglandins, Leukot. Essent. Fat. Acids* **66**, 211–220.

Kreutzberg G. W. (1996) Microglia: a sensor for pathological events in the CNS. *Trends Neurosci.* **19**, 312–8.

Krüger R., Müller T., Riess O. (2000) Involvement of α-synuclein in Parkinson's disease and other neurodegenerative disorders. *J. Neural Transm.* **107**, 31–40.

Krul E. S., Tang J. (1992) Secretion of apolipoprotein E by an astrocytoma cell line. *J. Neurosci. Res.* **32**, 227–238.

Kuo Y.-M., Li Z., Jiao Y., Gaborit N., Pani A. K., Orrison B. M., Bruneau B. G., et al.
(2010) Extensive enteric nervous system abnormalities in mice transgenic for
artificial chromosomes containing Parkinson disease-associated alpha-synuclein
gene mutations precede central nervous system changes. *Hum. Mol. Genet.* **19**,
1633–50.

Kurtz A., Zimmer A., Schnutgen F., Bruning G., Spener F., Muller T. (1994) The
expression pattern of a novel gene encoding brain-fatty acid binding protein
correlates with neuronal and glial cell development. *Development* **120**, 2637–2649.

Lee E. J., Kim H. C., Cho Y. Y., Byun S. J., Lim J. M., Ryoo Z. Y. (2005a) Alternative
promotion of the mouse acyl-CoA synthetase 6 (mAcsl6) gene mediates the
expression of multiple transcripts with 5'-end heterogeneity: genetic organization of
mAcsl6 variants. *Biochem. Biophys. Res. Commun.* **327**, 84–93.

Lee E. J., Kim H. C., Cho Y. Y., Byun S. J., Lim J. M., Ryoo Z. Y. (2005b) Alternative
promotion of the mouse acyl-CoA synthetase 6 (mAcsl6) gene mediates the
expression of multiple transcripts with 5'-end heterogeneity: genetic organization of
mAcsl6 variants. *Biochem. Biophys. Res. Commun.* **327**, 84–93.

Lee M., Hyun D., Halliwell B., Jenner P. (2001) Effect of the overexpression of wild-type
or mutant alpha-synuclein on cell susceptibility to insult. *J. Neurochem.* **76**, 998–
1009.

Lee S., Park S. M., Ahn K. J., Chung K. C., Paik S. R., Kim J. (2009) Identification of the
amino acid sequence motif of alpha-synuclein responsible for macrophage
activation. *Biochem. Biophys. Res. Commun.* **381**, 39–43.

Levi G., Minghetti L., Aloisi F. (1998) Regulation of prostanoid synthesis in microglial
cells and effects of prostaglandin E2 on microglial functions. *Biochimie* **80**, 899–
904.

Lewin T. M., Kim J. H., Granger D. A., Vance J. E., Coleman R. A. (2001) Acyl-CoA synthetase isoforms 1, 4, and 5 are present in different subcellular membranes in rat liver and can be inhibited independently. *J. Biol. Chem.* **276**, 24674–24679.

Li X., Melief E., Postupna N., Montine K. S., Keene C. D., Montine T. J. (2015) Prostaglandin E2 receptor subtype 2 regulation of scavenger receptor CD36 modulates microglial Ab42 phagocytosis. *Am. J. Pathol.* **185**, 230–239.

Liu J. W., Almaguel F. G., Bu L., Leon D. D. De, Leon M. De (2008) Expression of E-FABP in PC12 cells increases neurite extension during differentiation: involvement of n-3 and n-6 fatty acids. *J. Neurochem.* **106**, 2015–2029.

Liu J. W., Montero M., Bu L., Leon M. De (2015) Epidermal fatty acid-binding protein protects nerve growth factor-differentiated PC12 cells from lipotoxic injury. *J. Neurochem.* **132**, 85–98.

López G. H., Ilincheta de Boschero M. G., Castagnet P. I., Giusto N. M. (1995) Age-associated changes in the content and fatty acid composition of brain glycerophospholipids. *Comp. Biochem. Physiol. B. Biochem. Mol. Biol.* **112**, 331–343.

Lotharius J., Brundin P. (2002) Impaired dopamine storage resulting from alpha-synuclein mutations may contribute to the pathogenesis of Parkinson's disease. *Hum. Mol. Genet.* **11**, 2395–407.

Marcheselli B. L., Scott V. L., Reddy T. S., Bazan N. G. (1988) Quantitative analysis of acyl group composition of brain phospholipids, neutral lipids, and free fatty acids, in *Neuromethods 7 Lipids Relat. Compd.*, (Boulton A. A., Baker G. B., Horrocks L. A., eds), pp. 83–110. Humana Press, Clifton, NJ.

Marszalek J. R., Kitidis C., Dirusso C. C., Lodish H. F. (2005) Long-chain acyl-CoA synthetase 6 preferentially promotes DHA metabolism. *J. Biol. Chem.* **280**, 10817–

10826.

Martin G. G., Huang H., Atshaves B. P., Binas B., Schroeder F. (2003) Ablation of the Liver Fatty Acid Binding Protein Gene Decreases Fatty Acyl CoA Binding Capacity and Alters Fatty Acyl CoA Pool Distribution in Mouse Liver [?] *Biochemistry* **42**, 11520–11532.

Marzo V. Di, Bisogno T., Sugiura T., Melck D., Petrocellis L. De (1998) The novel endogenous cannabinoid 2-arachidonoylglycerol is inactivated by neuronal-and basophil-like cells - connections with anandamide. *Biochem. J.* **331**, 15–19.

Marzo V. Di, Deutsch D. G. (1998) Biochemistry of the Endogenous Ligands of Cannabinoid Receptors. *Neurobiol. Dis.* **5**, 386–404.

Mashek D. G., Li L. O., Coleman R. A. (2006) Rat long-chain acyl-CoA synthetase mRNA, protein, and activity vary in tissue distribution and in response to diet. *J. Lipid Res.* **47**, 2004–2010.

Matsuda L. A., Lolait S. J., Brownstein M. J., Young A. C., Bonner T. I. (1990) Structure of a cannabinoid receptor and functional expression of the cloned cDNA. *Nature* **346**, 561–564.

Mauch D. H., Nägler K., Schumacher S., Göritz C., Müller E. C., Otto A., Pfrieger F. W. (2001) CNS synaptogenesis promoted by glia-derived cholesterol. *Science* **294**, 1354–1357.

McGeer P. L., Schwab C., Parent A., Doudet D. (2003) Presence of reactive microglia in monkey substantia nigra years after 1-methyl-4-phenyl-1,2,3,6-tetrahydropyridine administration. *Ann. Neurol.* **54**, 599–604.

Mecha M., Carrillo-Salinas F. J., Feliú A., Mestre L., Guaza C. (2016) Microglia activation states and cannabinoid system: Therapeutic implications.

Mecha M., Feliú a., Carrillo-Salinas F. J., Rueda-Zubiaurre a., Ortega-Gutiérrez S.,

Sola R. G. de, Guaza C. (2015) Endocannabinoids drive the acquisition of an alternative phenotype in microglia. *Brain. Behav. Immun.* **49**, 233–245.

Medeiros A. I., Serezani C. H., Lee S. P., Peters-Golden M. (2009) Efferocytosis impairs pulmonary macrophage and lung antibacterial function via PGE2/EP2 signaling. *J. Exp. Med.* **206**, 61–68.

Miller R. H., Raff M. C. (1984) Fibrous and protoplasmic astrocytes are biochemically and developmentally distinct. *J. Neurosci.* **4**, 585–592.

Milner R., Campbell I. L. (2003) The extracellular matrix and cytokines regulate microglial integrin expression and activation. *J. Immunol.* **170**, 3850–8.

Moore S. A., Yoder E., Murphy S., Dutton G. R., Spector A. A. (1991) Astrocytes, not neurons, produce docosahexaenoic acid (22:6 omega-3) and arachidonic acid (20:4 omega-6). *J. Neurochem.* **56**, 518–524.

Motoi Y., Aizawa T., Haga S., Nakamura S., Namba Y., Ikeda K. (1999) Neuronal localization of a novel mosaic apolipoprotein E receptor, LR11, in rat and human brain. *Brain Res.* **833**, 209–215.

Mukhopadhyay S., Howlett A. C. (2001) CB1 receptor-G protein association. Subtype selectivity is determined by distinct intracellular domains. *Eur. J. Biochem.* **268**, 499–505.

Munro S., Thomas K. L., Abu-Shaar M. (1993) Molecular characterization of a peripheral receptor for cannabinoids. *Nature* **365**, 61–65.

Muoio D. M., Lewin T. M., Wiedmer P., Coleman R. A. (2000) Acyl-CoAs are functionally channeled in liver: potential role of acyl-CoA synthetase. *Am. J. Physiol. Endocrinol. Metab.* **279**, 1366–1373.

Murphy C. C., Murphy E. J., Golovko M. Y. (2008) Erucic Acid is Differentially Taken up and Metabolized in Rat Liver and Heart. *Lipids* **43**, 391–400.

Murphy E. J. (1998) L-FABP and I-FABP expression increase NBD-stearate uptake and cytoplasmic diffusion in L cells. *Am J Physiol Gastrointest Liver Physiol* **275**, 244–249.

Murphy E. J. (2010) Brain fixation for analysis of brain lipid-mediators of signal transduction and brain eicosanoids requires head-focused microwave irradiation: An historical perspective. *Prostaglandins Other Lipid Mediat.* **91**, 63–67.

Murphy E. J., Barcelo-Coblijn G., Binas B., Glatz J. F. C. (2004) Heart fatty acid uptake is decreased in heart fatty acid-binding protein gene-ablated mice. *J. Biol. Chem.* **279**, 34481–34488.

Murphy E. J., Horrocks L. A. (1993) A model for compression trauma: pressure-induced injury in cell cultures. *J. Neurotrauma* **10**, 431–444.

Murphy E. J., Owada Y., Kitanaka N., Kondo H., Glatz J. F. C. (2005) Brain arachidonic acid incorporation is decreased in heart fatty acid binding protein gene-ablated mice. *Biochemistry* **44**, 6350–6360.

Murphy E. J., Prows D. R., Jefferson J. R., Schroeder F. (1996) Liver fatty acid-binding protein expression in transfected fibroblasts stimulates fatty acid uptake and metabolism. *Biochim. Biophys. Acta* **1301**, 191–196.

Murphy E. J., Prows D. R., Stiles T., Schroeder F. (2000a) Liver and intestinal fatty acid-binding protein expression increases phospholipid content and alters phospholipid fatty acid composition in L-cell fibroblasts. *Lipids* **35**, 729–738.

Murphy E. J., Rosenberger T. A., Horrocks L. A. (1997) Effects of maturation on the phospholipid and phospholipid fatty acid compositions in primary rat cortical astrocyte cell cultures. *Neurochem. Res.* **22**, 1205–1213.

Murphy E. J., Rosenberger T. a, Patrick C. B., Rapoport S. I. (2000b) Intravenously injected [1-14C]arachidonic acid targets phospholipids, and [1-14C]palmitic acid

targets neutral lipids in hearts of awake rats. *Lipids* **35**, 891–898.

Murphy M. G. (1984) Increasing membrane polyunsaturated fatty-acid content augments cyclic AMP formation and prostaglandin production in NIE-115 neuroblastoma. *Prog. Neuropsychopharmacol. Biol. Psychiatry* **8**, 529–537.

Murphy M. G. (1995) Effects of exogenous linoleic acid on fatty acid composition, receptor-mediated cAMP formation, and transport functions in rat astrocytes in primary culture. *Neurochem. Res.* **20**, 1365–1375.

Myers-Payne S. C., Hubbell T., Pu L., Schnütgen F., Börchers T., Wood W. G., Spener F., Schroeder F. (1996) Isolation and characterization of two fatty acid binding proteins from mouse brain. *J. Neurochem.* **66**, 1648–1656.

Nagano T., Kimura S. H., Takemura M. (2010) Prostaglandin E2 reduces amyloid beta-induced phagocytosis in cultured rat microglia. *Brain Res.* **1323**, 11–17.

Nakane S., Oka S., Arai S., Waku K., Ishima Y., Tokumura A., Sugiura T. (2002) 2-Arachidonoyl-sn-glycero-3-phosphate, an arachidonic acid-containing lysophosphatidic acid: occurrence and rapid enzymatic conversion to 2-arachidonoyl-sn-glycerol, a cannabinoid receptor ligand, in rat brain. *Arch. Biochem. Biophys.* **402**, 51–8.

Narayanan V., Guo Y., Scarlata S. (2005) Fluorescence studies suggest a role for alpha-synuclein in the phosphatidylinositol lipid signaling pathway. *Biochemistry* **44**, 462–470.

Neary J. T., Pilar Gutierrez M. del, Norenberg L. O., Norenberg M. D. (1987) Protein phosphorylation in primary astrocyte cultures treated with and without dibutyryl cyclic AMP. *Brain Res.* **410**, 164–168.

Osono Y., Woollett L. A., Herz J., Dietschy J. M. (1995) Role of the low density lipoprotein receptor in the flux of cholesterol through the plasma and across the

tissues of the mouse. *J. Clin. Invest.* **95**, 1124–1132.

Outeiro T. F., Lindquist S. (2003) Yeast Cells Provide Insight into Alpha-Synuclein Biology and Pathobiology. *Science (80-.).* **302**, 1772–1775.

Owada Y. (2008) Fatty acid binding protein: localization and functional significance in the brain. *Tohoku J. Exp. Med.* **214**, 213–220.

Owada Y., Kondo H. (2003) Fatty acid binding proteins of the brain, in *Cell. proteins their Fat. acids Heal. Dis.*, (Duttaroy A. K., Spener F., eds), pp. 253–265. Wiley-VCH Verlog GmbH & Co., Weinheim.

Owada Y., Yoshimoto T., Kondo H. (1996) Spatio-temporally differential expression of genes for three members of fatty acid binding proteins in developing and mature rat brains. *J. Chem. Neuroanat.* **12**, 113–122.

Pagotto U., Cervino C., Vicennati V., Marsicano G., Lutz B., Pasquali R. (2006a) How many sites of action for endocannabinoids to control energy metabolism? *Int. J. Obes.* **30**, 39–43.

Pagotto U., Marsicano G., Cota D., Lutz B., Pasquali R. (2006b) *The emerging role of the endocannabinoid system in endocrine regulation and energy balance*.

Park J.-Y., Paik S. R., Jou I., Park S. M. (2008) Microglial phagocytosis is enhanced by monomeric α-synuclein, not aggregated α-synuclein: Implications for Parkinson's disease. *Glia* **56**, 1215–1223.

Payton J. E., Perrin R. J., Woods W. S., George J. M. (2004) Structural determinants of PLD2 inhibition by alpha-synuclein. *J. Mol. Biol.* **337**, 1001–9.

Perrin R. J., Woods W. S., Clayton D. F., George J. M. (2000) Interaction of human alpha-Synuclein and Parkinson's disease variants with phospholipids. Structural analysis using site-directed mutagenesis. *J. Biol. Chem.* **275**, 34393–8.

Pitas R. E., Boyles J. K., Lee S. H., Foss D., Mahley R. W. (1987) Astrocytes synthesize

apolipoprotein E and metabolize apolipoprotein E-containing lipoproteins. *Biochim. Biophys. Acta* **917**, 148–161.

Poirier J., Baccichet A., Dea D., Gauthier S. (1993) Cholesterol synthesis and lipoprotein reuptake during synaptic remodelling in hippocampus in adult rats. *Neuroscience* **55**, 81–90.

Polymeropoulos M. H., Lavedan C., Leroy E., Ide S. E., Dehejia A., Dutra A., Pike B., et al. (1997) Mutation in the alpha-synuclein gene identified in families with Parkinson's disease. *Science* **276**, 2045–7.

Poppelreuther M., Rudolph B., Du C., Großmann R., Becker M., Thiele C., Ehehalt R., Füllekrug J. (2012) The N-terminal region of acyl-CoA synthetase 3 is essential for both the localization on lipid droplets and the function in fatty acid uptake. *J. Lipid Res.* **53**, 888–900.

Posse de Chaves E. I., Rusinol A. E., Vance D. E., Campenot R. B., Vance J. E. (1997) Role of lipoproteins in the delivery of lipids to axons during axonal regeneration. *J. Biol. Chem.* **272**, 30766–30773.

Prows D. R., Murphy E. J., Schroeder F. (1995) Intestinal and liver fatty acid binding proteins differentially affect fatty acid uptake and esterification in L-cells. *Lipids* **30**, 907–910.

Radin N. S. (1988) Lipid extraction, in *Neuromethods 7 Lipids Relat. Compd.*, (Boulton A. A., Baker G. B., A H. L., eds), pp. 1–62. Humana Press, Cifton, NJ.

Raghavan R., Kruijff L. de, Sterrenburg M. D., Rogers B. B., Hladik C. L., White C. L. (2004) Alpha-Synuclein Expression in the Developing Human Brain. *Pediatr. Dev. Pathol.* **7**, 506–516.

Ramakrishnan M., Jensen P. H., Marsh D. (2006) Association of alpha-synuclein and mutants with lipid membranes: spin-label ESR and polarized IR. *Biochemistry* **45**,

3386–95.

Rapoport S. I., Chang M. C., Spector A. A. (2001) Delivery and turnover of plasma-derived essential PUFAs in mammalian brain. *J. Lipid Res.* **42**, 678–685.

Regoeczi E., Taylor P. (1978) The net weight of the rat liver. *Growth* **42**, 451–6.

Richie-Jannetta R., Nirodi C. S., Crews B. C., Woodward D. F., Wang J. W., Duff P. T., Marnett L. J. (2010) Structural determinants for calcium mobilization by prostaglandin E2 and prostaglandin F2alpha glyceryl esters in RAW 264.7 cells and H1819 cells. *Prostaglandins Other Lipid Mediat.* **92**, 19–24.

Richter-Landsberg C., Gorath M., Trojanowski J. Q., Lee V. M.-Y. (2000) alpha-synuclein is developmentally expressed in cultured rat brain oligodendrocytes. *J. Neurosci. Res.* **62**, 9–14.

Robert J., Montaudon D., Hugues P. (1983) Incorporation and metabolism of exogenous fatty acids by cultured normal and tumoral glial cells. *Biochim. Biophys. Acta* **752**, 383–395.

Robinson P. J., Noronha J., DeGeorge J. J., Freed L. M., Nariai T., Rapoport S. I. (1992) A quantitative method for measuring regional in vivo fatty-acid incorporation into and turnover within brain phospholipids: review and critical analysis. *Brain Res. Brain Res. Rev.* **17**, 187–214.

Rojanathammanee L., Murphy E. J., Combs C. K. (2011) Expression of mutant alpha-synuclein modulates microglial phenotype in vitro. *J. Neuroinflammation* **8**, 44.

Rosenberger T. A., Oki J., Purdon A. D., Rapoport S. I., Murphy E. J. (2002) Rapid synthesis and turnover of brain microsomal ether phospholipids in the adult rat. *J. Lipid Res.* **43**, 59–68.

Rosenberger T. A., Villacreses N. E., Contreras M. a, Bonventre J. V, Rapoport S. I. (2003) Brain lipid metabolism in the cPLA2 knockout mouse. *J. Lipid Res.* **44**, 109–

117.

Seeger D. R., Murphy C. C., Murphy E. J. (2016) Astrocyte arachidonate and palmitate uptake and metabolism is differentially modulated by dibutyryl-cAMP treatment. *Prostaglandins, Leukot. Essent. Fat. Acids* **110**, 16–26.

Sellner P. A., Chu W., Glatz J. F. C., Berman N. E. J. (1995) Developmental role of fatty acid-binding proteins in mouse brain. *Dev. Brain Res.* **89**, 33–46.

Sharon R., Bar-Joseph I., Mirick G. E., Serhan C. N., Selkoe D. J. (2003) Altered Fatty Acid Composition of Dopaminergic Neurons Expressing alpha-Synuclein and Human Brains with alpha-Synucleinopathies. *J. Biol. Chem.* **278**, 49874–49881.

Sharon R., Goldberg M. S., Bar-Josef I., Betensky R. A., Shen J., Selkoe D. J. (2001) alpha-Synuclein occurs in lipid-rich high molecular weight complexes, binds fatty acids, and shows homology to the fatty acid-binding proteins. *Proc. Natl. Acad. Sci. U. S. A.* **98**, 9110–5.

Shavali S., Brown-Borg H. M., Ebadi M., Porter J. (2008) Mitochondrial localization of alpha-synuclein protein in alpha-synuclein overexpressing cells. *Neurosci. Lett.* **439**, 125–8.

Smith B. S. (1970) A comparison of 125-I and 51-Cr for measurement of total blood volume and residual blood content of tissues in the rat; evidence for accumulation of 51-Cr by tissues. *Clin. Chim. Acta.* **27**, 105–8.

Stachowska E., Baśkiewicz-Masiuk M., Dziedziejko V., Adler G., Bober J., Machaliński B., Chlubek D. (2007) Conjugated linoleic acids can change phagocytosis of human monocytes/macrophages by reduction in Cox-2 expression. *Lipids* **42**, 707–16.

Staub F., Winkler A., Peters J., Goerke U., Kempski O., Baethmann A. (1995) Clearance and metabolism of arachidonic acid by C6 glioma cells and astrocytes. *Neurochem. Res.* **20**, 1449–1456.

Straiker A., Wager-Miller J., Hu S., Blankman J., Cravatt B., Mackie K. (2011) COX-2 and fatty acid amide hydrolase can regulate the time course of depolarization-induced suppression of excitation. *Br. J. Pharmacol.* **164**, 1672–1683.

Strokin M., Sergeeva M., Reiser G. (2003) Docosahexaenoic acid and arachidonic acid release in rat brain astrocytes is mediated by two separate isoforms of phospholipase A $_2$ and is differently regulated by cyclic AMP and Ca $^{2+}$. *Br. J. Pharmacol.* **139**, 1014–1022.

Subramaniam S. R., Federoff H. J. (2017) Targeting Microglial Activation States as a Therapeutic Avenue in Parkinson?s Disease. *Front. Aging Neurosci.* **9**, 176.

Svennerholm L. (1968) Distribution and fatty acid composition of phosphoglycerides in normal human brain. *J. Lipid Res.* **9**, 570–579.

Swanson L. W., Simmons D. M., Hofmann S. L., Goldstein J. L., Brown M. S. (1988) Localization of mRNA for low density lipoprotein receptor and a cholesterol synthetic enzyme in rabbit nervous system by in situ hybridization. *Proc. Natl. Acad. Sci. U. S. A.* **85**, 9821–9825.

Tanji K., Imaizumi T., Yoshida H., Mori F., Yoshimoto M., Satoh K., Wakabayashi K. (2001) Expression of alpha-synuclein in a human glioma cell line and its up-regulation by interleukin-1beta. *Neuroreport* **12**, 1909–12.

Tanji K., Mori F., Imaizumi T., Yoshida H., Matsumiya T., Tamo W., Yoshimoto M., et al. (2002) Upregulation of alpha-synuclein by lipopolysaccharide and interleukin-1 in human macrophages. *Pathol. Int.* **52**, 572–7.

Teismann P., Schulz J. B. (2004) Cellular pathology of Parkinson?s disease: astrocytes, microglia and inflammation. *Cell Tissue Res.* **318**, 149–161.

Teunissen C. E., Veerhuis R., Vente J. De, Verhey F. R. J., Vreeling F., Boxtel M. P. J. van, Glatz J. F. C., Pelsers M. A. L. (2011) Brain-specific fatty acid-binding protein

is elevated in serum of patients with dementia-related diseases. *Eur. J. Neurol.* **18**, 865–871.

Trexler A. J., Rhoades E. (2009) Alpha-synuclein binds large unilamellar vesicles as an extended helix. *Biochemistry* **48**, 2304–6.

Ulvestad E., Williams K., Bjerkvig R., Tiekotter K., Antel J., Matre R. (1994) Human microglial cells have phenotypic and functional characteristics in common with both macrophages and dendritic antigen-presenting cells. *J. Leukoc. Biol.* **56**, 732–40.

Veerkamp J. H., Zimmerman A. W. Fatty acid-binding proteins of nervous tissue. *J. Mol. Neurosci.* **16**, 133–142.

Walter L., Franklin A., Witting A., Wade C., Xie Y., Kunos G., Mackie K., Stella N. (2003) Nonpsychotropic cannabinoid receptors regulate microglial cell migration. *J. Neurosci.* **23**, 1398–405.

Watkins P. A., Maiguel D., Jia Z., Pevsner J. (2007) Evidence for 26 distinct acyl-coenzyme A synthetase genes in the human genome. *J. Lipid Res.* **48**, 2736–2750.

Wilkin G. P., Marriott D. R., Cholewinski A. J., Wood J. N., Taylor G. W., Stephens G. J., Djamgoz M. B. (1991) Receptor activation and its biochemical consequences in astrocytes. *Ann. N. Y. Acad. Sci.* **633**, 475–488.

Williard D. E., Harmon S. D., Kaduce T. L., Spector A. A. (2002) Comparison of 20-, 22-, and 24-carbon n-3 and n-6 polyunsaturated fatty acid utilization in differentiated rat brain astrocytes. *Prostaglandins, Leukot. Essent. Fat. Acids* **67**, 99–104.

Wilms H., Rosenstiel P., Romero-Ramos M., Arlt A., Schäfer H., Seegert D., Kahle P. J., et al. (2009) Suppression of MAP kinases inhibits microglial activation and attenuates neuronal cell death induced by alpha-synuclein protofibrils. *Int. J. Immunopathol. Pharmacol.* **22**, 897–909.

Yin C., Zhou S., Jiang L., Sun X. (2012) Mechanical injured neurons stimulate astrocytes

to express apolipoprotein E through ERK pathway. *Neurosci. Lett.* **515**, 77–81.

Zhang W., Wang T., Pei Z., Miller D. S., Wu X., Block M. L., Wilson B., et al. (2005) Aggregated alpha-synuclein activates microglia: a process leading to disease progression in Parkinson's disease. *FASEB J.* **19**, 533–542.

Zhou W., Hurlbert M. S., Schaack J., Prasad K. N., Freed C. R. (2000) Overexpression of human alpha-synuclein causes dopamine neuron death in rat primary culture and immortalized mesencephalon-derived cells. *Brain Res.* **866**, 33–43.